Contribution to the uplink PHY/MAC analysis for the IOT and BAN applications

Claire Goursaud

No d'ordre NNT : HDR 2017 005

HABILITATION À DIRIGER DES RECHERCHES
opérée au sein de
L'INSTITUT NATIONAL DES SCIENCES APPLIQUÉES DE LYON ET L'UNIVERSITÉ CLAUDE BERNARD LYON 1

ÉCOLE DOCTORALE EDA 160
ÉLECTRONIQUE, ÉLECTROTECHNIQUE ET AUTOMATIQUE
(E.E.A.)

CLAIRE GOURSAUD
Date de soutenance : 01 Décembre 2017

CONTRIBUTION TO THE UPLINK PHY/MAC ANALYSIS FOR THE IOT AND BAN APPLICATIONS

Devant le jury composé de :

FIJALKOW, Inbar	Professeure des universités, *Université Paris Seine, Université Cergy Pontoise*	Présidente
DOHLER, Mischa	Professeur des universités, *King's College London*	Rapporteur
KOIVUNEN, Visa	Professeur des universités, *Aalto University*	Rapporteur
CIBLAT, Philippe	Professeur des universités, *Telecom Paris Tech, Université de Paris-Saclay*	Rapporteur
BEYLOT, André-Luc	Professeur des universités, *Toulouse INP*	Examinateur
GUÉRIN LASSOUS, Isabelle	Professeure des universités, *Université Claude Bernard - Lyon 1*	Examinateur
GORCE, Jean-Marie	Professeur des universités, *INSA Lyon*	Examinateur
FOURTET, Christophe	Co-fondateur, Directeur technique, *SigFox*	Invité

Contents

Chapter 1

Introduction

It has been more than 35 years since the first commercial telecommunication system was deployed for phone calls purpose, named $1G$. Over the last 3 decades, the world has witnessed the evolution of this primary network, toward to the currently deployed $4G$ and the forthcoming $5G$ as depicted in Fig.1.1.

$1G$, launched in 1981 was based on analog transmissions, and dedicated to phone calls. In the early $1990s$, was deployed with the first digital system $2G$, able to send small messages (SMS and MMS). Apart from the physical device size, the main improvement brought by $2G$ was the digital processing that improves reliability and handover among cells.

In $2000s$, $3G$ was deployed, relying on spread spectrum techniques to improve the link capacity by adapting the transmission to the channel conditions. These higher data transfer capabilities were used to serve new applications such as Internet browsing or multimedia transmissions.

In early 2009, $4G$ was deployed. In contrast to $3G$, $4G$ was more data oriented. It uses jointly all-IP packet switched network, OFDMA (Orthogonal Frequency Division Multiple Access) and MIMO (Multiple Input Multiple Output) to provide enough capacity for applications such as IP telephony, gaming services, high-definition mobile TV, video conferencing, and 3D television.

The upcoming new generation, namely $5G$, is expected to be deployed by 2020, targeting IoT (Internet of Things) applications. Behind this buzzword, we can find many interpretations. IoT is commonly defined as *a global infrastructure for the information society, enabling advanced services by interconnecting (physical and virtual) things based on existing and evolving inter-operable information and communication technologies* [Itu]. In other words, along with communication dedicated devices, any objects, animals or people could be provided with unique identifiers and the ability to transfer data over a network. In practice, $5G$ is targeting at providing even higher data rates (typically of Gbps order) to fulfill the demand of new multimedia applications (for a small class of devices, typically smartphones and/or tablets), while absorbing the traffic (individually low) from a very high number of nodes. The data

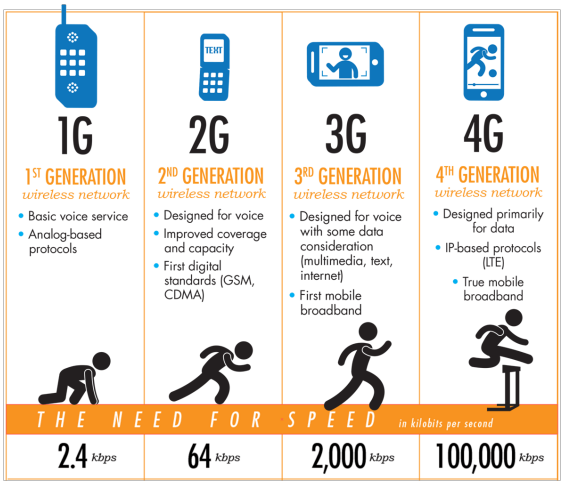

FIGURE 1.1: 1G to 4G evolution [1G417]

rate increase is expected to be reached with new techniques [ARS16]. The first one is the use of millimeter-wave communications [Rap+13]. Indeed, the historical radio spectrum band (700 MHz to 2.6 GHz) is currently saturated. Besides, as carrier frequency increases, the transmission band can be larger, thus increasing the data transfer rate. In addition, spatial multiplexing with Massive MIMO [Lu+14] or SDMA (Spatial Division Multiple Access) [PK11] are studied.

In a complementary direction to throughput increase, there is a need for handling an unseen number of devices (forecast to be between 20 [Edd15] to 50 billions devices [Eva11] in 2020). Indeed, the fruitful research made on WSNs (Wireless Sensor Networks) has paved the way for inexpensive, low powered miniature components that are able to sense their environment and transfer this collected data for processing. The definition of IoT is extending this concept by adding the ability of connection to the Internet, and the ability to uniquely identified all these sensors. One may expect that most of the devices deployed in IoT network will only have a small amount of data to share (e.g.for smart parking, smart metering, animal tracking,...). However, in contrast to the data rate challenge which mainly concerns the downlink transmission, the radio resource management for a huge number of nodes is particularly challenging for the uplink, especially for low quantities of individual information. Indeed, while resource reservation guarantees successful transmission (at least without endogenous collisions), this is at the cost of additional transmissions before sending the intended data. The latter should thus be kept as low as possible to save the resources for the useful data transmission. In this context, I have focused on the uplink transmissions of data in a WSN or IoT network, for two main reasons:

- First, it was a logical continuation of my thesis research activities. Indeed, during my PhD, I worked on the uplink in optical fiber networks. I studied OCDMA (Optical Code Division Multiple Access), which enables to provide simultaneous and asynchronous access to the optical fiber to several users. While shifting from optical to wireless communications, keeping the same multiple access goal was natural.

- Secondly, in my opinion, the uplink is more challenging, and interesting to treat. We have witnessed during the last couple of decades, the evolution of cellular communications to provide higher and higher data rates for downlink. On the contrary, the uplink remains a different problem and seems to be more open one.

During the last 10 years, I have thus considered ways to efficiently transmit information from one or several nodes to a BS (Base Station), a sink, or a specific node. In the work presented in this manuscript, I start from the principle that the channel state is not easy to obtain. This is specially the case for fast varying channels. The main hypothesis is that, the transmitting node has no (or very little) information on the signal propagation conditions, and on the channel occupation by other potential users. The recurring question in my research work was thus *how can we achieve the best performance, with almost no knowledge of the channel*. The objective is thus to design schemes that permit blind or opportunistic transmission of the data with the best reliability, without previous knowledge of the channel state. However, such schemes might depend on the channel specificities. We can distribute my contributions on two main cases, depending on the application context:

- Shadowing channel: this modeling was used to study WBANs (Wireless Body Area Networks). In such networks, the movements of the body parts cause time-varying shadowing effects for the on-body channels. Indeed, the direct link (or LOS (Line Of Sight)) can be obstructed by a body part, causing attenuation of the received signal. The work I conducted on WBAN is presented in chapter 2.

- Propagation and interference channel: this modeling was considered for wider networks such as WSN, and LPWAN (Low Power Wide Area Network). In such networks, path loss and fading are the main components needed to express the useful signal power at the reception side. In addition, one may also take into account the contribution due to the other simultaneous transmissions. The work conducted on this direction is presented in chapter 3.

In the following, I will present a summary the main results to which I have contributed, before presenting my research perspectives.

Bibliography

[1G417] 1G4G. In: (2017). URL: http://blog.commscopetraining.com/cellular-wireless-watch-the-evolution/.

[ARS16] Mamta Agiwal, Abhishek Roy, and Navrati Saxena. "Next generation 5G wireless networks: A comprehensive survey". In: *IEEE Communications Surveys & Tutorials* 18.3 (2016), pp. 1617–1655.

[Edd15] Nathan Eddy. "Gartner: 21 Billion IoT Devices To Invade By 2020". In: *InformationWeek, Nov* 10 (2015).

[Eva11] Dave Evans. "The internet of things: How the next evolution of the internet is changing everything". In: *CISCO white paper* 1.2011 (2011), pp. 1–11.

[Itu] "ITU-T Y.4000/Y.2060". In: (June 2012).

[Lu+14] Lu Lu et al. "An overview of massive MIMO: Benefits and challenges". In: *IEEE journal of selected topics in signal processing* 8.5 (2014), pp. 742–758.

[PK11] Zhouyue Pi and Farooq Khan. "An introduction to millimeter-wave mobile broadband systems". In: *IEEE communications magazine* 49.6 (2011).

[Rap+13] Theodore S Rappaport et al. "Millimeter wave mobile communications for 5G cellular: It will work!" In: *IEEE access* 1 (2013), pp. 335–349.

Chapter 2

Contributions in the WBAN context

2.1 What is a WBAN ?

WBAN (Wireless Body Area Network) refers to a specific network, where nodes are deployed on (or in) one or several persons [Cav+14]. These nodes are lightweight devices that are able to sense their environment and/or biological features of the person, and have wireless communication capabilities to transmit such data to a collection and processing point. One may note that BANs (Body Area Networks) share almost the same definition, but without considerations of the wireless transmission capabilities. WBAN is thus a sub-category of BAN. However, as most BANs have wireless links, the two acronyms usually refer to the same thing.

Such kind of network has attracted significant attention [Che+11][CKC08][BAu12][PW10]. Indeed, the targeted applications for such a network are numerous: from leisure (interactive games, sport entertainment) to medical applications (biological constant monitoring, rehabilitation), along with specific needs such as additional protection for firemen or servicemen during their operations, or for professional cyclists to provide additional information to their managers during their competition. All these applications share the following requirements as recommended by the IEEE TG6 [Zhe+08]:

- Low energy consumption: to ensure a long lifetime to the sensors and avoid battery replacement, monitoring should be energy efficient.
- Harmless wave: as nodes are placed close to the human body (even inside), the emitted waves must insure that they do not affect the surrounding tissues or organs. Keeping the emission power as low as possible is a good way to verify this constraint and the previous one.
- Coexistence with other systems: the wireless transmission protocol must ensure that 2 or more BANs can coexist in the same vicinity. The BANs may even cooperate for a better reliability. In addition, BANs must not interfere on other existing systems. Indeed, the usual band used for BAN applications is the ISM (Industrial, Scientific and Medical) radio band, which is open to unlicensed transmissions with signal specifications.

Besides, they also have their specific requirements:

- Delay: interactive gaming requires a very low latency, while collecting information from a cyclist does not suffer from small delay.
- Reliability: heart monitoring requires high reliability in the case of heart attack detection, while one of the periodic message on the heart rhythm can be lost without vital impact.
- Data rate: this constraint depends on the size of the data to transfer.
- Transmission range: even if one can expect that BAN communications are performed in a body area (thus targeting at most 2m transmissions), WBAN network definition is larger.

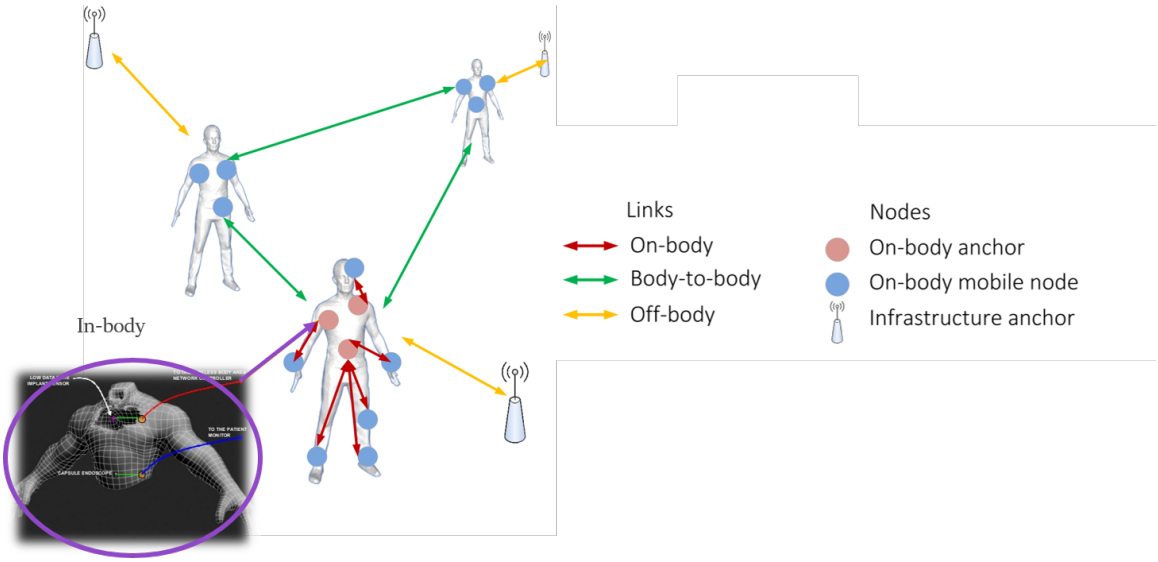

FIGURE 2.1: WBAN various kinds of links

Indeed, several kinds of links have been identified in a WBAN as presented in Fig.2.1 [MDD14]

- In-body (part of intra-BAN communications): this link involves at least one device inside the person body. This link is used when monitoring internal features such as blood composition, or needing to actuate a device (for instance an internal defibrillator, or insulin pump).
- On-body (part of intra-BAN communications): the sender and receiver are placed on the same person. This link is used when a sensor needs to send its information to a sink for processing or to a gateway for further relaying.
- Body-to-body (inter-BAN communication): in this case, the sender and receiver are on two different people. This case is used when the two WBANs cooperate, or when the persons are not considered individually, but rather as a group.
- Off-body (beyond-BAN communication): transmission is performed between one node placed on a person, and an infrastructure gateway. This link is used by the body sink to offload its data to other networks, or in localization purpose.

The main applications considered in my work were medical monitoring for non-vital functions, and localization applications. As a consequence, the in-body link is not considered, contrarily to the others. As regard to the requirements, data rates can be kept at a low level, and the constraint on delay is loose.

Besides, the close vicinity of the human body affects the signal propagation, leading to a specific radio channel. Indeed, the body modifies the conditions of propagation the electromagnetic waves, and even sometimes acts as an obstacle to the direct path transmission. This specific channel shape, and more specifically the correlation between the different channels has thus to be considered for realistic performance evaluation of such network. As such, I present the work done for evaluating this specific channel, and the performance obtained with these realistic propagation conditions. In particular, I propose solutions to provide better reliability while keeping the emitted power as low as possible, as well as results obtained for localization purpose.

The work presented in the following sections was mainly realized by a postdoc *Lusheng Wang* and 2 PhD students under my co-supervision: *Paul Ferrand*, and *Arturo Guizar*.

2.2 Characterization of the WBAN links channel and their correlation

In order to have accurate evaluation of the WBANs performances, it is mandatory to use an accurate channel model. Although other measurements campaigns have been conducted since, when starting this work, very few data and models were available to the scientific community. The first ones were for static analysis and were performed in 2002 and 2003 [HRH02] [Zas+03] to characterize the body effect on the channel variations. The body shape impact was studied in [TAK09], multi-path depending on the surrounding environment was modelized in [IEE]. Finally, [Rob11] focused on the person position.

To complete, dynamic analysis was also performed. [CCS09] [SC08] confirmed that the channel stability was linked to the body movements. However, they also showed that fading was more significant than shadowing in a multi-path environment (such as in the indoor case). Similar studies have been presented in [YSP09] and [Min+08], with different mobility scenarios.

However, there are two characterization items that were missing in the previous studies:

- The correlation between any two links of the WBAN (i.e. full-mesh topology). The closest study was [CCS09], where the topology was a star one.
- The channel characteristics to external nodes, for the off-body case. [CDO14] considers a static case, while [RD12] provides high level channel modeling for the mobility case.

Thus, we have conducted two measurements campaigns in order to have these parameters (full-mesh and spatio-temporal correlation) for a realistic case, described in the following sections.

HiKoB sensors-based platform

The two campaigns have been performed by using the same sensor nodes: the FOX sensors [Hik]. They are produced by *HiKoB* society [HF]. The advantage of these sensors is that they enable us to perform the measurement campaign without physical constraints. Indeed, thanks to their internal memory card, and their battery powered features, no cables are required. In particular, this permits to run outside experiments, and to achieve any human movement without external constraints or bias in the human behavior.

These FOX sensors are equipped with the radio chipset Atmel AT86RF231 [Atm], whose characteristics are reported in Table 2.1. At the receiver side, we used the *ED* (Energy Detection) Atmel metric. This is the mean of the received *RSSI* over 8 modulated symbols, and ranges from -91 dBm, to -8 dBm, with a relative precision of 1 dB.

Modulation	Offset-QPSK with spreading
Radio frequency	2408-2480 MHz
Inter-channel spacing	5 MHz
Maximal emission power (precision)	3 dBm (2 mW) $\pm$ **3 dB**
Sensitivity	-101 dBm at 250 Kbps
Antenna	Patch (integrated to the FOX circuit)
Polarization and gain	Omnidirectionnal (1 dBi)
Noise figure	6 dB
Access control layer	Based on IEEE 802.15.4 norm

TABLE 2.1: FOX main characteristics.

As the goal was to identify the correlation between any 2 links during the movement, we had to define a protocol to capture simultaneous and coherent link information. Ideally, a simultaneous estimation of all links would have been expected. However, this was not possible due to :

- The half-duplex feature of the radio chips that prevents a node to listen to the incoming signals while transmitting.

- The difficulty to separate each incoming signal and to associate each of them to the appropriate sender. An approach based on CDMA could be appropriate, but canno be implemented in the chips we have.

Thus, in order to guarantee that the links' values are obtained for exactly the same movement, a TDMA-based transmission algorithm was used as shown in 2.2. We thus made the assumption that the channel coherency time is larger than the time needed to scan all emitters (≤ 1.5ms each).

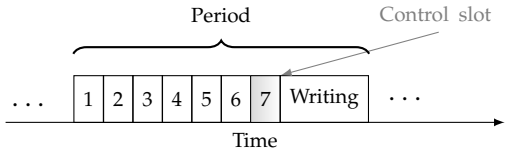

FIGURE 2.2: Measurement TDMA-based protocol

At a given slot, the scheduled emitter transmits, while all the other nodes listen to this one, and estimate the corresponding *ED*. Once all nodes have transmitted, an additional slot is reserved for a control node to trigger the data saving, and to increment the measure identifier. Finally, data are stored during the *writting slot*. One may note that the number of nodes is flexible, to be adapted to the WBAN size.

First measurement campaign : on-body links

In the first measurement campaign [Fer13], the FOX sensors were deployed on the body as presented on Fig.2.3, with two almost fixed nodes (hip and torso), and 4 highly mobile nodes (hands and feet)(both right and left). We have considered a walking scenario, in an outdoor place (stadium, with 30m walk), and indoor one (hallway of the Chappe building at INSA Lyon, with 40m walk).

This campaign has led to three main results.

The *first contribution* concerns the temporal behavior of the links. Indeed, one can easily identify on Fig.2.4 periods of 1s, corresponding to a walking cycle. This confirms that shadowing is mainly related to the body movement.

Besides, we can also observe that all presented links do not have the same temporal stability. We have thus evaluated the channel coherency time, by computing the signal autocorrelation function. Results obtained for a targeted cut-off value of 0.5 on indoor and outdoor measures are reported in Table 2.2 and Table 2.3 respectively.

From this analysis, we have confirmed the initial hypothesis. Indeed, the coherency time is larger than the frame duration (13ms for the 6 nodes), especially for the outdoor case. In

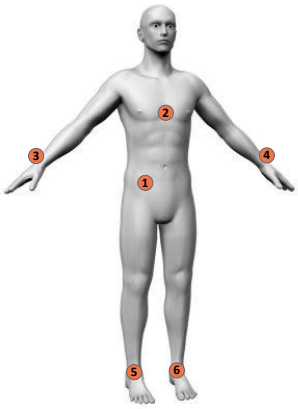

FIGURE 2.3: Nodes' position during the first campaign.

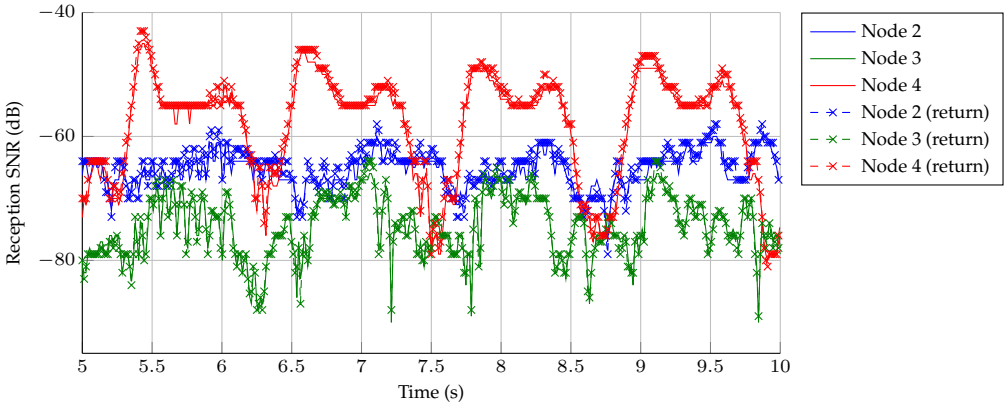

FIGURE 2.4: *ED* between node 1 (hip) from (solid line) or to (dashed line) nodes 2 (torso), 3 and 4 (hands), during 4 periods of walking movement.

Nodes	1	2	3	4	5	6
1	∅	35	17	47	21	38
2	25	∅	24	18	37	27
3	16	26	∅	19	25	35
4	52	19	19	∅	31	45
5	22	40	24	33	∅	21
6	33	26	32	39	21	∅

TABLE 2.2: Coherency time (ms), for any nodes set, for an indoor walking scenario.

Nodes	1	2	3	4	5	6
1	∅	84	77	134	60	36
2	86	∅	168	57	119	113
3	81	164	∅	62	118	52
4	131	46	59	∅	38	76
5	55	104	120	44	∅	38
6	38	98	55	78	37	∅

TABLE 2.3: Coherency time (ms), for any nodes set, for an outdoor walking scenario.

addition, we can note that this metric is highly dependent on the considered link, and the environment. In particular, links suffering from a higher level of multi-path (due to their low average power, or to the presence of reflectors such as in the indoor case) logically present a smaller coherency time.

The *second contribution* concerns the link symmetry. Indeed, we took advantage of having almost simultaneous link quality on the direct and the reverse link to analyze the link symmetry. For the links subject to multi-path, the knowledge of the direct link is not sufficient to predict the reverse link, especially when the received power is low (as can be seen for example on Fig.2.5(b)). This is due to the fading random contribution. However, more surprisingly, even for low multi-path case, there is a mismatch between the two links. Indeed, one can observe on Fig.2.5(a) that there is a shift between the experimental positions and the ideal linear equation $y = x$. To further this statement, a statistic test, namely *ANOVA* was performed. This has confirmed that the nodes used to form the link, even though they have the same nominal characteristics, can not be switched. Actually, this is due to the radio chip manufacturing imperfection. Nonetheless, the introduced bias is constant and can be compensated for if it is correctly estimated. Overall, one should apply a correction term when using the sensed *ED* to predict the reverse link *ED*.

The *third contribution* concerns the correlation between the links. We have shown that

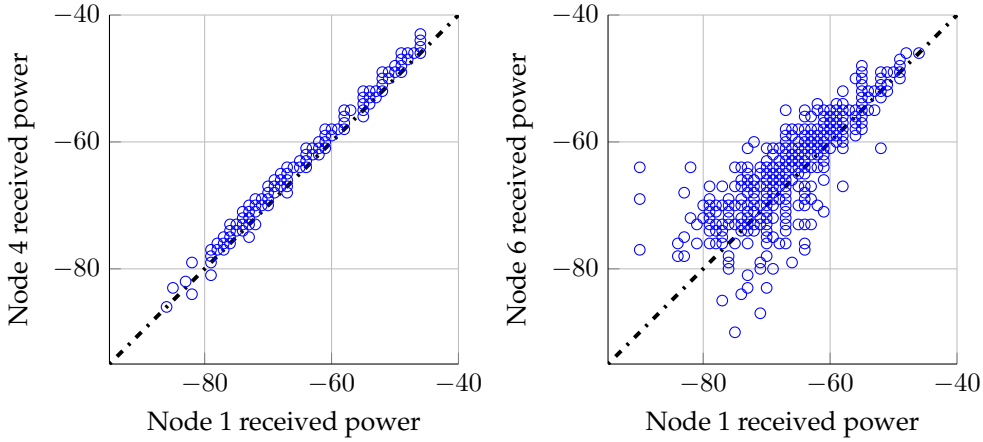

(a) Node 1 ↔ node 4

(b) Node 1 ↔ node 6

FIGURE 2.5: Repartition of the *ED* couples for the direct and reverse link

the correlation between the *ED* of 2 links is not pertinent over a long period, even for the outdoor scenario where multi-path effect is low. Indeed, in this case, the correlation matrix was different for each iteration of the same measure case. This implies that many other parameters are impacting and prevent us from either predicting the channel state of a link when having knowledge of the others, or to identify a specific movement by computing such metric. Nonetheless, the correlation matrix (for a subset of selected links) was more stable across the several periods in any given iteration. As a consequence, this is in favor of predicting the next step of a given iteration, but for a limited temporal window.

Second measurement campaign: on-body, body-to-body and off-body links

To complete the work presented in the previous section, a similar campaign was performed [Gui16], with additional features:

- Supplementary HiKoB nodes were deployed, to characterize off-body and body-to-body links. 4 nodes were fixed in the infrastructure for the off-body links, while 12 were deployed on 1 or several persons depending on the targeted scenario. Among the 12 nodes, 1 was used as a control one, to be able to check during the measurement that the HiKoB platform is recording the intended data.
- Complementary radio chips were also deployed, to evaluate the channel propagation conditions for UWB (Ultra-Wide Band) signals. To this aim, we used two different equipments. However, we obtained very little data to process from these measures. Indeed, for the first one, the platform IR-UWB TCR developed by the CEA [Lac+09], suffered from a problem undetected during the acquisition. The retrieved data were too oversampled to be useful. For the second one, a commercial platform from Be-Spoon, made of a smartphone and six nodes (also called *tag*), we obtained data for a star-topology, so only for a limited number of links. As a consequence, the channel values used in the following work were the ones from the narrow band HiKoB platform.
- Joint motion capture was performed: while recording link quality, the optical system Vicon [Vicst] was detecting the position of all the deployed nodes at a 100Hz rate, as well as any significant body part. This feature is highly relevant as:
  - it permits to couple the links quality with the exact environment conditions.
  - the measured positions will be used as a reference to evaluate the localization algorithm in further studies.

This measurement campaign was run in a Vicon dedicated gymasium at ENS/IRISA Cachan Bretagne, France (platform "Immermove"). One may note that multi-path was highly

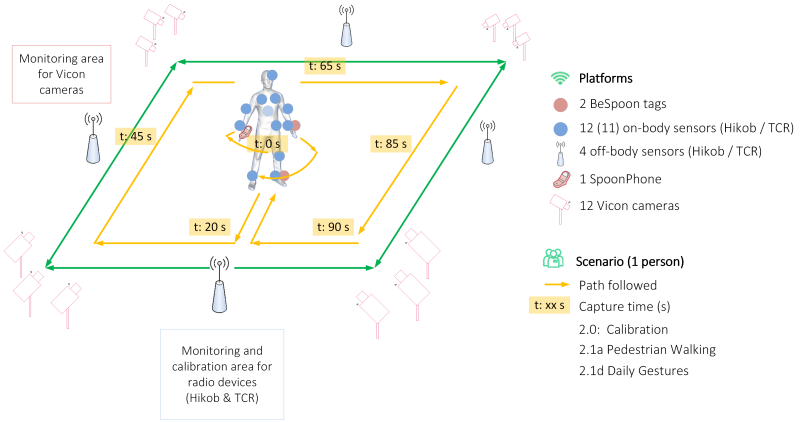

FIGURE 2.6: Experimental scenarios for the large scale individual motion capture (LSIMC.)

reduced compared to realistic cases, as reflecting walls were distant from the measurement area. Multi-path was mainly due to floor reflections.

In this context, we have defined diverse configurations (Fig.2.6), corresponding to the targeted application of the ANR project:

- LSIMC (Large Scale Individual Motion Capture): the objective is to be able to identify the posture and the absolute position of a person, while evolving in a wide area.
- CGN (Coordinated Group Navigation): the objective is to position all group's member, either relatively to each other, or absolutely with respect to the infrastructure.

Each scenario of about 3 minutes was run four times in case of measurement failure. Indeed, complete on-line verification was not possible (for instance, it took 6 months to get all the usable Vicon files due to time-consuming post processing).

Once obtained, the Vicon data were processed by the IETR research team to feed them into their PyLayer simulator. The body shape (based on multi-cylinder model), posture and position was reconstituted, which allows us to also identify the obstructed and non-obstructed links. Then, an additional post-processing was needed to pair them with the HiKoB data:

- In sampling frequency: the two systems were using different sampling frequency (10ms period for Vicon and $\approx$ 26ms for HiKoB). Thus, decimation/interpolation techniques were used.
- In time: the synchronization was performed by using several methods. First, a rough synchronization was obtained by identifying at the beginning of the data a specific gesture (quick raising arms above the head). Then, we used the correlation properties to refine the synchronization. We defined l_{sh} as the link *ED* expectation when knowing the position of the nodes and the environment. By considering free space propagation model, l_{sh} is proportional to the reciprocal of the squared distance. We completed this estimation by an empirical value of 15dB attenuation in case body obstruction is detected. The correlation factor between l_{sh} and *ED* was computed for all the links. One can observe on Fig.2.7 that for some links l_{sh} and *ED* fit perfectly, while differences are observed for others. However, as HiKoB nodes were jointly synchronized, the synchronization of a link permits the synchronization of the others.

Finally, to be able to exploit all these data at a communication layer, a joint PyLayer-WSNet simulator was enabled. WSNet is an event-driven simulator for large scale wireless sensor networks, developed in the CITI laboratory, that permits to modularly define and simulate any communication layer, from PHY to application layer. In this work, PyLayer has been used to provide both mobility model, and the channel temporal impulse response for any link. However, the exact impulse response exploitation requires a more sophisticated

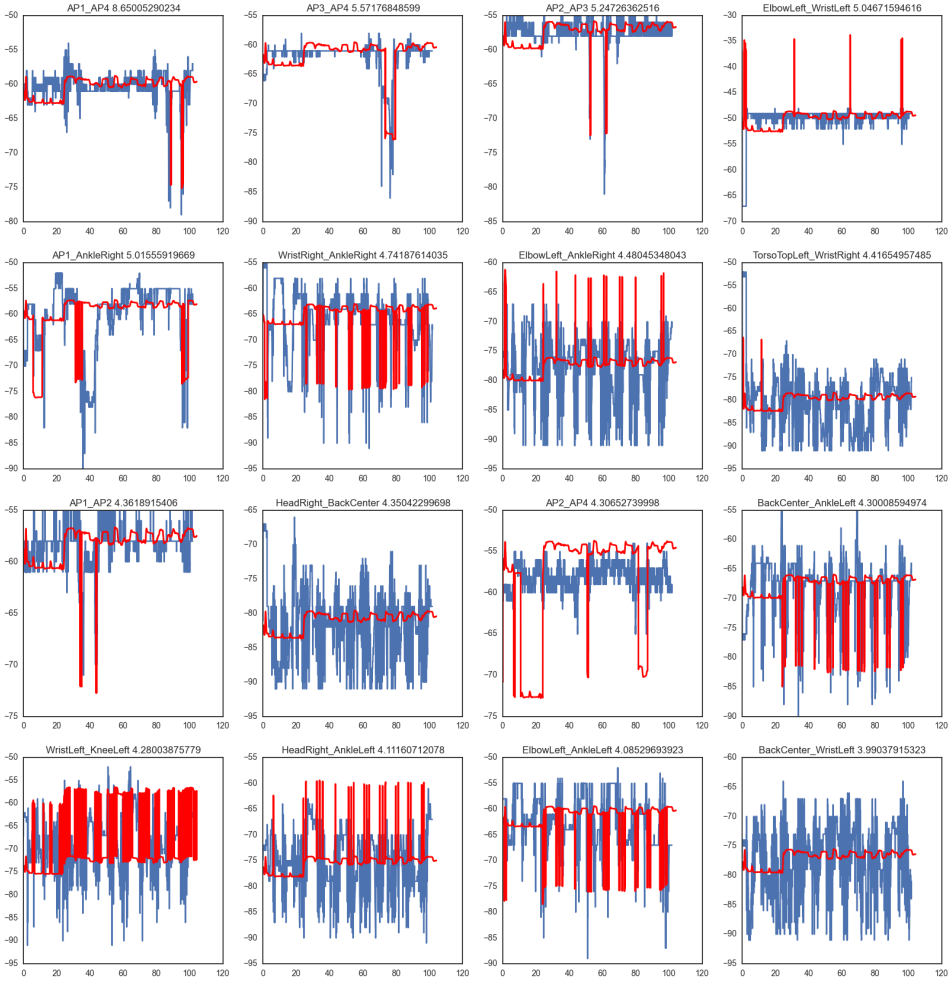

FIGURE 2.7: Comparison of *ED* (blue) and dhs (red) for the links presenting the best correlation factor

receiver model than the one available WSNet. Due to the lack of time, we have not focused on this issue. We have thus used the received power. This latter was estimated by two methods:

- R1, where the paths amplitude are squared and summed: $R_1 = \sum_{k=0}^{K-1} |\alpha_k|^2$ with K the number of considered paths, α_k the amplitude of the path
- R2, when also considering the paths delays: $h(\tau) = \sum_{k=0}^{K-1} \alpha_k \delta(\tau - \tau_k)$ with τ_k the path delay

To validate these models, we have compared them to the measurement data. An example is available on Fig.2.8. We have identified that the second model was more accurate as it was considering the fading due to multi-path. However, theory and measurement do not perfectly match. In fact, for the off-body link, when the direct link is available, the estimation is accurate. However, when there is an obstruction, the model is not sufficient to accurately describe the channel quality. In a similar way, for on-body links, the body effect can not be neglected. Thus, the PyLayer estimated reception power will be used when wanting to take into account only the distance and the shadowing impact, while measures will be used when studying the realistic case.

These data are then exploited by the WSNet simulator. We choose to interface the two simulators by using a data base, created beforehand by PyLayer, and exploited by WSNet at its will. To this aim, we have modified several modules of the WSNet initial features. One may note, that these modules were made to use PyLayer or measurement information,

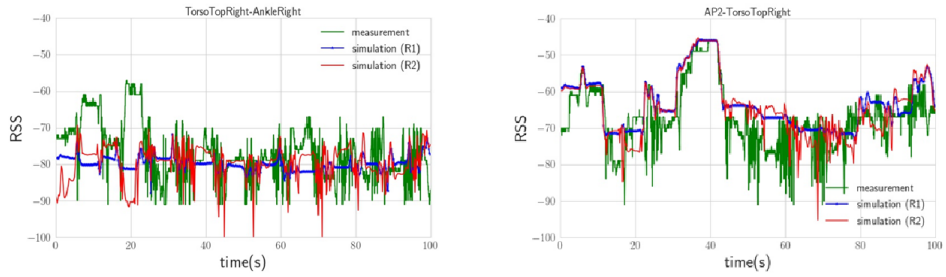

(a) On body : Right Torso - Right foot (b) Off body AP2 - Right torso

FIGURE 2.8: Reception power comparison of measurement (Hikob FOX, green) for an on-body and an off-body link with the 2 models: R_1 (blue), R_2 (red)

but also to use defined behavior (for instance linear movement for the mobility model, or a statistical channel model).

Conclusion

These measurement campaigns provided a rich and accurate framework describing the correlated links quality for WBANs, where classical models are not sufficient to accurately predict it.

One may regret that such results were available for narrow band transmission only, due to the unfortunate UWB equipments failure during the campaign.

Nonetheless, thanks to the completeness of the narrow band measurements (simultaneous measure of link, position, and context), we have a highly tunable framework, which permits to take into account the intended channel feature (distance, shadowing, and/or fading). Such framework has thus been exploited in the following work.

Finally, we can verify on Fig.2.7, that the links encounter various channel conditions at the same time, and over time. In such context, cooperation between the nodes may permit to counteract the temporary bad channel conditions. The objective is thus to evaluate the benefits of such cooperation, for various application examples.

2.3 Cooperation in a WBAN

In this section, we focus on the cooperation within a single WBAN. Any node can serve as a relay for the ones that face bad transmission conditions. We thus study the relay-channel building block presented in Fig.2.9. To keep a low energy consumption, we have theoretically evaluated the best power allocation between the source (S) and the relay (R) so as to maximize the end-to-end success probability, when knowing the shadowing states (s_{SD}, s_{SR} and s_{RD}).

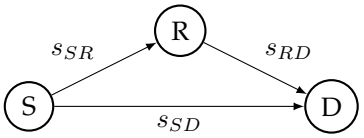

FIGURE 2.9: Relay channel, with shadowing effect on each link.

We note $\bar{\gamma}_{SD}$, $\bar{\gamma}_{SR}$ et $\bar{\gamma}_{RD}$ the SNR ((Signal to Noise Ratio), of the links $S \to D$, $S \to R$ and $R \to D$ respectively. These SNR can be expressed as:

$$\bar{\gamma}_{SD} = \delta s_{SD}\bar{\gamma} \qquad \bar{\gamma}_{SR} = \delta s_{SR}\bar{\gamma} \qquad \bar{\gamma}_{RD} = (1-\delta) s_{RD}\bar{\gamma} \tag{2.1}$$

with $\bar{\gamma}$ the the equivalent SNR available at the source, and δ the power ratio allocated to the source ($1-\delta$ being allocated to the relay).

PER and OP analysis

By considering that, when a link suffers from Rayleigh or Rice fading, its PER (Packet Error Rate) can be written [WG03] as $p(\bar{\gamma}_i) = G_{c,i}\bar{\gamma}_i^{-1}$, with $\bar{\gamma}_i$ the SNR, and $G_{c,i}$ the coding gain constant. We have deduced three optimum ratio δ, depending on the way the relay is used:

- Multihop: destination does not receive information directly from the source, $\delta_1 = \frac{\sqrt{\beta_{SR}}}{\sqrt{\beta_{SR}}+\sqrt{\beta_{RD}}}$
- Partial cooperation: destination listen to the source transmission, then to the relay one, $\delta_2 = \begin{cases} \frac{\beta_{SR}-4\beta_{RD}+\sqrt{\beta_{SR}(\beta_{SR}+8\beta_{RD})}}{4(\beta_{SR}-\beta_{RD})} & \text{if } \beta_{SR} \neq \beta_{RD} \\ \frac{2}{3} & \text{otherwise} \end{cases}$
- Full cooperation: destination listen to the source transmission, then to a joint transmission between source and relay, $\delta_3 = 1 + \frac{\beta'_{SR}}{\beta'_{RD}} - \sqrt{\left(\frac{\beta'_{SR}}{\beta'_{RD}}\right)^2 + \frac{\beta'_{SR}}{\beta'_{RD}}}$

with $\beta_{SD} = \frac{s_{SD}}{G_{c,SD}}$ $\beta_{SR} = \frac{s_{SR}}{G_{c,SR}}$ $\beta_{RD} = \frac{s_{RD}}{G_{c,RD}}$ $\beta'_{SR} = \frac{s_{SR}}{G_{c,SD}G_{c,SR}}$ $\beta'_{RD} = \frac{s_{RD}}{G_{c,MRC}}$

From this theoretical analysis, we have been able to show that the full cooperation scenario is better than the others. But when the $S \to R$ link is less reliable, the difference with the partial cooperation scenario decreases.

If the shadowing state is not known, the power allocation can not be optimally performed. However, we can evaluate the outage probability. For a relay channel, it can be expressed as the conditional expectation of the packet error function, over the shadowing states, i.e. over three variables for the complete relay scheme. To simplify the analysis, we have reduced the network freedom degrees to two, by considering two particular cases: 2-hop, and relay with a perfect link between relay and destination as shown in Fig.2.10. In particular, we observed the performance for correlated links, as presented in Fig.2.11, with ρ the correlation coefficient. Negative ρ describes a case where a link is bad while the other is good; and a positive ρ leads to a similar behavior of the two links.

We can verify that 2-hop is better suited for positively correlated and uncorrelated links, while the perfect link is more indicated for negative correlation case. This confirms that the correlation between the links is a necessary information when considering cooperation.

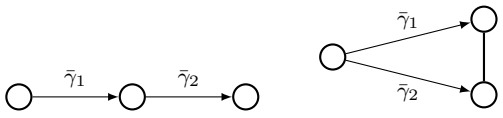

(a) 2-hop (b) Perfect $R \to D$ link

FIGURE 2.10: Simplified models for outage probability study.

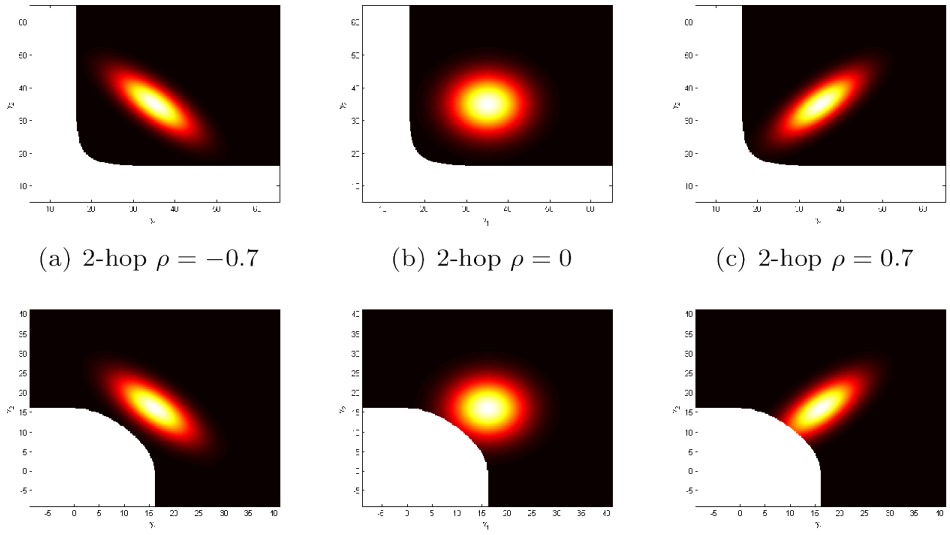

(a) 2-hop $\rho = -0.7$ (b) 2-hop $\rho = 0$ (c) 2-hop $\rho = 0.7$

(d) Perfect link $\rho = -0.7$ (e) Perfect link $\rho = 0$ (f) Perfect link $\rho = 0.7$

FIGURE 2.11: Correlation impact on the outage probability. White space is the outage area, while colors indicate the probability density for a bi-variate gaussian distribution.

This theoretical relay analysis has been completed by the study with the measured links values. We consider the foot (node D) as the source, the hip (A) as the receiver, and we elect one of the wrist nodes (I or K) as the relay. Source and relay are transmitting at the same power. We have first extracted the correlation parameters, as reported in Table 2.4.

	$A \leftrightarrow I$	$A \leftrightarrow D$	$D \leftrightarrow I$
$A \leftrightarrow I$	1	0.29	-0.04
$A \leftrightarrow D$	0.29	1	-0.34
$D \leftrightarrow I$	-0.04	-0.34	1

	$A \leftrightarrow K$	$A \leftrightarrow D$	$D \leftrightarrow K$
$A \leftrightarrow K$	1	-0.38	0.48
$A \leftrightarrow D$	-0.38	1	0.47
$D \leftrightarrow K$	0.48	0.47	1

TABLE 2.4: Correlation matrix for the 2 potential relay channels.

We consider both the real case (correlated one) and hypothetic one were links would be uncorrelated, but with the same shadowing distribution. We can see on Fig.?? that not considering the correlation leads to a further underestimation of the outage probability.

Besides, for high targeted PER threshold $P^\star$, the use of a relay can be counterproductive, as the source is more efficient by using all the power (thus transmitting 3dB higher than when the relay is used). Finally, we can note that the relay choice is important as node K leads to better performance than node I.

Capacity analysis

Finally, if we consider a stable AWGN channel (at least during the observation moment), we can also characterize the relay channel by its capacity (as defined by Shannon [Sha48]). We have shown that, for the half-duplex, decode and forward case, the capacity is upper-bounded by:

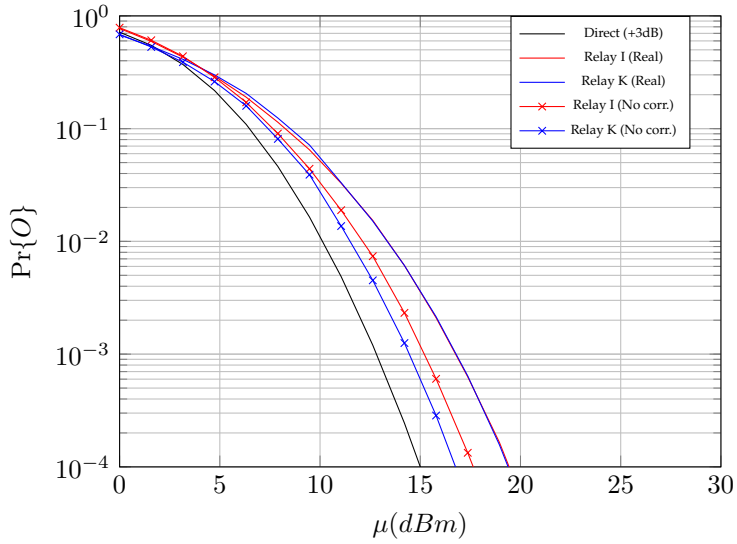

(a) $P^\star = 0.1$

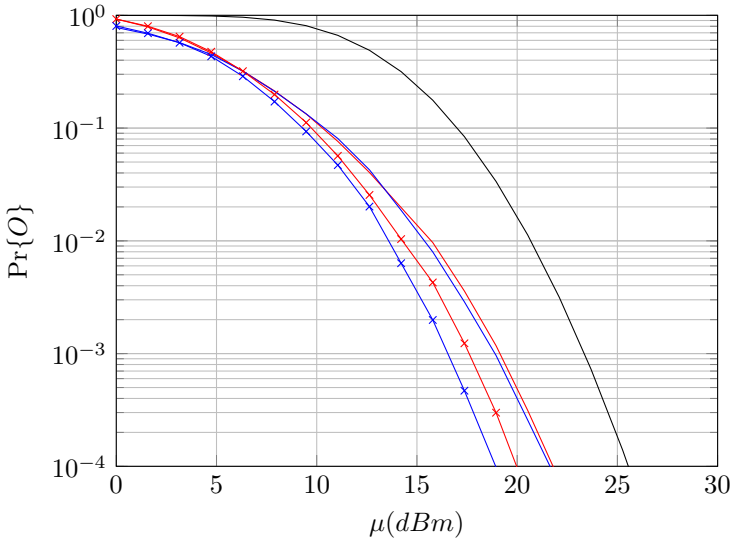

(b) $P^\star = 0.05$

FIGURE 2.12: Outage probability comparison for 2 relay choices, and 2 targeted PER $P^\star$.

$$C \leq \frac{1}{2}\left(\log\left(1 + 2\frac{(|s_{SD}|^2 + |s_{RD}|^2)|s_{SR}|^2}{|s_{SR}|^2 + |s_{RD}|^2}\bar{P}_{\text{tot}}\right)\right) \tag{2.2}$$

with P_{tot} the power to be distributed

As a consequence, the best choice for the relay node is the one that maximizes the $logarithm$ argument, i.e. is given by:

$$I^\star = \arg\max_{i\in\{1,\ldots,N\}} \frac{|s_{S,i}|^2(|s_{S,D}|^2 + |s_{i,D}|^2)}{|s_{S,i}|^2 + |s_{i,D}|^2} \tag{2.3}$$

The argument corresponds to the harmonic mean of $|h_{S,i}|^2$ and $|h_{i,D}|^2$, with an additional effect of the $S \rightarrow D$ channel. This is our first criteria for the relay election. We have also considered the Mean Harmonic metric (MH), where we compute the harmonic mean of the relay-destination link modulus to elect the relay; and the direct path performances. We have compared the mean capacity for the two criteria to no-relay case (direct), in the same scenario

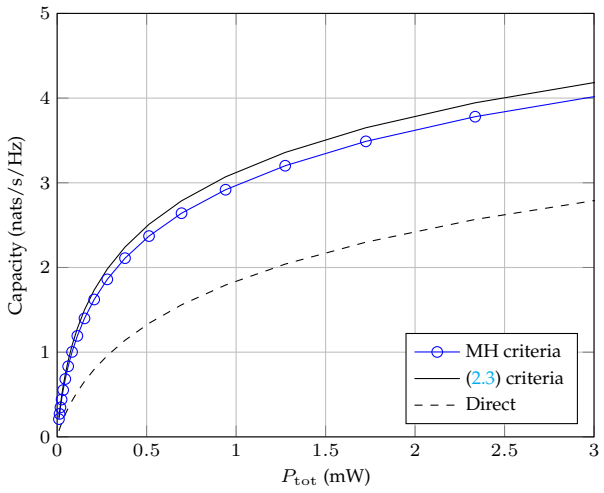

FIGURE 2.13: Mean capacity comparison for different relay selection criteria in a BAN, for an outdoor walking scenario.

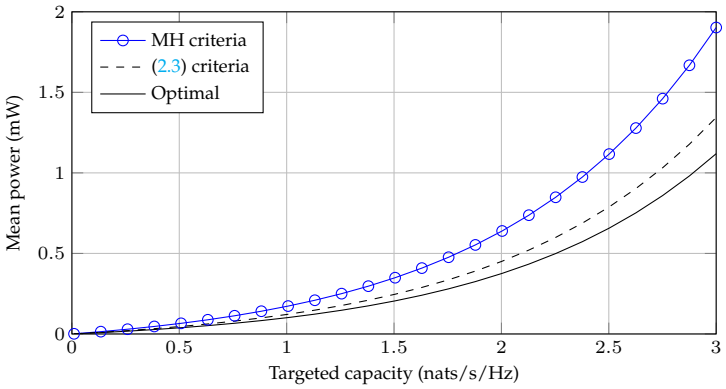

FIGURE 2.14: Comparison of the minimal power needed for a targeted capacity, for an outdoor walking scenario, and with beacon relaying protocol.

than previously (transmission between the foot and the hip), on Fig.2.13.

We can verify that the capacity criteria leads to better use of the channel. However, one may note that this optimum was obtained by considering that the channel was perfectly known at the receiver. We thus conclude this analysis by evaluating a realistic relay protocol. We consider that the coordinator (placed at the hip in this scenario) sends a beacon containing the links quality observed during the previous transmission. The node with the best quality starts transmitting, and relays the beacon to ensure that the destination gets it. We plot on Fig.2.14, the mean power needed to satisfy the capacity when electing the relay nodes with the different criteria, compared to the optimal case (channel is perfectly known).

We can observe that the imperfect knowledge on the channel state induces an additional power consumption. This is due to the fact that the used metrics for the relay selection suffer from two imprecisions: in time (as some were obtained in the previous transmission), and in accuracy (as some are estimated based on the reverse link). Thus, the optimization process is not optimal.

In this work, we have highlighted the relaying protocol benefit compared to direct path only. We have evaluated its theoretical performances in the ideal case (perfect channel estimation), and in a more realistic case. We have evaluated the performances degradation due to imperfect channel knowledge, within a relay channel (as the power is not optimally distributed over the transmitting nodes), but also when electing the relaying node within a WBAN.

2.4 Benefiting from cooperation between 2 WBANs

In this section, we now focus on the presence of several WBANs in the same vicinity. In this case, cooperation can be performed by two means:

- Cooperative scheduling: WBANs coordinators organize their transmission resources by considering the presence of the other WBANs
- Cooperative transmission: WBANs are collaborating by relaying to each others the transmitted data.

The cooperative transmission has been discarded because of privacy and security issues. Indeed, WBAN messages usually convey personal and critical data. Sharing this data with other WBAN opens a potential breach that can be exploited by a malicious WBAN to corrupt or inject false data. On the contrary, the cooperative scheduling is mandatory, as it is needed to ensure co-existence of WBANs. Resources can be shared in two fashions:

- Orthogonal resource sharing: each WBAN uses distinct resources. For example, in a 2 WBAN context, each WBAN transmits half of the time [Pat+09]. However, this drastically limits the transmissions for each WBAN.
- Non-orthogonal transmissions: resources are shared by the WBANs. This obviously leads to interference. Nonetheless, We have proposed and studied an optimum scheduling strategy that permits to minimize the interference effect.

To do so, we considered the case of two WBANs. Each was composed of one coordinator, collecting data from its N sensors, forming a star topology. Coordinators communicate with each other to guarantee time synchronization between the two WBANs, and exchange information on the links quality:

- RSS: intra-BAN Received Signal Strength
- RIS: inter-BAN Received Interference Strength

Inter-BAN interference level depends on the distance, the shadowing and the multi-path component. Shadowing is highly correlated between inter-BAN links (such links are likely to be respectively obstructed at the same time due to an obstacle in-between the WBANs, and the mutual orientation of the WBANs [MD16]). Thus, when there is an obstacle, interference is low for all nodes. Consequently, we have focused on the non-obstructed case, where interference can be effective. Therefore, the direct path has a strong contribution, and we have considered a free space propagation model.

1-BAN optimization.

In a first step, we have considered the case were a WBAN (B_2) has defined its transmission strategy, i.e. the transmission slots assigned to each sensor. The other WBAN (B_1) designs its own strategy to maximize its transmission capabilities.

We adapted a famous Chinese story "horse racing". Two sets of horses, (each composed of one superior, one medium and one inferior) were planed to compete. One set was owned by the king, so these horses were better in every category. To have chances to win, the competitor shifted the horses such as his inferior horse races the king's superior horse, his superior horse with the king's medium one, and his medium one with the king's inferior one. By doing so, there was a chance that he won the two last races. In our case, the competitors are the WBANs, and the horses are the sensors. The horse strength category maps to the RSS and RSI seen from B_1 point of view. The objective is to find the best number of shifts that permits to have the best SNR for B_1. One may note that, in contrast to the horse race where only one horse can win, in the WBAN context we can have a win-win situation. Indeed, both WBANs can be simultaneously successful due to path-loss which modifies the relative received powers among the WBANs. Besides, as each coordinator orders the sensors from its own observation on their strengths, the ordering might be different for the 2 coordinators.

This can be observed on Fig.2.15 which represents the PDR (Packet Delivery Ratio) as a function of the number of shifts. Circles and squares represent PDRs of the active BAN

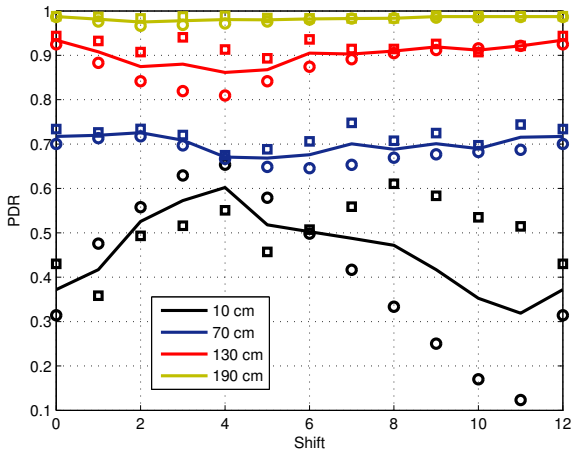

FIGURE 2.15: The effect of shifts in horse racing scheduling.

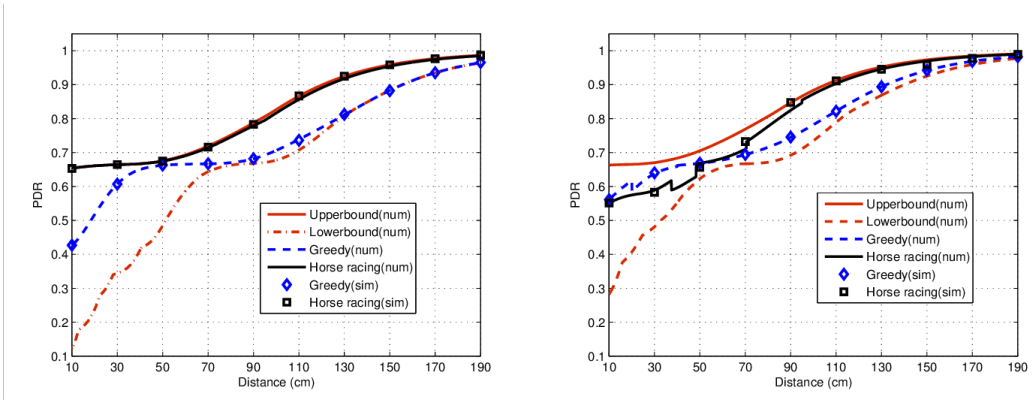

(a) Left-side BAN (b) Right-side BAN

FIGURE 2.16: Performance comparison of 1-BAN scheduling strategies.

and the inactive BAN, respectively, and curves represent average PDR of the two BANs. Analysis was made in the case where two persons wearing WBANs are standing side-by-side and motionless with a certain distance in between. Each BAN contains 12 sensors, along with the coordinator. 0 shift corresponds the strategy were RSS and RSI are sorted from the strongest to the weakest, and thus the strongest RSS competes with the strongest RSI. Cyclic shifting is then performed on the RSS for the other shift values.

We can observe that the best strategy for a WBAN is not necessarily the worst for the other one. Besides, the distance between the WBANs highly influence the performances.

We now compare on Fig.2.16 the horse racing strategy to other classical algorithms: the Hungarian algorithm [Kuh55] with time complexity, $O(N^3)$, which is quite efficient compared with full search. But it is still too resource demanding for a mobile coordinator, and too long regards to the channel coherency time. We also use the greedy algorithm[Cor+01] which step by step modifies the strategy toward a better one. The greedy algorithm is fast, however the optimal solution is not always reached. Both numerical analysis (theoretical computation of the SNR using Matlab)(curves), and simulations (with WSNet)(symbols) were performed. The upperbound and lowerbound are obtained by Hungarian algorithm.

We can observe that for the left-side WBAN, the proposed horse racing algorithm performances are very close to the upperbound, while it is less tight for the right-side WBAN. Thus, the left-side WBAN has succeeded in finding its optimal strategy, but at the expense of degraded performances for the other WBAN. In practice, this latter would then consider modifying its strategy, as treated below.

2-BAN case

In this case, both BANs are alternately active to change their own strategies, with purpose of maximizing their own utilities. This behavior is known as a game. Thus, we have theoretically studied two ways of reaching Nash Equilibrium (state in which no BAN benefits from changing unilaterally its strategy), i.e., PSNE (Pure Strategy NE, were the strategy is fixed) and MSNE (Mixed Strategy NE, where pure strategies are assigned with a selection probability). In particular, we have shown that there exist an infinite number of MSNE with equal probability on the strategies (referred to as Theorem 2 in the figures), and proposed an algorithm (DCS Distributed Cooperative Strategy)) detailed in [Wan+13], which prevents from the two BANs doing antagonist decisions, and at least converge to a state where the each BAN let the other win half time. Results are presented on Fig.2.17.

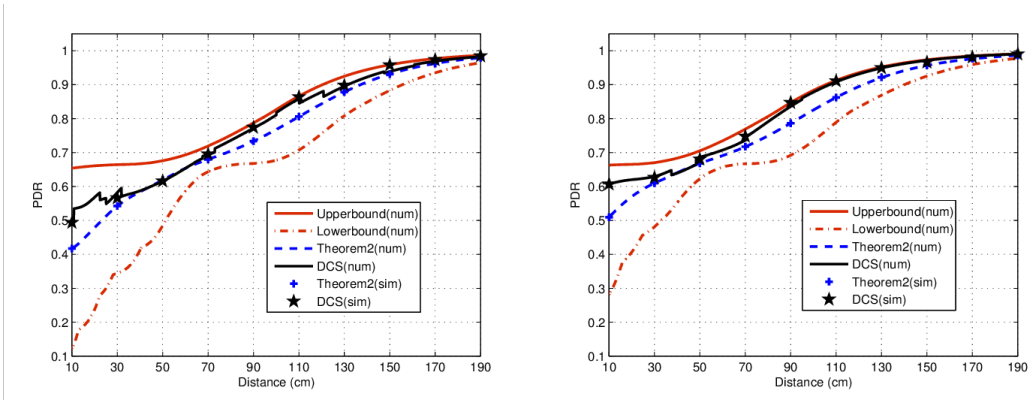

(a) Left-side BAN (b) Right-side BAN

FIGURE 2.17: Performance comparison of 2-BAN concurrent scheduling strategies.

We can observe that no WBAN performance reaches the upperbound. However, the system is more fair between the 2 WBANs. We have thus shown that it is possible to design a lightweight algorithm that permits to handle the interference in a fair way for multi-BAN coexistence. We were planning to extend this study to case were the sensors do not have the same function and require different QoS. In this case, we planned to weight their utilities before summation, to favor the critical applications.

2.5 How to use WBANs for localization ?

In this section, we use WBAN for localization and posture detection. To this aim, we have to retrieve information on the distance, the position and/or the movement of each body part. This can be done by using localization systems, such as:

- optical systems: external camera capture the person behavior without additional equipment [MHK06] [Pop07], or track previously installed tags as used in the measurement campaign [Vicst]. Precision is very high, but the infrastructure cost as well.
- magnetic systems: nodes sense the reference magnetic field [BN10]. The sensitivity to potential metallic pieces on the body (e.g. zipper, ring), prevents from using this technology in WBAN context.
- mechanical system: the person wears an exoskeleton that detects the movement [KW08]. Such skeleton reduces the freedom of movement.
- inertial systems: inertial sensors such as accelerometers, gyroscopes, magnetometer [Mor73] [Sak+96] [TP05] are used. They provide a good precision, while permitting mobile application.

However, all these systems require to had additional features to the WBAN transmitting node. Another option is to take advantage of the informations that can be captured by the radiochip:

- received power strength (RSS): this feature is not pertinent when the channel pathloss is affected by other parameters than distance. As WBAN suffer from shadowing and fading, this can be discarded.
- angle of arrival (AoA): this requires the use of an antenna array so as to evaluate the differential time of arrival to each element, but this is to expensive to be popularly deployed.
- time of arrival (ToA): thanks to this measure (and to the departure time stamp), the time of flight, thus, the distance can be evaluated. This metric will be used in our work.

Due to the propagation speed of the signals, the time of arrival needs to be obtained with a good precision (10 ns time error corresponds to 3 cm error). Thus, IR-UWB (Impulse Radio-Ultra Wide Band)(with OOK modulation) signals are used [Xia+10] [Ham+13], to take advantage of their high time resolution due to impulse-like shape. Once this value is obtained, we can deduce the person posture by following this workflow:

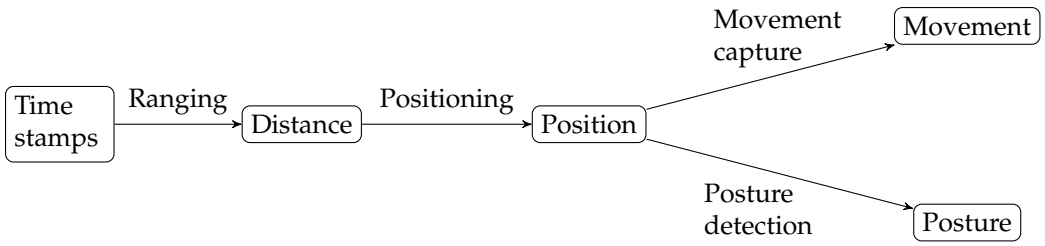

FIGURE 2.18: Posture/movement identification workflow

Ranging At the first step, the distance is estimated by computing the observed ToA. The basic protocol is 2-Way Ranging protocol (2WR), where a single round-trip is performed (in red on Fig.2.19). But, for better accuracy, and less sensitivity to clock drift, we have considered the 3-Way Ranging protocol (3WR), where an additional transmission is added, as shown on Fig.2.19.

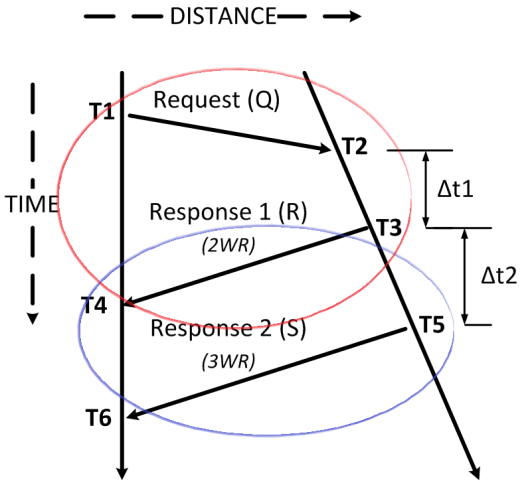

FIGURE 2.19: 2-WR et 3-WR protocols for UWB based localization

More precisely, node i first transmits a request packet to node j. Node j answers with 1 (resp 2) packets separated by a predefined delay response for the 2WR (resp 3WR) protocol. These response packets contain the request packet ToA at node j, and the time of departure of the 2 response packets. By using its complementary knowledge of the time of arrival/departure, node i computes the estimated distance as follows:

$$\hat{d}_{ij}(t) = \frac{1}{2}c\left[((T_4 - T_1) - (T_3 - T_2))\right] \tag{2.4}$$

for the 2WR, with c is light celerity (i.e. $c = 3 * 10^8 m/s$).

$$\hat{d}_{ij}(t) = \frac{1}{2}c\left[((T_4 - T_1) - \Delta t1) - ((T_6 - T_4) - \Delta t2)\right] \tag{2.5}$$

for the 3WR protocol.

Positioning To evaluate the position of a node, we need specific nodes called anchors, to define the coordinate system. This latter can be local (for instance if anchors are located on the body) or global (if fixed external nodes are used). The node first evaluate its relative distances toward the anchors (4 for a 3D positioning), than position algorithms are applied such as the classical ones (Linear Least Square Error (LLSE), Time Difference of Arrival (TDOA) [Xia+10]) or statistical cooperative techniques (Maximum Likelihood (ML), Cooperative Constrained (CDWMDS) [HDR14]). In this work, we used the simplest one TDOA to easily test our transmission protocols.

Posture and movement identification Finally, once the position data of specific body parts are obtained, we can aggregate them to either have the whole picture of the person and detect its posture by comparison with a database set; or to analyze their evolution along time to identify the movement. This is more a data processing issue, and will not be addressed in this work.

In theory, all this workflow leads to accurate localization. However, WBANs context induce specific issues, especially due to the inherent body mobility, which impact both the estimated distances and the success probability of the transmitted packets. The work presented hereafter has tackled the problem of such mobility during the localization algorithm. All simulations were done with WSNet.

Ranging protocol study in mobility case

The mobility is clearly the most specific feature of WBANs compared to other networks. As the person is moving, its nodes are as well. Thus, as shown on Fig.2.20, the distance between 2 nodes (so in particular between a node and an anchor) is changing. However, the distance

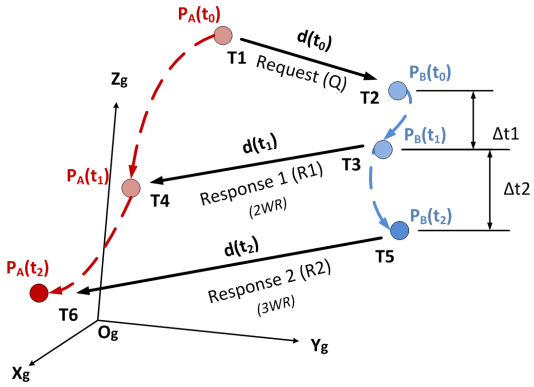

FIGURE 2.20: Protocole Three Way Ranging

computation 2.5 was defined for a constant distance during the measurement. This brings three questions:

1. Is the mobility impact significant ?
2. Which distance can be considered as estimated ? We have proposed 3 distances: d_{ref1} observed at the beginning of the measure, d_{ref2} observed at the end of the measure, and d_{avg} the average between the 2 previous ones. We will refer to these distances as *reference distances*.
3. What are the main impacting parameters ?

To answer these questions, we have considered a toy case, where one node is moving back and forth linearly (30 cm amplitude) with respect to an anchor. Distance is estimated via 3WR protocol, and we compute the RMSE (Root Mean Squared Error) metric for error estimation:

$$RMSE = \sqrt{\frac{\sum^{N} |d_{ref} - d_{est}|^2}{N}} \tag{2.6}$$

Error evolution is plotted on Fig.2.21, as a function of three system parameters: the node's speed, and the delays $\Delta t1$ and $\Delta t2$. We can thus answer to the previous questions:

1. Impact is important as the error ranges from 0 to 17cm. The mobility is thus an important parameter to take into account in the localization protocol.
2. We can observe that d_{ref1} is always better estimated than the others. This is due to the fact that the two first transmissions evaluate the distance, while the third one permits to correct the clock drift. Thus, the estimated distance is logically related to the actual distance at the beginning of the ranging protocol.
3. Node's speed has clearly an impact on the error, but is an inherent external feature of the ranging process. On the contrary, $\Delta t1$ is more impacting than $\Delta t2$, for the same reason than in question 2.

As a consequence, mobility must not be neglected in the ranging protocol, and one should favor a short $\Delta t1$ to ensure better distance accuracy.

Positioning protocol study in mobility case

In the previous section, the node was performing its ranging with only one anchor to estimate one distance. If the node needs to obtain its position, the ranging must be done with 4 anchors. By following the same logic than previously, we can identify that, as the node is moving, when performing the ranging to each anchor successively, the obtained distances will not correspond to the same position. This leads to additional error on the position estimation.

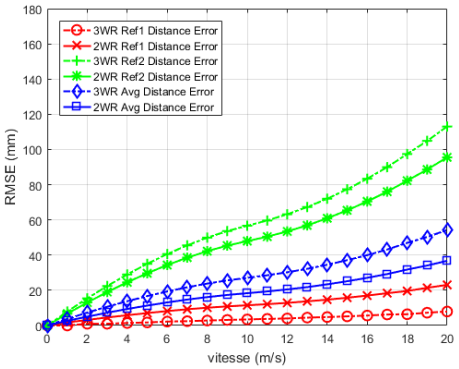

(a) Estimated distance RMSE for 2WR/3WR as a function of the node's speed

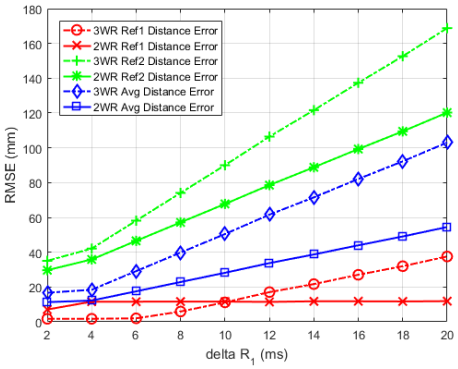

(b) Estimated distance RMSE for 2WR/3WR as a function of the 1^{st} response packet delay $\Delta t1$

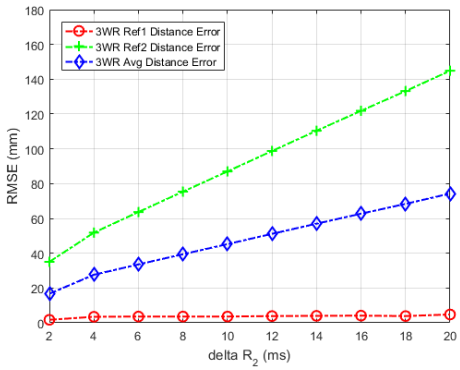

(c) Estimated distance RMSE for 2WR/3WR as a function of the 2^{nd} response packet delay $\Delta t2$

FIGURE 2.21: Mobility impact on the distance estimation

Ideally, one needs simultaneous distance estimations, with the best distance accuracy. However, as only one transmission is possible at a given time, a tradeoff has to be made between the following extreme cases:

- distances are evaluated successively: in this case, we get the better distance accuracy, but he worst consistency between the distances.
- request packets are sent to all anchors, then all anchors send their response 1, then they send their response 2. In this case, distances are less accurate as the 3WR protocol with a given anchor is diluted over time, but distances are consistent as the estimation has been done over almost the same temporal window.

We have tested these protocols along with intermediate ones for the linear scenario (the anchors are fixed, the node is moving linearly as presented previously), and for the Yoga scenario (mobility traces were obtained during the measurement campaign). We have applied a variable speed coefficient so as to be able to accelerate the movement, and test the robustness to higher speeds. The error was evaluated with RMSE as previously, by considering the position instead of the distance. We have confirmed [Gui+14] that a compromise should be done, and that the best strategy, (called B-S1 in our work), is the one presented in Fig.2.22. In this strategy, the requests packets are broadcast to all anchors simultaneously. Then each anchor completes its 3WR ranging protocol at its turn.

This preliminary work has served as a starting point for the more realistic case where posture detection needs several moving nodes to be simultaneously detected. Once again, there is a tradeoff between the accuracy of each individual position and the consistency of these positions to identify a posture. We have defined the posture detection accuracy metric as the sum of errors made on the nodes' position. We thus have targeted two goals: best

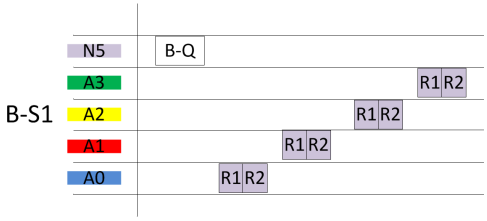

FIGURE 2.22: Scheduling strategy S1 with broadcast request

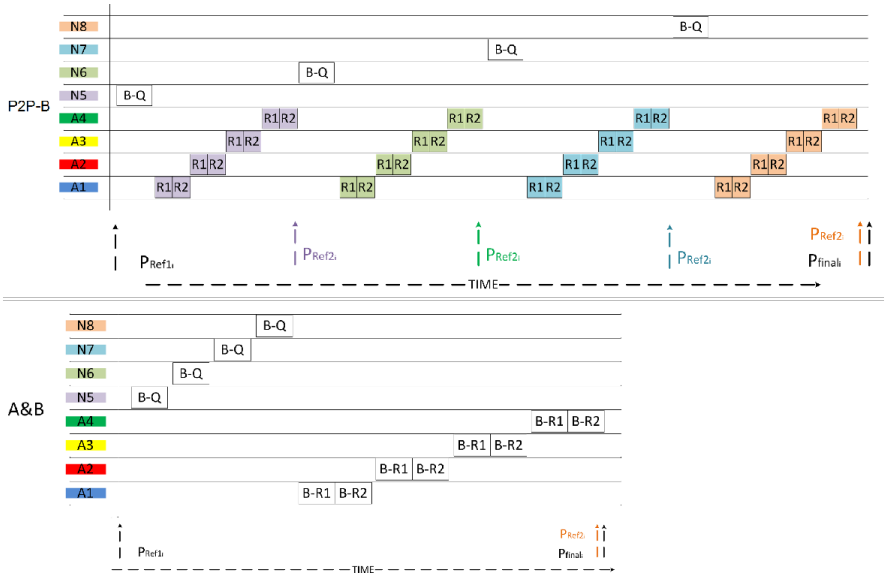

FIGURE 2.23: Scheduling algorithms P2P-B et A&B

individual accuracy, and smallest protocol duration to have all the positions. To do so, we have designed several protocols based on B-S1, and compared their performances to three positions cases: the posture at the beginning (and the end) of the scheduling strategy, and an *artificial posture* obtained by the individual positions of each node when its individual positioning protocol was finished. From this analysis, we have identified two relevant strategies presented on Fig.2.23:

- P2P-B: strategy B-S1 is applied to each node, one at a time. This one improves accuracy of estimated node positions, and provides the best estimation of the artificial posture.
- A&B: nodes broadcast the request packets at their turn, then each anchors broadcast its aggregated first and second response. One may note that the aggregated response lasts longer as it contains the time stamps intended for all the nodes. This strategy is more adapted for movement capture as it better estimates the global posture (specifically the final one).

Once the best global scheduling strategy were identified, we further the study by considering the slot allocation within this scheduling. Indeed, nodes do not evolve with the same speed, and are thus more or less impacted by the delays encountered in the scheduling strategy. As a consequence, we have classified the nodes into three categories depending on their mobility level: *low*, *medium*, *high*. We have defined four allocations strategies as presented in Fig.2.24

We have observed that, for P2P-B scheduling, NS1 (resp NS3) is the best one to get the initial (resp final) posture. Indeed, in NS1 (resp NS3), the ranging slots of the most mobile nodes are placed at the beginning of the protocol frame (resp at the end). Thus, their estimated position is closest to the initial (resp final) one, and they induce less impact on the overall performances. On the contrary, the artificial posture is not impacted by such slot allocation as the nodes' order does not impact the accuracy of each node position estimation.

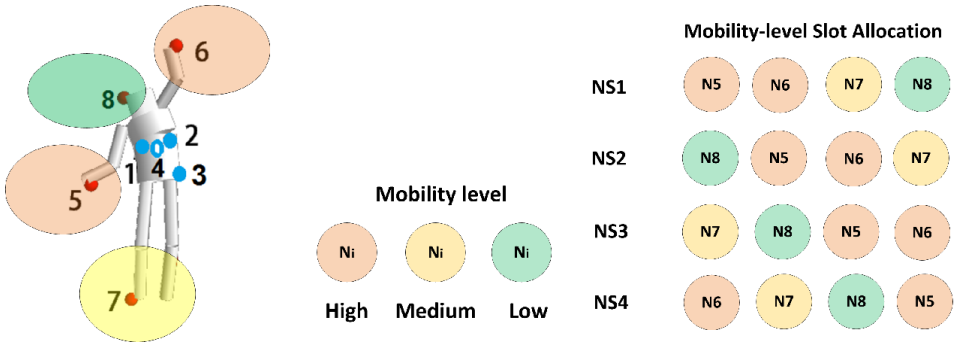

FIGURE 2.24: Slots allocation slots (NS_k) as a function of the mobility level with 4 mobile nodes.

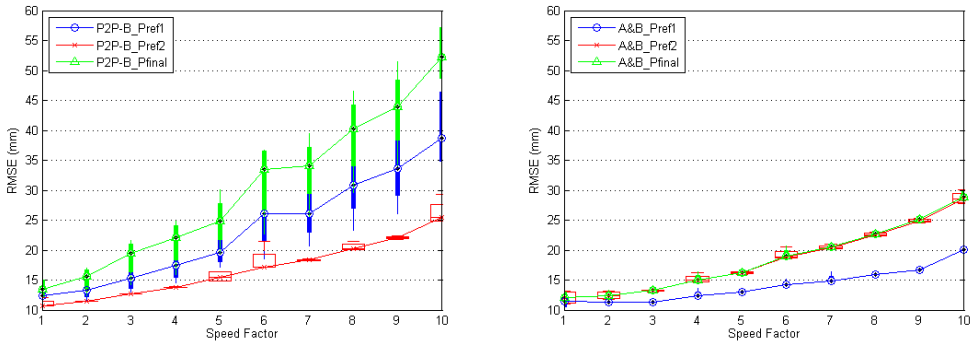

(a) RMSE for P2P-B

(b) RMSE for ANB

FIGURE 2.25: RMSE statistics over the various allocation scenarios, in the Yoga case

As a consequence, if targeting a specific posture, one should carefully design the slot allocation depending on the node's speed. On the other hand, if only individual positions are targeted, any slot allocation may work. Similarly, estimating individual positions is a good metric when no information on the individual nodes mobility is assumed.

In addition, A&B is not sensitive to the allocation, as shown in Fig.2.25. We have reported the error statistics across the different allocation scenarios. Contrarily to P2P-B, where we observe a high variation by respect to the median, A&B presents almost null deviation, and much lower error. Thus, the good distance coherency in A&B is more beneficial than the individual distance accuracy permitted in P2P-B.

Localization study with a realistic channel

In the previous studies, in order to tackle the mobility impact on the localization protocols, the transmission channel was considered as perfect: no attenuation, no shadowing, and no fading. The obtained results were thus valid for realistic mobility patterns, but for (unrealistic) reliable transmission conditions. However, in practice, any packet of the localization protocol can be lost, leading to the impossibility of estimating the distance/position/posture. To evaluate this impact, we have considered three channel models:

- empirical path loss channel model based on the on-body CM3 channel (Anechoic chamber) [YSP09]. This channel model provides information of the distance impact.
- simulated channel calculated with the PyLayers ray-tracing simulator [Mhe+14]. This channel model provides information on the distance and the body obstruction impact.

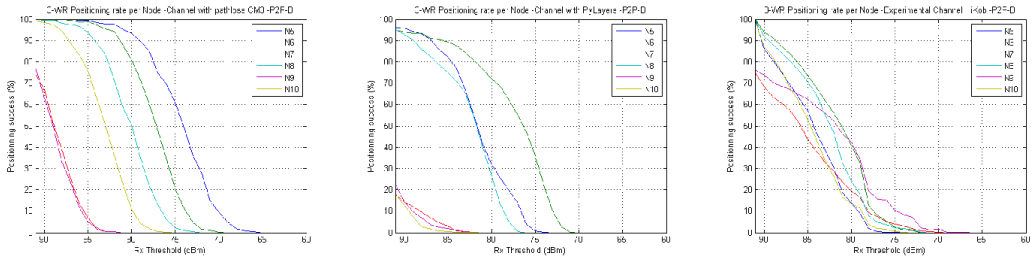

(a) P_{succ} for the empirical channel (b) P_{succ} for the simulated channel (c) P_{succ} for the experimental channel

FIGURE 2.26: Success positioning probability (P_{succ}) with 3WR and P2P-B.

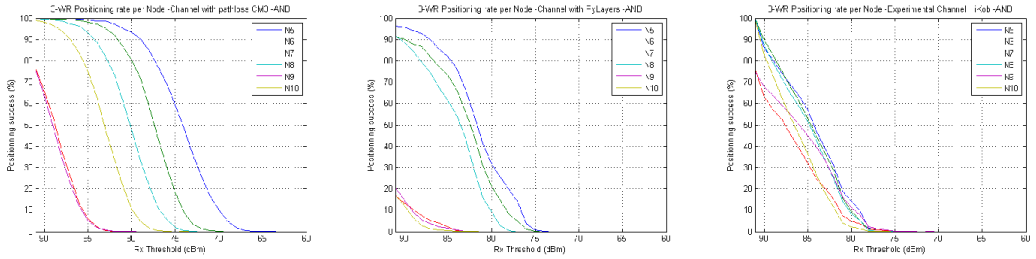

(a) P_{succ} for the empirical channel (b) P_{succ} for the simulated channel (c) P_{succ} for the experimental channel

FIGURE 2.27: Success positioning probability (P_{succ}) with 3WR and A&B.

- experimental traces obtained by measurement during the campaign 2.2. This channel adds unpredictable channel characteristics such as fading due to multi-path, and specific wave propagation nearby the body.

We have considered a -10 dBm emission power, and null antenna gains. We model the channel as an erasing one: a packet is lost if the received power is lower than the sensitivity threshold (ρ). If a packet is lost during the protocol, we declare the positioning status as failed. We thus define P_{succ} as the positioning success probability, which is the ratio of successfully estimated positions over the total number of attempts.

In our preliminary study on a walking scenario, we have verified that the node's positioning success probability decreases with the presence of shadowing. We also found that 2WR is less sensitive than 3WR as less packets are required in the protocol. However, during the 3WR protocol, if only one response packet is lost, ranging can still be obtained by considering a 2WR protocol with the remaining packets. Thus, as 2WR is less precise than 3WR, we have suggested to always use 3WR protocol, and compute the distance with 3WR or 2WR depending on the actual received packets.

In addition, to compare the choice of the scheduling algorithm (P2P-B or A&B), and analyze the channel impact, we have plotted on Fig.2.26 and Fig.2.27 the positioning success probability as a function of the received power threshold ρ, for exactly the same walking scenario. We can observe that shadowing degrades the performances as case (b) is worse than case (a). However, we can see in (c) that, in the practical case, this shadowing effect can be leveraged by creeping waves or multi-path, especially for the weak nodes (N7, N9, N10). Furthermore, we can also observe that A&B is more sensitive to channel loss. Indeed, due to its broadcast and aggregated features, the loss of a packet impacts several positions. Thus, there is also a tradeoff between positioning success and position accuracy. We can imagine a protocol that switches from P2P-B to A&B depending on the success probability.

However, we have observed that, for most positioning failures, it was due to a bad connectivity with one anchor, while channel with other mobiles nodes seems more reliable. As a consequence, we propose a distributed-cooperative algorithm to increase the localization

performance of WBAN nodes. We have investigated a cooperative protocol in which a defective anchor can be replaced by a mobile node. To do so, we have considered three LQE (Link Quality Estimator):

- P_{succ} the positioning success probability, which permits to identify the nodes that have difficulties to obtain their positions
- R_{succ} the ranging success probability, which permits to identify the anchors that should be replaced by mobile nodes
- L_{ik} the link quality distribution, which permits to quantify the link quality between the node and another mobile node.

Based on these metrics, we have proposed an algorithm for the positioning cooperation. We have divided it into two steps:

- failure identification based on the long-term LQE P_{succ} and R_{succ}. For each node i, if P_{succi} is lower than a quality level α, node i is put in the set nodes that have to change at least one of their anchors. Then, the node with the worst P_{succ} is the first one to enter the new anchor selection. The anchor that has the worst R_{succ} is detected to be changed.
- replacement node election based on the short-term LQE L_{ik}. From the observed link quality between node i and the potential new anchor, we compute the expected $P_{succexp}$ if this modification was done. Then, we use one of these 2 decision methods:
  1. the mobile node(s) that lead(s) to a better $P_{succexp}$ is (are) elected as anchor(s) for node i.
  2. additionally to method 1, a node can not choose as an anchor a node that has a worst P_{succ} than him (so as to avoid circular anchoring between the mobile nodes), and the $P_{succexp}$ is weighted by the long term LQE R_{succ} so as to avoid to make a change that would be pertinent for a limited time. One may note that the P_{succ} additional constraints also guarantee the feasibility of the protocol. Indeed, it is needed that the nodes elected as anchors achieve their positioning before the ones that use them. However, if circular anchoring is authorized, it is not possible within a frame.

The observed positioning probability of each mobile node is plotted on Fig.2.28, for the three channels models, and the two scheduling algorithms P2P-B and A&B. First, one may note that, for some cases, cooperation permits to have positioning (for instance for nodes $N7$ and $N9$) while its was not possible previously. Thus, for these nodes, the cooperation is necessary.

Furthermore, method 2 leads to reduced performance for some nodes, but clearly permits to bring more fairness between the nodes. Indeed, nodes that mostly need the cooperation are served first, and thus benefit from the cooperation by choosing the anchors that are best adapted to them. On the other hand, the other nodes have less potential nodes at their disposal when comes their turn. Thus the benefit may decrease.

Finally, we can observe that the cooperative algorithms bring better improvement in the experimental channel case, than in the other cases. As a consequence, such algorithms are well fitted for dynamic and highly variable channel which is a positive thing. Furthermore, no hypothesis was made on the channel characteristics. Such protocol can thus adapt opportunistically to any body shape, and propagation conditions.

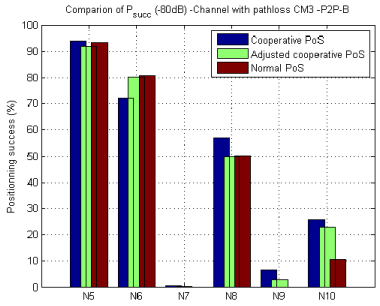

(a) P_{succ} with empirical channel and P2P-B

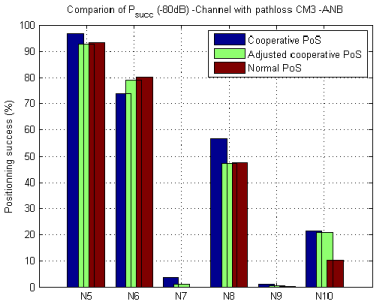

(b) P_{succ} with empirical channel and A&B

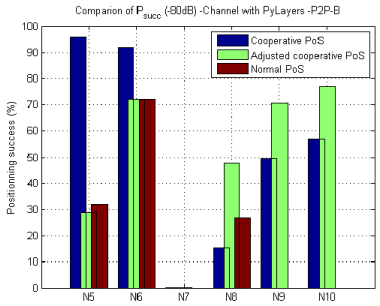

(c) P_{succ} with simulated channel and P2P-B

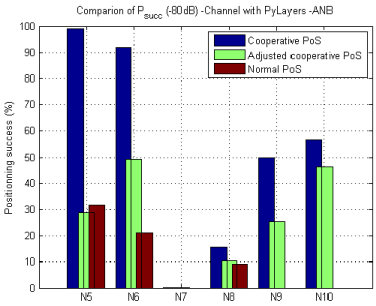

(d) P_{succ} with simulated channel and A&B

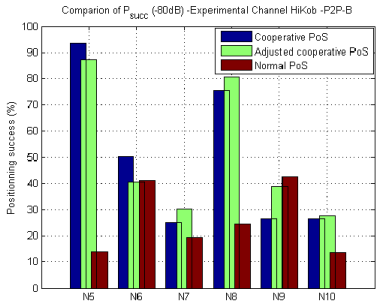

(e) P_{succ} with experimental channel and P2P-B

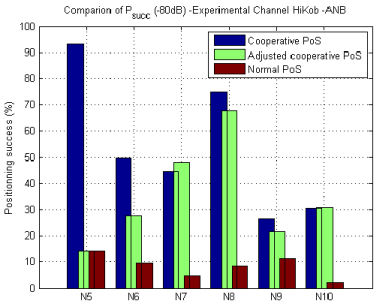

(f) P_{succ} with experimental channel and A&B

FIGURE 2.28: Success positioning rate for P2P-B and A&B, non-cooperative protocol (red), cooperative method 1 (blue) and cooperative method 2 (green).

2.6 Conclusion

In this work, we have mainly evaluated the compromise that has to be done for the localization (accuracy of each individual feature vs accuracy of the set; positioning accuracy vs positioning success), and proposed strategies to reach better performances, at each level of the process.

Such study should be completed by considering the accumulated error in the cooperation process. Indeed, the virtual anchors, even though they benefit from good localization conditions are also prone to error. Thus, they do not provide a perfectly reliable position as reference to their associated nodes. This error might cumulate with the one studied in the previous work.

Besides, we should also extend the study to the inter-BAN case, for group navigation context (for instance). In this case, the inter-BAN links correlation due to potential obstruction between the bodies should be exploited to design a smart strategy. We can even exploit the horse-racing based strategy to permit to perform localization in several nearby BAN. Thus, the protocol would have two optimization goals: ensuring limited interference across BANs, while ensuring accurate localization. It is very likely that the optimal scheduling is not the same in both cases, and that an additional compromise has to be reached.

Finally, in the work presented in this chapter, we have considered WBANs with two main application cases: data transmission and localization. In both cases, we have used a methodology that I believe is appropriate: combination of experiments to ground truth the research directions along with theoretical derivations to be as generic as possible. Unfortunately, it was not possible to compare the results obtained for the two application cases, as the metrics are different. Nonetheless, these studies focused on complementary applications for BANs, and thus provide an insight of BANs performances in real case.

These realistic results were possible thanks to the experimental campaigns that we did. Part of the collected data has been exploited in this work, but there are much more data sets that are still unexploited.

Bibliography

[Atm] *AT86RF231*. http://www.atmel.com/devices/at86rf231.aspx. 2012.

[BAu12] Deena M Barakah and Muhammad Ammad-uddin. "A survey of challenges and applications of wireless body area network (WBAN) and role of a virtual doctor server in existing architecture". In: *Intelligent Systems, Modelling and Simulation (ISMS), 2012 Third International Conference on*. IEEE. 2012, pp. 214–219.

[BN10] Jorg Blankenbach and Abdelmoumen Norrdine. "Position estimation using artificial generated magnetic fields". In: *2010 International Conference on Indoor Positioning and Indoor Navigation* (2010). DOI: 10.1109/ipin.2010.5646739. URL: http://dx.doi.org/10.1109/IPIN.2010.5646739.

[Cav+14] Riccardo Cavallari et al. "A survey on wireless body area networks: Technologies and design challenges". In: *IEEE Communications Surveys & Tutorials* 16.3 (2014), pp. 1635–1657.

[CCS09] S. L. Cotton, G. A. Conway, and W. G. Scanlon. "A Time-Domain Approach to the Analysis and Modeling of On-Body Propagation Characteristics Using Synchronized Measurements at 2.45 GHz". In: *IEEE Transactions on Antennas and Propagation* 57.4 (2009), pp. 943–955. ISSN: 0018-926X. DOI: 10.1109/TAP.2009.2014521.

[CDO14] Simon Cotton, Raffaele D'Errico, and Claude Oestges. "A review of radio channel models for bodycentric communications". Anglais. In: *Radio Science* 49.6 (2014), pp. 371–388. ISSN: 1944-799X. DOI: 10.1002/2013RS005319. URL: http://hdl.handle.net/2078.1/146953.

[Che+11] Min Chen et al. "Body area networks: A survey". In: *Mobile networks and applications* 16.2 (2011), pp. 171–193.

[CKC08] Jae Myeong Choi, Heau-Jo Kang, and Yong-Seok Choi. "A study on the wireless body area network applications and channel models". In: *Future Generation Communication and Networking, 2008. FGCN'08. Second International Conference on*. Vol. 2. IEEE. 2008, pp. 263–266.

[Cor+01] Thomas H Cormen et al. "Greedy algorithms". In: *Introduction to algorithms* 1 (2001), pp. 329–355.

[Fer13] Paul Ferrand. "Communications coopératives dans les réseaux autour du corps humain". PhD thesis. Lyon, INSA, 2013.

[Gui+14] Arturo Guizar et al. "Impact of MAC scheduling on positioning accuracy for motion capture with ultra wideband body area networks". In: *Proceedings of the 9th International Conference on Body Area Networks*. ICST (Institute for Computer Sciences, Social-Informatics and Telecommunications Engineering). 2014, pp. 365–371.

[Gui16] Arturo Guizar. "Communications coopératives dans les réseaux autour du corps humain pour la capture du mouvement". PhD thesis. INSA Lyon, 2016.

[Ham+13] Jihad Hamie et al. "On-body TOA-based ranging error model for motion capture applications within wearable UWB networks". In: *Journal of Ambient Intelligence and Humanized Computing* (Dec. 2013). ISSN: 1868-5137. DOI: 10.1007/s12652-013-0215-6. URL: http://link.springer.com/10.1007/s12652-013-0215-6.

[HDR14] Jihad Hamie, Benoit Denis, and Cedric Richard. "Decentralized Positioning Algorithm for Relative Nodes Localization in Wireless Body Area Networks". In: *Mobile Networks and Applications* 19.6 (Nov. 2014), pp. 698–706. ISSN: 1383-469X. DOI: 10.1007/s11036-014-0543-6. URL: http://link.springer.com/10.1007/s11036-014-0543-6.

[HF] sensor HiKoB FOX. *"http://www.hikob.com/hikob-fox"*. URL: http://www.hikob.com/hikob-fox.

[Hik] *HiKoB FOX sensor*. http://www.hikob.com/hikob-fox. 2012.

[HRH02] P. S. Hall, M. Ricci, and T. M. Hee. "Measurements of on-body propagation characteristics". In: *Antennas and Propagation Society International Symposium, 2002. IEEE*. Vol. 2. 2002, 310–313 vol.2. DOI: 10.1109/APS.2002.1016087.

[IEE] IEEEStd802.15.4a. In: ().

[Kuh55] Harold W Kuhn. "The Hungarian method for the assignment problem". In: *Naval Research Logistics (NRL)* 2.1-2 (1955), pp. 83–97.

[KW08] Midori Kitagawa and Brian Windsor. *MoCap for Artists: Workflow and Techniques for Motion Capture*. Focal Press, 2008. ISBN: 0240810007, 9780240810003.

[Lac+09] D. Lachartre et al. "A 1.1nJ/b 802.15.4a-compliant fully integrated UWB transceiver in 0.13 x00B5;m CMOS". In: *2009 IEEE International Solid-State Circuits Conference - Digest of Technical Papers*. 2009, 312–313,313a. DOI: 10.1109/ISSCC.2009.4977433.

[MD16] Francesco Mani and Raffaele D'Errico. "A spatially aware channel model for body-to-body communications". In: *IEEE Transactions on Antennas and Propagation* 64.8 (2016), pp. 3611–3618.

[MDD14] Mickael Maman, Benoît Denis, and Raffaele D'Errico. "Research trends in wireless body area networks: From On-Body to Body-to-Body cooperation". In: *Medical Information and Communication Technology (ISMICT), 2014 8th International Symposium on*. IEEE. 2014, pp. 1–5.

[Mhe+14] Meriem Mhedhbi et al. "Human Body Perturbed Antenna Integration In Indoor Propagation Simulator". In: *Journées scientifiques 2014 de l'URSI France*. Paris, France, Mar. 2014. URL: https://hal.archives-ouvertes.fr/hal-01122245.

[MHK06] Thomas B. Moeslund, Adrian Hilton, and Volker Krüger. "A survey of advances in vision-based human motion capture and analysis". In: *Computer Vision and Image Understanding* 104.2-3 (2006), pp. 90–126. ISSN: 1077-3142. DOI: 10.1016/j.cviu.2006.08.002. URL: http://dx.doi.org/10.1016/j.cviu.2006.08.002.

[Min+08] D. Miniutti et al. *Narrowband Channel Characterization for Body Area Networks*. IEEE P802.15-08-0421-00-0006 "https://mentor.ieee.org/802.15/dcn/08/15-08-0421- 00-0006-narrowband-channel-characterization-for-ban.pdf". 2008.

[Mor73] J.R.W. Morris. "Accelerometry—A technique for the measurement of human body movements". In: *Journal of Biomechanics* 6.6 (1973), pp. 729 –736. ISSN: 0021-9290. DOI: http://dx.doi.org/10.1016/0021-9290(73)90029-8. URL: http://www.sciencedirect.com/science/article/pii/0021929073900298.

[Pat+09] RK Patro et al. "Samsung MAC proposal for IEEE 802.15 TG6 body area networks". In: *IEEE P802* (2009), pp. 15–09.

[Pop07] Ronald Poppe. "Vision-based human motion analysis: An overview". In: *Computer Vision and Image Understanding* 108.1–2 (2007). Special Issue on Vision for Human-Computer Interaction, pp. 4 –18. ISSN: 1077-3142. DOI: http://dx.doi.org/10.1016/j.cviu.2006.10.016. URL: http://www.sciencedirect.com/science/article/pii/S1077314206002293.

[PW10] Maulin Patel and Jianfeng Wang. "Applications, challenges, and prospective in emerging body area networking technologies". In: *IEEE Wireless communications* 17.1 (2010).

[RD12] R. Rosini and R. D'Errico. "Off-Body channel modelling at 2.45 GHz for two different antennas". In: *2012 6th European Conference on Antennas and Propagation (EUCAP)*. 2012, pp. 3378–3382. DOI: 10.1109/EuCAP.2012.6206591.

[Rob11] C. Roblin. "Analysis of the channel power delay profile of WBAN scenarios in various indoor environments". In: *Ultra-Wideband (ICUWB), 2011 IEEE International Conference on*. 2011, pp. 545–549. DOI: 10.1109/ICUWB.2011.6058905.

[Sak+96] T. Sakaguchi et al. "Human motion capture by integrating gyroscopes and accelerometers". In: *Multisensor Fusion and Integration for Intelligent Systems, 1996. IEEE/SICE/RSJ International Conference on*. 1996, pp. 470–475. DOI: 10.1109/MFI.1996.572219.

[SC08] W. G. Scanlon and S. L. Cotton. "Understanding on-body fading channels at 2.45 GHz using measurements based on user state and environment". In: *Antennas and Propagation Conference, 2008. LAPC 2008. Loughborough*. 2008, pp. 10–13. DOI: 10.1109/LAPC.2008.4516852.

[Sha48] Claude E Shannon. "A mathematical theory of communication, Part I, Part II". In: *Bell Syst. Tech. J.* 27 (1948), pp. 623–656.

[TAK09] K. Takizawa, T. Aoyagi, and R. Kohno. "Channel Modeling and Performance Evaluation on UWB-Based Wireless Body Area Networks". In: *2009 IEEE International Conference on Communications*. 2009, pp. 1–5. DOI: 10.1109/ICC.2009.5198820.

[TP05] Chin-Woo Tan and Sungsu Park. "Design of accelerometer-based inertial navigation systems". In: *Instrumentation and Measurement, IEEE Transactions on* 54.6 (2005), pp. 2520–2530. ISSN: 0018-9456. DOI: 10.1109/TIM.2005.858129.

[Vicst] Vicon. *http://www.vicon.com/*. last accessed September 2015. URL: http://www.vicon.com/.

[Wan+13] Lusheng Wang et al. "Cooperative scheduling for coexisting body area networks". In: *IEEE Transactions on Wireless Communications* 12.1 (2013), pp. 123–133.

[WG03] Zhengdao Wang and Georgios B Giannakis. "A simple and general parameterization quantifying performance in fading channels". In: *IEEE Transactions on Communications* 51.8 (2003), pp. 1389–1398.

[Xia+10] Zhu Xiao et al. "A survey on impulse-radio UWB localization". In: *Sci. China Inf. Sci.* 53.7 (2010), pp. 1322–1335. ISSN: 1869-1919. DOI: 10.1007/s11432-010-3102-1. URL: http://dx.doi.org/10.1007/s11432-010-3102-1.

[YSP09] K. Y. Yazdandoost and K. Sayrafian-Pour. *Channel Model for Body Area Network (BAN)*. IEEE P802.15-08-0780-09-0006; https://mentor.ieee.org/802.15/. 2009.

[Zas+03] T. Zasowski et al. "UWB for noninvasive wireless body area networks: channel measurements and results". In: *Ultra Wideband Systems and Technologies, 2003 IEEE Conference on*. 2003, pp. 285–289. DOI: 10.1109/UWBST.2003.1267849.

[Zhe+08] Bin Zhen et al. "TG6 technical requirements document (TRD)". In: *IEEE P802* (2008), pp. 15–08.

Chapter 3

Contributions in the LPWAN context

3.1 What is LPWAN ?

LPWAN (Low Power Wide Area Network) is a very recent term (appeared in 2013), referring to a very wide area network (up to several tens of kms range in rural areas). The objective of such network is to provide a connectivity to the Internet to a huge number of nodes deployed anywhere, in the IoT context. LPWAN gateways are thus needed to settle communication with the devices in their vicinity. To limit the operational cost of the operators, a limited access infrastructure is suitable. As a consequence, a collecting point should serve nodes deployed in a very wide area. However, this can not be obtained by tuning up the emission power, because it must be achieved while keeping a low energy consumption for the nodes to preserve the network lifetime.

In addition, LPWAN are characterized by the fact that ISM bands are usually used for transmissions as they are license-free, and thus permit to further reduce the network cost. Furthermore, LPWAN is expected to handle sporadic small data packets, thus targeting new applications such as smart cities, smart metering, logistics, wildlife monitoring and tracking, home automation and safety, etc.

All these applications pave the way for new markets, and new business operators. Besides, as the infrastructure cost is low, newcomers have joined the historical telecom operators by launching their proprietary transmission technology. Among them, we can cite SemTech along with LoRa Alliance with the LoRa technology, SigFox with UNB (Ultra Narrow Band), and Ingenu with RPMA (Random Phase Multiple Access).

FIGURE 3.1: Examples of targeted applications for LPWAN

Aside from the market, LPWAN network has recently fostered many academic works [Cen+16], [RKS17], [BDK16]. Indeed, this context reveals a new scientific challenge which is moving from the data rate expansion, to the forthcoming number of devices growth, and follow the path lead by dense WSN. To sum up, the objective is to define new techniques that verify:

- low energy consumption: data have to be sent with the least emission power, and with the smallest time duration,
- low device and infrastructure costs: BSs number should be the smallest, while devices have low computation capabilities,
- capability of handling burst transmission of small size packets,
- scalability and capability to handle a very high number of nodes,
- extended coverage.

Star-topology LPWAN

The second requirement is obtained, for the most shared vision, by a star topology with very long range (devices are directly communicating with the BS (Base Station)). To achieve such range, one can:

- increase the transmission power (but this solution is not acceptable due to the induced power consumption and potential health impact of increased wave exposure)
- design ultra sensitive receivers (but they are expensive, so could be deployed at the BS, but not at the node, preventing to deploy a downlink for distant nodes)
- design new transmission technologies. This is this last possibility that has been adopted by operators and scientific community. In practice, 2 main directions (surprisingly in the orthogonal way) have been taken:
  - spectrum spreading (LoRa with CSS (Chirp Spread Spectrum), or Ingenu with RPMA): data are sent on a much larger band than their baseband occupation. This frequency diversity permits to recover a signal even if its PSD (Power Spectral Density) is lower than the noise floor, because a specific pattern is search and provides interesting decoding gains. Besides, different codes that are verifying good correlation properties, can be affected to simultaneous transmitting devices, for multiple access purpose.
  - spectrum reducing (SigFox with UNB): data are sent are a very low rate with a simple modulation scheme, so as to ensure a minimal spectrum occupation. The advantage of such technique is that the perceived noise (after signal filtering) is reduced as it linearly depends on the signal spectrum occupation.

  For both techniques, the required received power is significantly reduced. Thus, for the same emission power than classical systems, an higher range can be reached without degrading the performances capabilities.

During the last seven years, I have considered the last technology, which was the first one to be commercially initiated for IoT purpose, i.e. UNB.

Multi-hop LPWAN

In addition to the interest to star-topology for LPWAN, the multi-hop topology has very recently being studied [BM+17]. This solution is inspired from the WSN where multi-hop was considered for energy savings [AY05]. The basic principle is to exploit the presence of intermediary nodes (called relays) to reach the final destination. By doing so, same transmission techniques and same emission power can be kept, but the functional coverage of the BS is increased.

When I joined the CITI laboratory, I started my research activities by considering such cooperative WSN. I will thus start this chapter by presenting this work, that is currently related to LPWAN, although purposelessly at that time (they were called large scale networks).

The work presented in the following sections, that aims at making the transmission reliable despite unreliable and unpredictable channel, was or is mainly realized by 3 PhD students under my co-supervision: *Anya Apavatjrut*, *Minh-Tien Do* and *Yuqi Mo*.

3.2 Multi-hop LPWAN

In classical point to point transmissions, for critical applications such as health monitoring or fire detection, reliability is usually ensured by using acknowledgment (ACK) and retransmission protocol. The data packet is sent until one succeeds in reaching destination, and ACK is also successfully received. Theoretically, such principle can be extended to multi-hop transmissions. However, the multi-hop transmissions may increase the overall transmission failure, as failure in one of the hop may lead to restart the whole transmission process. Besides, such ACK protocol floods the network with ACK packets, which is a waste of time/frequency and energy resources.

In this context, we have proposed the use of *fountain codes*. Such code family permits to have a reliable transmission with a limited ACK feedback.

3.2.1 Fountain codes principle

Fountain codes are a subcategory of FEC (Forward Error Correction) codes. Their goal is to introduce redundancy into the data flow such as the initial information is likely to be recovered in case of partial failure. When the channel characteristics are known, one can deduce the needed redundancy for a targeted successful transmission probability [Sha48]. Such codes can be used when the channel statistics can be evaluated and are stable long enough. Otherwise, the FEC might not be adapted (either inefficient or oversized). Fountain codes are useful in this case, as they intrinsically adapt to the transmission conditions.

Indeed, fountain codes are rateless erasure codes. This means that this code fights against the lost of some packets by adding redundancy between transmitted packets. The other feature is that the amount of redundancy is not defined previously to the transmission, but adapted on-the-fly regards to the actual transmission conditions. To do so, when information is to be sent from a source to a destination, it is first partitioned into K fragments. These fragments having equal length are randomly encoded together with a XOR operation to create an infinite sequence of encoded packets. At the reception side, once information can be extracted from the received encoded packets, an ACK is sent to acknowledge the correct reception of the whole information and to stop the transmission.

One may note that, in order to decode the received packets, the receiver needs to know which fragments are included in each packet. This can be done by including at the beginning of the packet either the list of the included fragments, or a generation key or identifier to recover the packet content. This overhead thus increase the initial packet size, and should be taken into account in the performances evaluation.

At the source side, several fountain codes family can be used. I recall here the principal ones.

Random Linear Fountain (RLF)

This is the optimal family. Each encoded packet is generated from a linear XOR combination of fragments uniformly selected with a $1/2$ probability. At the receiver, the matrix describing the encoded fragments in each received packet is built. Then, ML algorithm (Maximum Likelihood) is applied. The RLF coding method permits to maximize the probability for the matrix to be invertible, thus to recover the initial fragments. It was shown [Mac05] that, for a channel with success probability $1 - p_e$, the number of redundant packets is $\log_2(1/p_e)$. Unfortunately, such code needs high decoding capabilities (ML computation complexity of $\mathcal{O}(K^3)$).

Luby Transform codes (LT)

Luby proposed in [Lub+01] another family to reduce the decoding process. This latter is based on BP (Believed Propagation) algorithm, which principle is to "decode" first the packets that contain only one fragment. Then, these fragments are removed from the other received packet. The process iterates until all fragments are recovered. In Fig.3.2, f_1 and f_2 are first decoded from p_1 and p_2, then, their knowledge is used in p_4 or p_5 to get f_3.

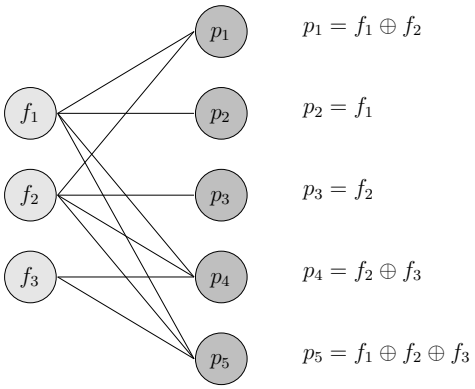

FIGURE 3.2: LT code represented as a bipartite graph

However, to permit such decoding algorithm, the packets should be encoded in a specific way. The key parameter is the degree of a packet. It is defined as the number of fragments that the packet contains. Luby proposed the RSD law (Robust Soliton Distribution), as the optimal one regards to the capacity and whose shape can be observed in Fig.3.3. These codes will be referred to as LT (Luby Transform).

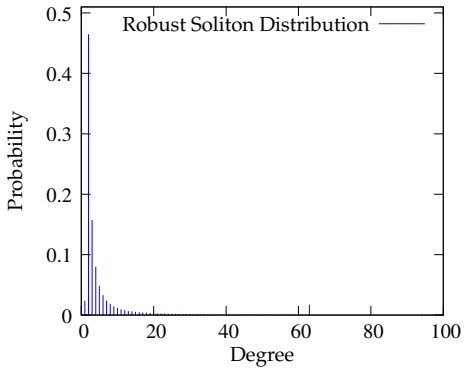

FIGURE 3.3: Robust Soliton Distribution

The encoding process is very simple as can be seen in Algo.1, as well as the decoding one previously described. However, recovery is obtained for about $K + \mathcal{O}(\sqrt{K}log^2(K))$ received packets which is slightly more than for the RLF. The algorithm complexity gain is obtained at the cost of additional transmissions.

Algorithm 1 : LT encoding

while no ACK is received **do**
  choose the degree d with RSD distribution
  randomly choose d fragments among the K, and XOR them
  send the concatenation between the overhead and the XORed fragments
end while

Improved fountain codes

The Raptor code is an improvement of LT, with a precoding step [Sho06] (usually LDPC (Low Density Parity Check) or Hamming code). When LDPC is used, the improved code is called Turbo [TB06]. The objective of these codes is to combine the efficiency of the precoder to the rateless feature of the fountain codes. However, they can be seen as fountain encoding of a specific message, thus study can be done separately. We will thus only focus on RLF and LT.

3.2.2 Fountain codes performances for a link

In this section, I present the study of the intrinsic performances of fountain codes when transmitting information from the source to the destination by using an erasure channel, defined by the PER (Packet Error Probability) $\text{PER} = 1 - (1 - \text{BER}(\delta))^{N_b}$, with BER the bit error rate, and N_b the number of bits in the packet. We also note $\gamma = 1 - \text{PER}$ as the success probability.

As with fountain codes, perfect reliability is obtained, the protocol efficiency is measured by the resources consumed by transmitted data. Thus, we consider the following performances metrics:

- energy: we modeled the energy consumption in three transmission states
  - transmitting state: $E_{tx} = \frac{N_b}{R} P_{txElec} + \alpha P_t$
  - receiving state: $E_{rx} = \frac{N_b}{R} P_{rxElec}$
  - idle state: $E_{idle} = T_{idle} P_{idleElec}$

  with P_{txElec} (resp P_{rxElec} and $P_{idleElec}$) the power consumed during emission (resp reception and idle state), T_{idle} the idle state duration, R the data rate (bit/s), α the amplificator coefficient, and P_t the emitted power.
- delay: we define it as the time interval needed to transfer the original message $\mathcal{M}$ to destination, i.e. until its K initial fragments are received and decoded. For a fair comparison with uncoded streams, we normalize this metric by K.

Small packet size

As fountain codes have been originally designed and optimized for multimedia applications where the amount of data is important, we have evaluated their performances for smaller information. Indeed, aside from the needed redundancy to compensate for the channel losses, fountain codes require an additional overhead (as transmission is done until all packets can be retrieved). Thus, we have evaluated if this overhead is or is not a limitation for small data size.

Point to point topology We have compared the RLF and LT performances (analytically, and with WSNet simulations), with a classical ARQ protocol. In this latter, each of the K fragments is repeatedly sent until an ACK is received at the source. Thus, an ACK needs to be sent for each fragment. We evaluate two cases, one with perfect ACK feedback, and the more realistic case of potential ACK loss.

We can observe on Fig.3.4 that, even in this toy-case, while the overhead has a negative impact for perfect ACK (dashed lines), the benefits is higher when realistic channel is considered (solid lines). Furthermore, we can also verify that fountain codes are more efficient when K increases.

In addition, we have also analyzed the emitted power effect on Fig.3.5. We observe the classical tradeoff between the low power case to save energy on the transmission on one packet, and high power case to prevent from multiple retransmissions. However, we can note that fountain code leads to the lowest energy consumption, thus validating their interest.

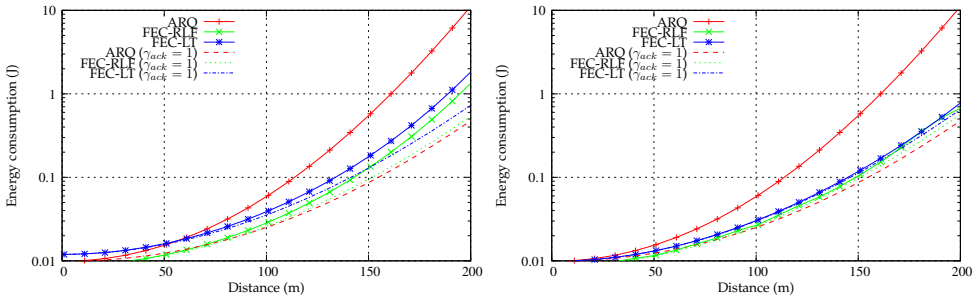

(a) K=10 (b) K=100

FIGURE 3.4: Energy consumption in point to point scenario, $K = 10$

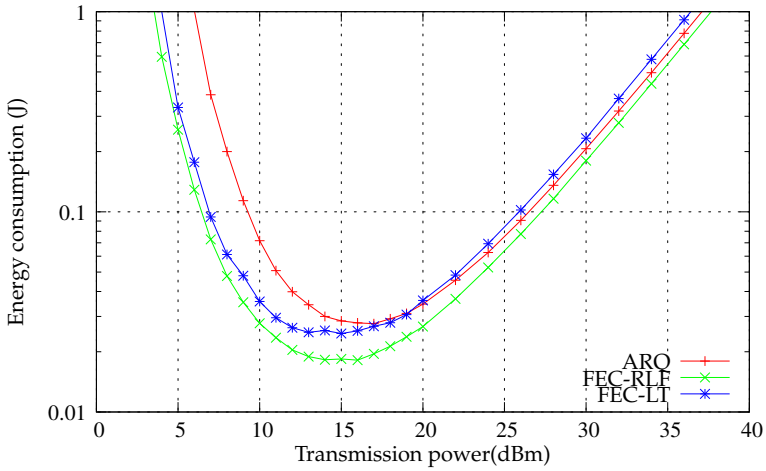

FIGURE 3.5: Energy consumption as a function of emitted power, $K = 100$

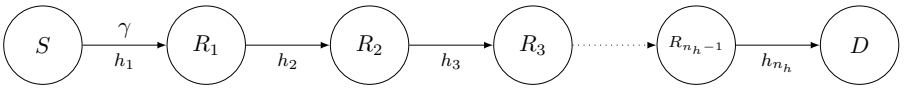

FIGURE 3.6: Multi-hop network

Multi-hop topology We now consider the case where the packets need to be relayed by intermediate nodes (uniformly spaced) before reaching destination.

We consider five relaying algorithms:

- **SB** (without coding, bloc relaying): no coding is used, and each relay waits for the entire set of fragments before forwarding them.
- **SP** (without coding, packet relaying): no coding is used, but each relay forwards a packet upon reception. Only destination acknowledges the received packets.
- **CB** (coding, bloc relaying): each nodes waits for being able to decode the entire set before acknowledging and relaying.
- **CP** (coding, packet relaying): each nodes forwards the received encoded packets upon reception. Destination acknowledges the received message.
- **CPR** (coding, packet relaying with retransmission): same scenario than before, but when a relay does not receive a packet, it uses the spare slot to retransmit a XOR of the latest ones.

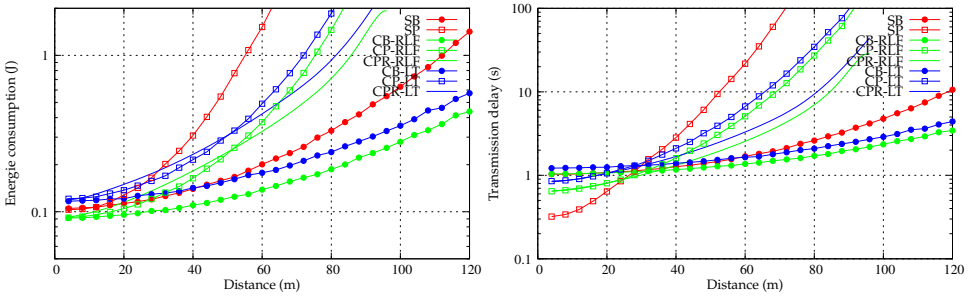

(a) Energy consumption (b) Transmission delay

FIGURE 3.7: Performance metrics of multi-hop scenario, $K = 10$

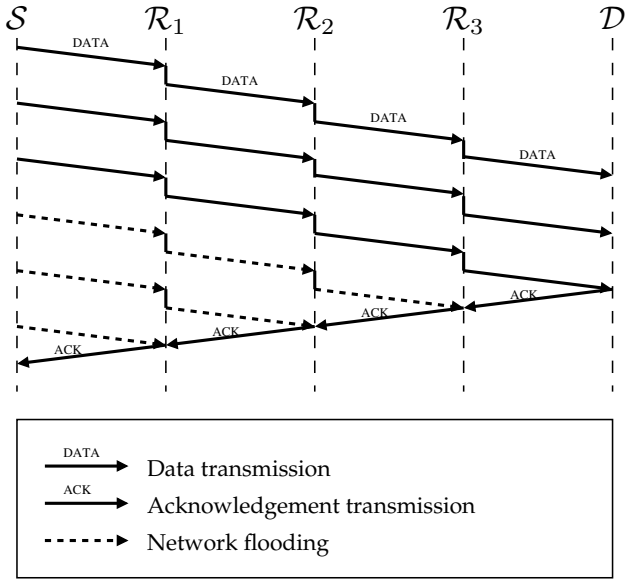

FIGURE 3.8: Overflow example (in dashed line) for a 4-hop network.

We can see on Fig.3.7, that bloc relaying (curves with the circle symbol) is the most energy efficient as each hop is optimally done. However, it is at the cost of an increased delay.

Finally, we have also tackled the specific issue of multi-hop networks with or without fountain codes, i.e., overflow. This phenomenon is observed at the end of the transmission. When the destination gets all the message, its sends an acknowledgement, but this one is not instantaneously received by the source. There is thus a laps of time during which un-needed coded packets are still sent, flooding the network Fig.3.8.

We have evaluated the overflow in scenario CB and CP, along with two new ones:

- **`CH`** `(coding, hybrid relaying)`: This is a combination between CP and CB. Each relay first uses CP, then, once it has succeeded in decoding the message, it switches to CB.
- **`CPR-XA`** `(coding, packet relaying with random XOR)`: each node relays a combination of two random packets in its buffer [PFS05].

Our simulated results in Fig.3.9 show that there are data packet overflow, but also ACK overflow when systemic ACK is required across the relays. We can note that CPR-XA offers the best performances, but also a better fairness among the relays as they support similar load and overflow. To conclude, fountain codes are suitable for small data size, and for multi-hop communications, as they reduce the energy consumption. However, depending on the other network constraints, the relaying algorithm should be adapted.

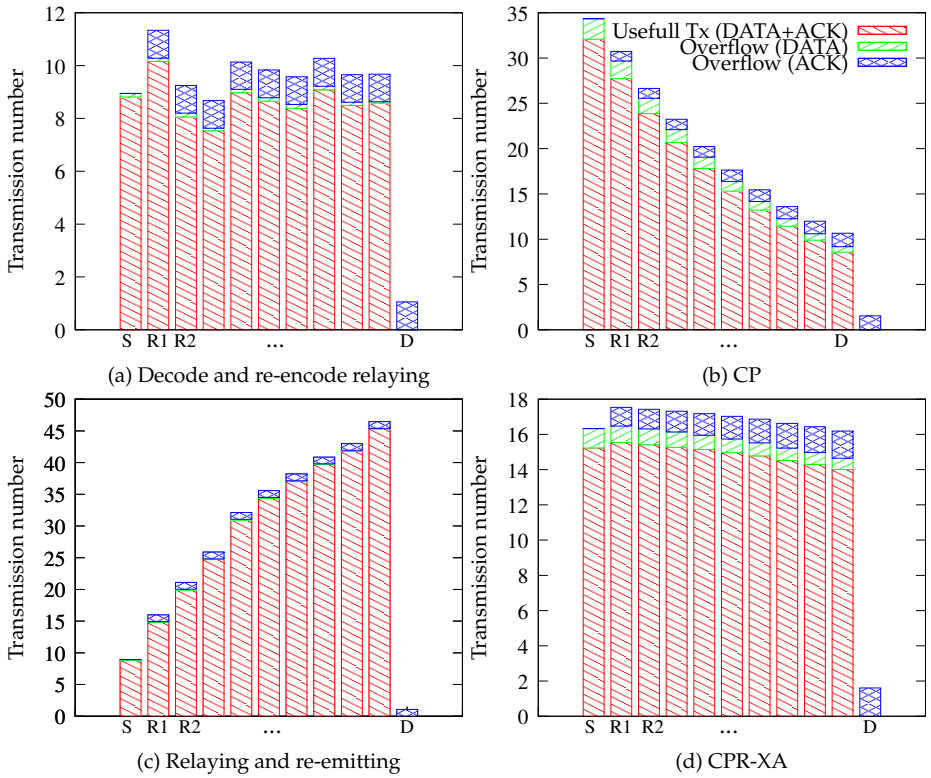

(a) Decode and re-encode relaying (b) CP

(c) Relaying and re-emitting (d) CPR-XA

FIGURE 3.9: Measured traffic for the diverse transmission scenarios, for $n_h = 10$ and $K = 5$

3.2.3 Fountain codes performances in a relay network

In the previous work, we have introduced XORing at the relay nodes (also known as Network coding [LYC03]) in the CPR-XA algorithm. This permits to improve the performances with a ML decoder. However, if BP is intended, the degree distribution modification due to the XORs might make the decoding to take more time or even to fail.

We have thus sought for a way to perform these XORs while keeping BP decoder.

Theoretical degree analysis

We first compute the resulting degree after the XOR between 2 packets. If these packets have no fragment in common, then the resulting degree will be the sum of their degrees $d_{xor} = d_1 + d_2$ with d_1 and d_2 the degrees of the original packets, and d_{xor} one the resulting packet. On the contrary,if 1 fragment is present in both packets as in Fig.3.10, the XOR operation will remove it from the XORed packet. Thus, for o common fragments, the final degree will be $d_{xor} = d_1 + d_2 - 2o$.

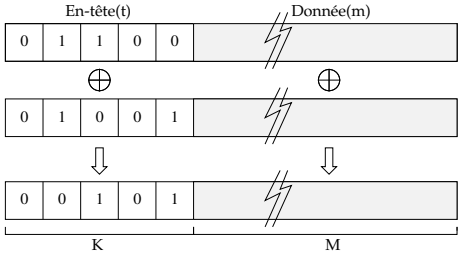

FIGURE 3.10: XOR of 2packets having a fragment in common

From this analysis, we have derived the new degree distribution for the XOR of 2 packets:

$$p_{dxor}(d_{xor}) = \sum_{d_1=1}^{K} \sum_{d_2=1}^{K} p_{d1}(d_1) p_{d2}(d_2) p_o(o = \frac{d_1 + d_2 - d_{xor}}{2} | d_1, d_2, K) \tag{3.1}$$

and extended it by iteration to the distribution for $e + 1$ XORed packets:

$$p_{dxor_e}(d_e) = \sum_{d_1=1}^{K} \sum_{d_0=1}^{K} p_{dxor_{e-1}}(d_1) p_0(d_0) p_o(o = \frac{d_1 + d_2 - d_{xor}}{2} | d_1, d_0, K) \tag{3.2}$$

with $p_{dxor_{e-1}}$ the degree distribution after e XORs, and $p_0(d_0)$ the initial degree distribution. $p_e(d_e) = p_{e-1}(d_1)$ for $e = 1$.

We have verified that RLF distribution is not affected by such XOR operations. However, LT distribution is completely modified, and tends to the RLF one as seen in Fig.3.11 for a high value of e.

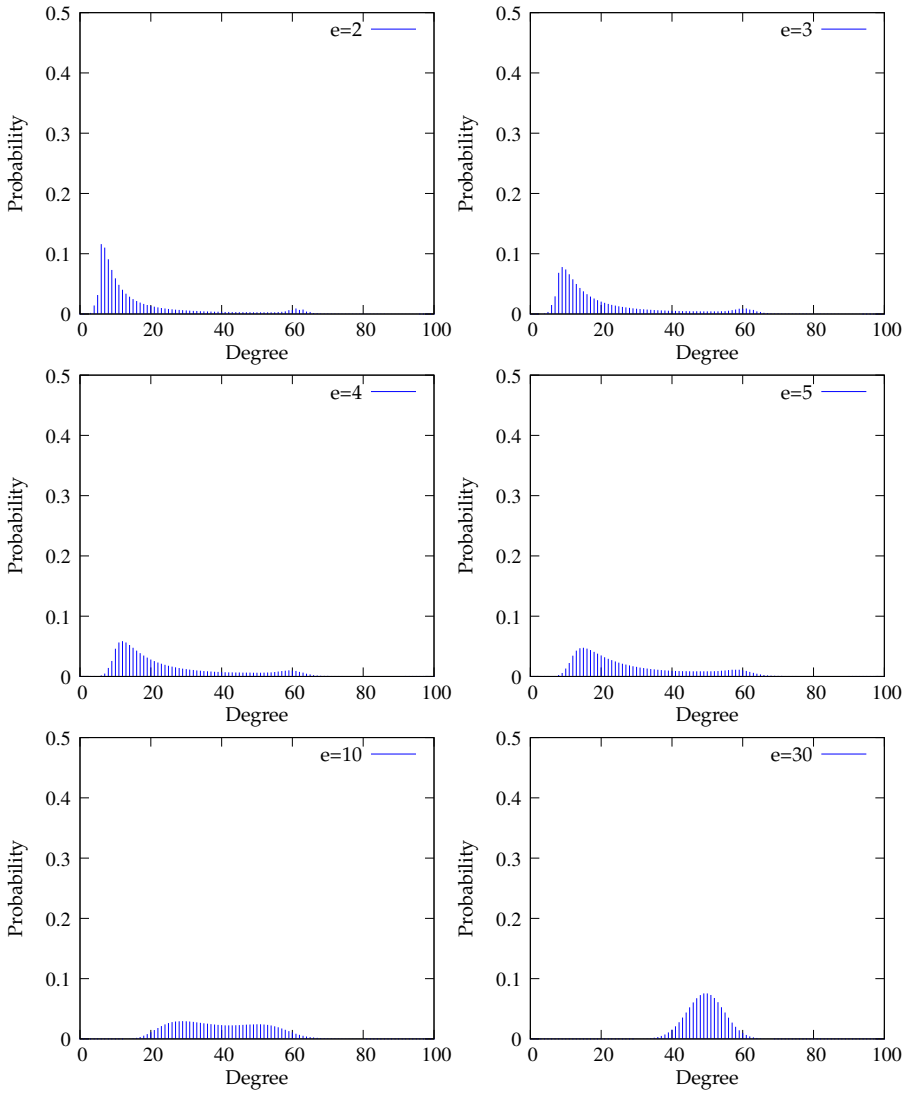

FIGURE 3.11: Degree evolution along e XORs steps for LT code

Algorithms to maintain the LT distribution

Theoretical approach Following this theoretical analysis, we have proposed this first algorithm for the relay node Algo2. The last packet is selected, then depending on its degree, the second packet is elected based on its degree as follows. From eq.3.1, we can deduce p_{choice} the distribution of degree selection so as to obtain LT distribution after the XOR. The second packet is selected according to this law.

Algorithm 2 : Theoretical approach

$p_1 \Leftarrow$last packet in memory, (has a degree d_1)
if p_1 does not exist **then**
  quit
else
  $d_2 \Leftarrow$ choose a degree according to p_{choice}
  $p_2 \Leftarrow$ packet of degree d_2 randomly picked in the memory
  if p_2 does not exist **then**
    quit
  end if
end if
$p_{xor} \Leftarrow p_1$ XOR p_2
send p_{xor}

Heuristic approach In the previous algorithm, although the degree distribution was conserved, the decoding process was inefficient due to the overrepresentation of some fragments at the expense of others. We have thus also considered an heuristic approach. The basic idea is to complete an adaptive number of XORs (bounded by maxround) so as to dynamically approach the targeted distribution, as presented in Algo.3.

Algorithm 3 : Heuristic approach

$d \Leftarrow$degree defined by Robust Soliton law
$p \Leftarrow$last received packet
$i \Leftarrow 0$
while $i < maxround$ **do**
  $p_{rand} \Leftarrow$randomly chosen in memory
  $p_{xor} \Leftarrow p$ XOR p_{rand}
  if (degree p_{xor}) is closer to degree d than degree(p) **then**
    $p \Leftarrow p_{xor}$
    if (p_{xor}) = d **then**
      quit
    end if
  end if
  $i \Leftarrow i$+1
end while
send p_{xor}

This algorithm performs faster than Algo.2, but packets of degree 1 is still difficult, even for high maxround. We have thus complemented this algorithm by Algo.4, where raw packets are also sent.

These algorithms have been tested in the same multi-hop network than previously, with a link success probability $\gamma = 0.4$. As decoding performances are studied, we consider perfect ACK. We test these algorithms, with the previously defined scenarios: CB, CP, and CPR. CPR-XT (resp CPR-XH) is for the theoretical (resp heuristic) algorithm.

On Fig.3.12, we can verify that CB leads to the best performances and is not impacted by the number of hops. Indeed, each hop is used at its best. Except from the latter, we can observe that when using ML, CPR-XR is the most efficient as it brings more diversity. On the contrary, the heuristic approach performs much better when BP is used. It thus

Algorithm 4 : Optimized heuristic approach

```
p ⇐last received packet
ξ ⇐ XOR probability
if degree(p)= 1 or 2 then
  if rand([0,1])<= ξ then
    apply algorithm 3
  else
    retransmit without XOR
  end if
else
  apply algorithm 3
end if
```

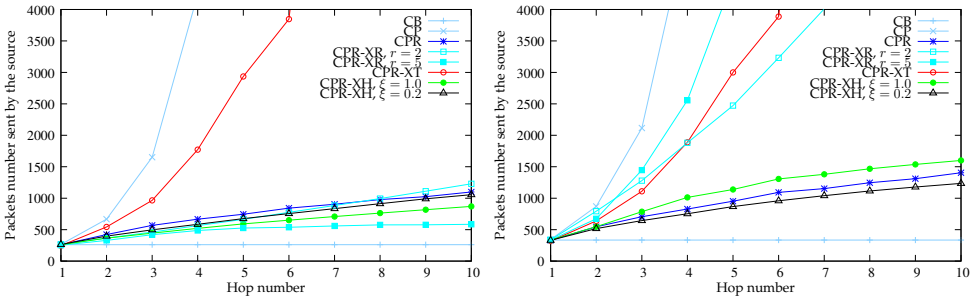

(a) ML (b) BP

FIGURE 3.12: Network performance

conforms that it is important to make a tradeoff between the fragment diversity and the degree distribution to ensure efficient BP decoding.

3.2.4 Network coding performances in a relay network

We now focus on the second atomic element in a cooperative network: the relay channel. We have seen in Section 2.3 that such topology logically permits to improve the performances compared to direct link transmission. However, this is obtained at the cost of additional transmissions. In this section, we use XOR operation at the relay to add diversity in the packets received at destination.

We consider the same topology than previously, and suppose that source and relay are assigned different time slots for their transmissions. Please note that, in this section, only network coding is performed: there is no fountain coding.

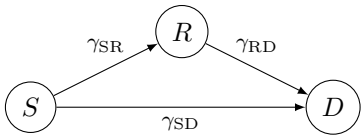

FIGURE 3.13: Relay channel

First, for comparison, if no coding is applied, the success probability of any packet is the probability that it is received on at least one path (direct path, or relay path):

$$\gamma = \gamma_{SD} + (1 - \gamma_{SD})(\gamma_{SR}\gamma_{RD}). \tag{3.3}$$

Secondly, for the XOR coding case, we have considered two cases:

1. the relay combines 2 packets consecutive from the source point of view. Unreceived packets are replaced by empty ones, so some relayed packets actually contains one received packet. This is referred to as Algo.5

2. when the relay received a packet, it performs XOR between the last 2 received packets, otherwise, no transmission is done. This is referred to as Algo.6.

We have identified that a packet p_i can be retrieved at the destination if one of these conditions is verified:

- p_i is received on the direct path. This is verified with a probability γ_{SD}.
- $p_i \oplus p_{i-1}$ is received on from the relay path, and p_{i-1} can be differently decoded, or was replaced by an empty packet at the relay. We use $\overrightarrow{\Gamma}$ to denote the upward decoding probability.
- $p_i \oplus p_{i+1}$ is received on from the relay path, and p_{i+1} can be differently decoded, or was replaced by an empty packet at the relay. We use $\overleftarrow{\Gamma}$ to denote the downward decoding probability.

From this, we have derived the mean network success probability, after the transmission of E packets from the source. For the Algo.5, we obtained:

$$\boxed{\gamma_{src_E} = \frac{1}{E} \cdot \sum_{i=1}^{E} (\gamma_{\mathrm{SD}} + (1-\gamma_{\mathrm{SD}})\gamma_{\mathrm{SR}}(\overrightarrow{\Gamma}_{src_i} + \overleftarrow{\Gamma}_{src_i} - \overrightarrow{\Gamma}_{src_i}\overleftarrow{\Gamma}_{src_i})).} \tag{3.4}$$

with

$$\overrightarrow{\Gamma}_{src_i} = \gamma_{\mathrm{RD}}(\gamma_{\mathrm{SD}} + (1-\gamma_{\mathrm{SD}})(\gamma_{\mathrm{SR}}\overrightarrow{\Gamma}_{src_{i-1}} + (1-\gamma_{\mathrm{SR}}))) \tag{3.5}$$

and

$$\overleftarrow{\Gamma}_{src_i} = \gamma_{\mathrm{RD}}(\gamma_{\mathrm{SD}} + (1-\gamma_{\mathrm{SD}})(\gamma_{\mathrm{SR}}\overleftarrow{\Gamma}_{src_{i+1}} + (1-\gamma_{\mathrm{SR}}))). \tag{3.6}$$

For the Algo.6, we obtained:

$$\boxed{\gamma_{rl_E} = \gamma_{\mathrm{SR}} \cdot \frac{1}{\gamma_{\mathrm{SR}} \cdot E} \cdot \sum_{i=1}^{\gamma_{\mathrm{SR}} \cdot E} \gamma_i + (1-\gamma_{\mathrm{SR}}) \cdot \gamma_{\mathrm{SD}}} \tag{3.7}$$

with

$$\gamma_i = \gamma_{\mathrm{SD}} + (1-\gamma_{\mathrm{SD}}) \cdot (\overrightarrow{\Gamma_i} + \overleftarrow{\Gamma_i} - \overrightarrow{\Gamma_i}\overleftarrow{\Gamma_i}) \tag{3.8}$$

and

$$\overrightarrow{\Gamma}_i = \gamma_{\mathrm{RD}} \cdot (\gamma_{\mathrm{SD}} + (1-\gamma_{\mathrm{SD}}) \cdot \overrightarrow{\Gamma}_{i-1}) \tag{3.9}$$

and

$$\overleftarrow{\Gamma_i} = \gamma_{\mathrm{RD}} \cdot (\gamma_{\mathrm{SD}} + (1-\gamma_{\mathrm{SD}}) \cdot \overleftarrow{\Gamma}_{i+1}). \tag{3.10}$$

After validation of these exact theoretical expressions, we have proposed an approximation. Indeed, they are based on recursive computation, which highly increases the complexity when the number of transmitted packets increases. We considered the Quasi Stationary State (QSR) by considering $E \to \infty$.

We obtained for Algo.5:

$$\boxed{\gamma_{src_{\mathrm{E}\to\infty}} = \gamma_{\mathrm{SD}} + (1-\gamma_{\mathrm{SD}})\gamma_{\mathrm{SR}}(2\Gamma_{src_{\mathrm{E}\to\infty}} - \Gamma^2_{src_{\mathrm{E}\to\infty}}).} \tag{3.11}$$

with

$$\Gamma_{src_{\mathrm{E}\to\infty}} = \frac{\gamma_{\mathrm{RD}}\gamma_{\mathrm{SD}} + \gamma_{\mathrm{RD}}(1-\gamma_{\mathrm{SD}})(1-\gamma_{\mathrm{SR}})}{1-\gamma_{\mathrm{RD}}(1-\gamma_{\mathrm{SD}})\gamma_{\mathrm{SR}}}. \tag{3.12}$$

We obtained for Algo.6:

$$\boxed{\gamma_{rl_{\mathrm{E}\to\infty}} = \gamma_{\mathrm{SR}} \cdot (\gamma_{\mathrm{SD}} + (1-\gamma_{\mathrm{SD}})(2\Gamma_{\mathrm{E}\to\infty} - \Gamma^2_{\mathrm{E}\to\infty})) + (1-\gamma_{\mathrm{SR}}) \cdot \gamma_{\mathrm{SD}}.} \tag{3.13}$$

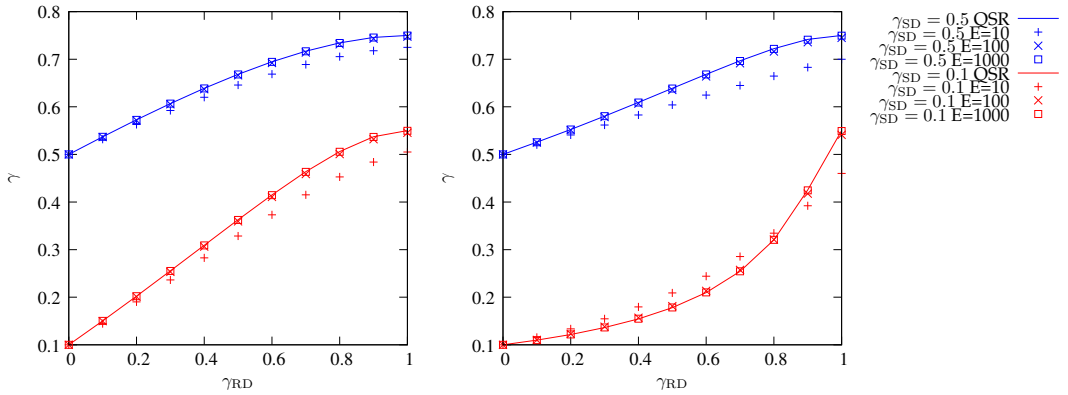

(a) Algorithm 5 (b) Algorithm 6

FIGURE 3.14: Success probability as a function of γ_{RD} for algorithms 5 and 6 (with $\gamma_{\mathrm{SD}} = 0.5$ et $\gamma_{\mathrm{SD}} = 0.1$) : QSR model and simulations for $E \in \{10, 100, 1000\}$.

with

$$\Gamma_{\mathrm{E}\to\infty} = \frac{\gamma_{\mathrm{RD}}\gamma_{\mathrm{SD}}}{1 - \gamma_{\mathrm{RD}}(1 - \gamma_{\mathrm{SD}})}. \tag{3.14}$$

We have verified on Fig.3.14, the accuracy of the approximation QSR when compared to simulation results, depending on the number of transmitted packets. We can observe first that the approximation is tight when more then 100 packets are sent, and loose precision under. Besides, we can note that Algo.5 performs better than Algo.6. This is due to the fact that, in the first one, more packets are sent, thus increasing the probability for a given packet to reach destination. The second is less performing, but is also less energy consuming.

Finally, to tradeoff between the performances and the energy consumption, we aimed at reducing the unnecessary transmissions. We defined a transmission rate $\tau \in [0, 1]$ for the relay.

We present on Fig.3.15, simulation results for the minimal total number of transmissions to be able to decode K packets, with the associated optimal τ. We can observe that Algo.5 performs better (i.e. N_{tx} is smaller) than the classical relaying or Algo.6, while targeting a higher τ. This signifies that with this algorithm, the relay is better exploited than in the other case. Thus, a more extensive use of the relay leads to better global efficiency.

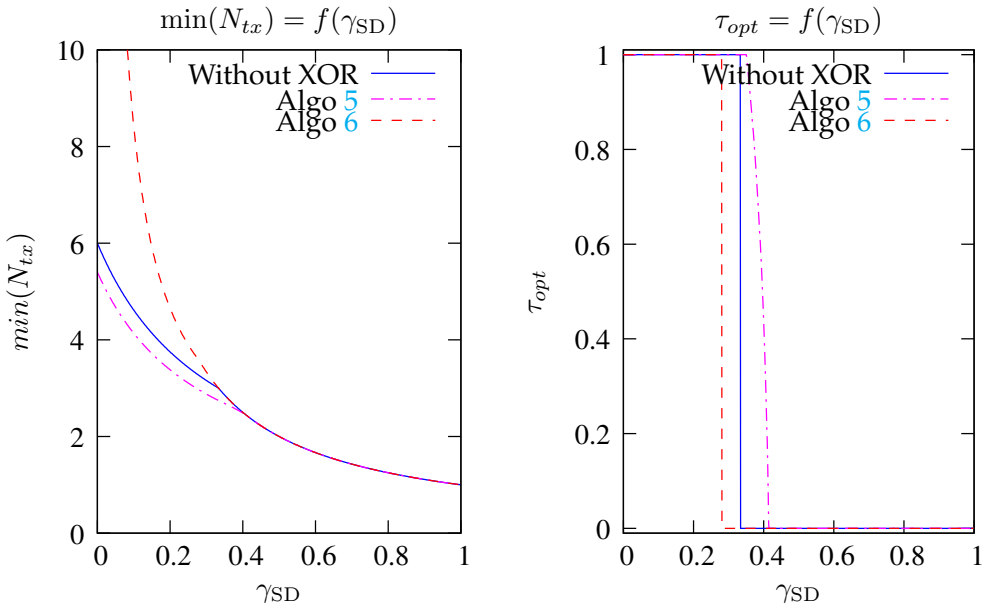

FIGURE 3.15: Minimal number of transmissions and optimal transmission rate as a function of γ_{SD} ($\gamma_{SR} = \gamma_{RD} = 0.5$).

3.2.5 Fountain codes performances in a relay network

Finally, we have merge all principles seen in the multi-hop and the relay channel topologies, to focus on a realistic deployment where nodes are distributed randomly in the area of interest, and aim at sending their data to a distant sink. In the previous studies, the topology was static and supposedly known: each node was having a predefined specific role.

However, in real cooperative networks, routing protocols have to be used to identify the role of each node. The defined path can be static, and for instance define a specific multi-hop path for any source-destination couple (in this case other relay overhearing the transmitted packets ignore them), or dynamic: the path(s) are opportunistically created during packet propagation in the network.

We have chosen a very simple dynamic routing protocol, based on gradient routing. In a preliminary step, the sink broadcast a specific message, that will be relayed by all nodes. This message contains a field that characterize the distance to the sink and will be increased at each relay. Thus, nodes will be able to evaluate to evaluate their minimal distance to the sink. We can observe on Fig.3.16 an example of the cost associated to nodes.

Once this step is done, data transmission can begin. When a node overhears a message coming for a node closer (or at the same distance) to the sink, it will discard the message, otherwise, it will consider it for relaying. Fig.3.17 represents the average number of transmitted packets per node for a communication between S and D. Unsurprisingly, nodes at proximity of the shortest path are more solicited.

In this section, we re-consider a LT coded source stream. The generated packets are broadcast by the source, intending the destination. If all the hearing nodes relay the packets, we would have a complex and inefficient combination of multi-hop an relay channel topology. Indeed, systemic retransmissions (aside from generating collisions if resource scheduling is not done properly) would result in an exponential growth of the transmission number when getting closer to the sink. We thus use the retransmission rate τ as proposed in Section 3.2.4. Besides, as in this study, we have observed that systemic XORing was not efficient, we also define ν as the probability that a relay transmits a XORed packet. Finally, if XORed is intended, we apply the heuristic Algo.4, to take advantage of its efficiency when dealing with LT codes and BP decoder. Thus, the relaying algorithm applied in any node is given by Algo.7

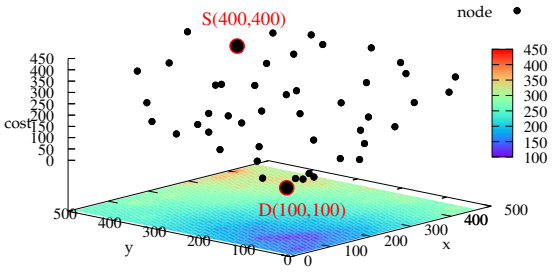

FIGURE 3.16: Positions and costs associated to node for a gradient algorithm

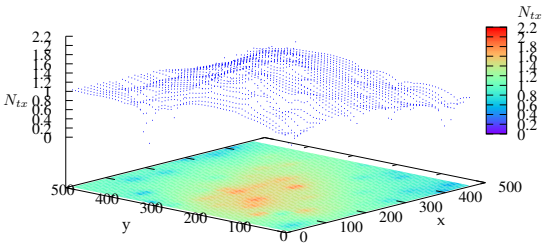

FIGURE 3.17: Transmission number per node for a $S \rightarrow D$ communication

Algorithm 7 : Relaying macro-algorithm for node R

$F_{max} \Leftarrow K$
if R receives a packet p **then**
  Add p in the FIFO whose size is F_{max};
  if rand $([0,1])\, leq\tau$ **then**
    if rand $([0,1])\, leq\nu$ **then**
      Apply algorithm 4
    else
      $p_{new} = p$
    end if
    transmit p_{new}
  end if
end if

We do not consider in this study the acknowledgment part, and suppose that transmission is finished when the destination has successfully decoded all fragments with BP decoder.

We present here the performances for a 50 nodes network, deployed over $500 \times 500m$. $M = 50$ messages are sent by the source, each divided into $K = 100$ fragments for LT encoding. We observed several metrics:

- `Success rate` This is given by the ratio between the successfully decoded fragments and sent fragments. We can observe three areas on Fig.3.18: reliable, unreliable, and transition one. Contrarily to the others, in the transition part, performances are highly dependent on the XORing rate ν, and that high ν is more performing.

- `Energy and delay` We observe in Fig.3.19 and Fig.3.20 consistent behavior than for the success rate: when the relaying rate is low, the network is spending more (inefficient) energy to try to complete the transmission, which is thus during longer in average.

- `Redundancy` We define redundancy μ as the ratio between the actually received packets number, and the number of needed packets to decode. We can observe on Fig.3.21 that the network coding indeed permits to diversify the information received at the destination.

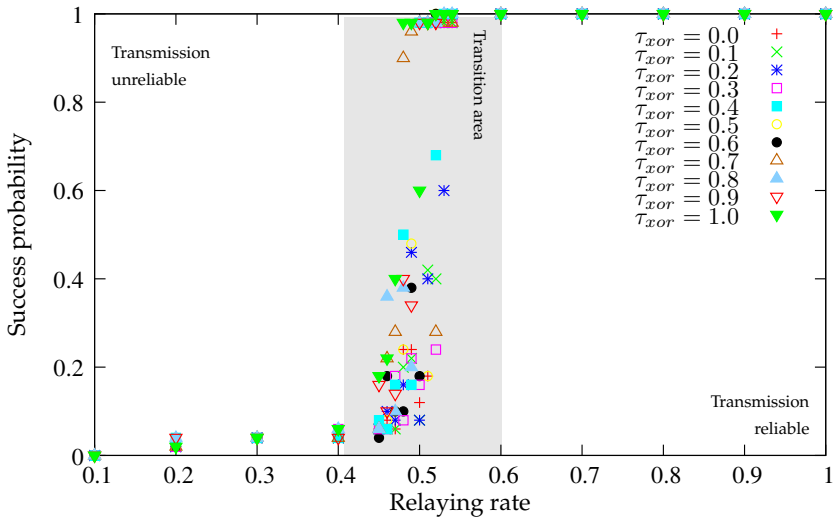

(a) Success probability

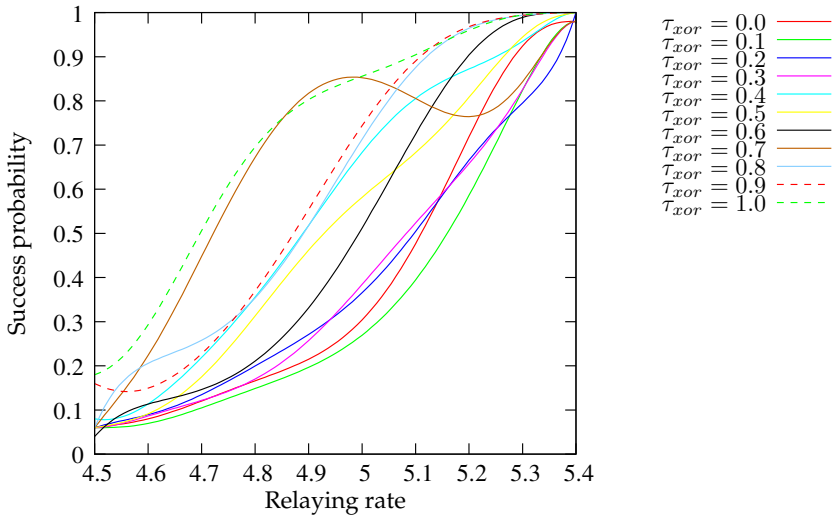

(b) Success probability in the transition area, obtained with the smoothing method of Bezier curves

FIGURE 3.18: Transmission success rate

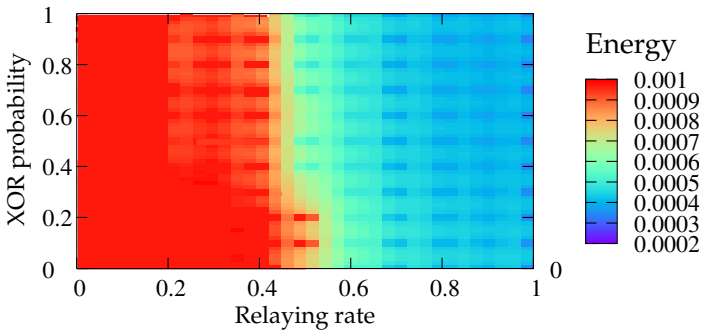

(a) Energy consumption as a function of the relaying rate and the network coding probability

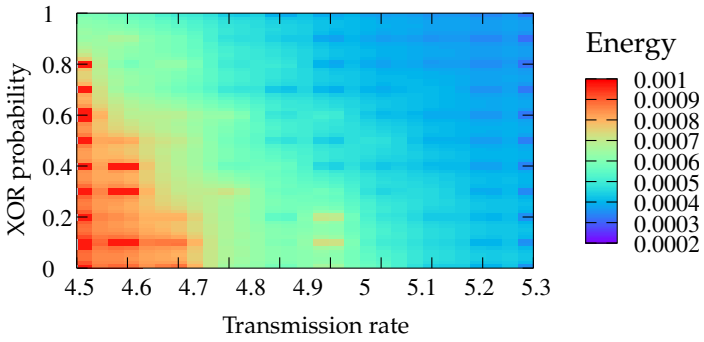

(b) Energy consumption as a function of the relaying rate and the network coding probability for the transition area

FIGURE 3.19: Network energy consumption

From this study, we can conclude that multi-hop is a way to extend coverage of the network. However, careful design of the relaying protocol should be done. We have proposed an algorithm to be jointly used with gradient-routing, and shown its good performances. However, one may note that relaying nodes where supposed to be:

- altruist: they are always willing to help further nodes although this leads to faster energy depletion for them
- on listening mode: relays were always listening to the channel to identify any packet to forward. This is also energy consuming compared to idle state.

In a case where all nodes belong to the same network/institution, such behavior is possible, as the help of relaying nodes permits to decrease the overall energy consumption. However, for distinct networks deployed in the same area but for different applications, reward must be considered to instantiate such cooperation.

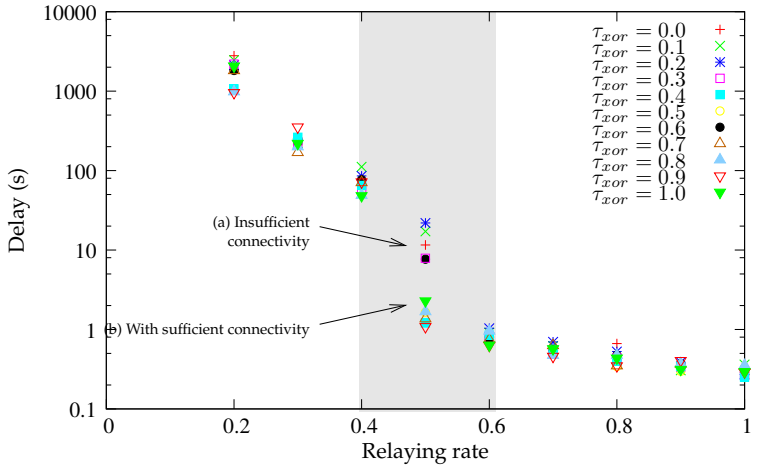

(a) Transmission delay

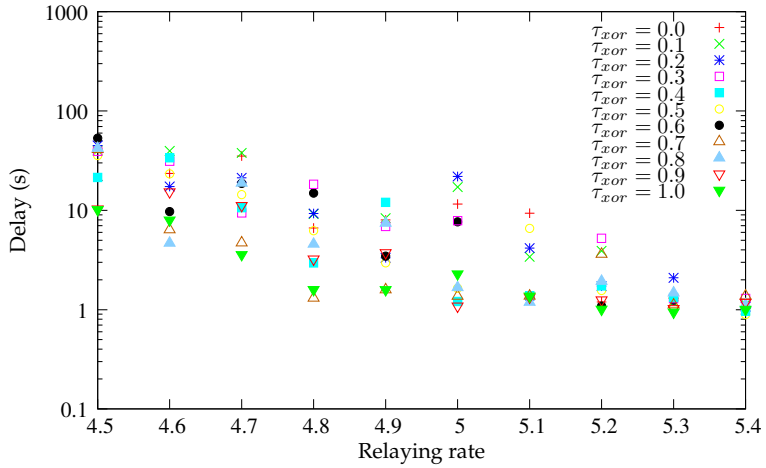

(b) Transmission delay in the transition area

FIGURE 3.20: Transmission delay

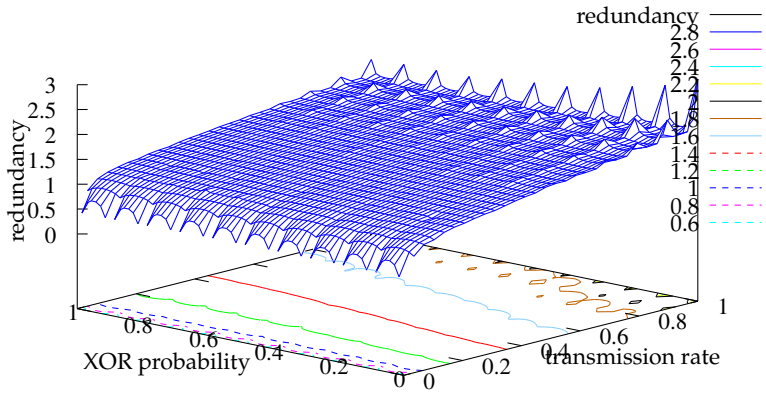

FIGURE 3.21: Redundancy as a function of XOR probability and the relaying rate

3.3 IoT : UNB

The second way to cover a wide area is to use long range transmission techniques. In this section, I will present the work made on SigFox's UNB networks. Although Sigfox's network is deployed worldwide and renowned to be efficient for low-throughput point-to-point transmissions, the capacity network based on this technology is not well-known. In particular, the behavior of a huge amount of non-synchronized operating nodes in a geographically extensive area around a base-station has not been studied yet.

3.3.1 UNB definition

Ultra-narrow-band systems are defined such that each individual node occupies an extremely narrow frequency band to transmit its signal. This frequency band is significantly smaller than the bandwidth of the channel and is usually around a few hundred Hz. In 2004, Walker [Wal]; [Zha13] first proposed the use of VMSK (Very Minimum Shift Keying) to compress data transmission in the smallest possible band. However, in practice, this modulation technique took a step forward but did not reach the claimed ultra narrow frequency occupancy [Karst]; [Xia03].

In this work, the ultra narrow band occupancy is obtained by transmitting at a very low data rate (100bps). The transmitted signal thus occupies a band of about $b = 100$ Hz, inside a typical possible band of 192kHz to 2MHz. A key parameter of such system is the oscillator precision which induces an offset between the targeted frequency and the actual one. The currently available technology only permits factoring components with a standard deviation around 2-20 ppm (the state of the art components reaches at best 0.25 ppm [Per+13]). For example, for an operating frequency band of $f = 800$ MHz and a typical oscillator jitter $d_f = 0.25 - 2$ ppm, the uncertainty of carrier frequency positioning would be around $D_f = 200 - 1600$ Hz which is bigger than the transmission band occupied by an individual node. In this case, i.e., when the frequency uncertainty is higher than the signal bandwidth, the system is referred to as UNB.

3.3.2 UNB: single cell design

The atomic network element is the star topology, where base-stations centered on large cells receive the data from a huge amount of source nodes spread over. From the receiver's point of view, as shown in Fig.3.22, the monitored bandwidth B is filled with a combination of narrow-banded signals randomly located in time and frequency. Their demodulation relies on efficient SDR (Software Design Radio) algorithms designed to analyze the total band, to detect transmitted signals and to retrieve sent data. This is done with a FFT block applied to the received signal followed by an adaptive detector which aims at identifying the spectral signatures of the transmitted UNB signals. So, any uncontrolled frequency shift at any transmitter is not problematic if this shift is fixed during the short message duration. One may note that oscillators also suffer from an additional shift while heating during transmission, but this feature is also managed in SigFox's BS. For each detected transmission, the appropriate frequency band is filtered and demodulated with a standard BPSK demodulator.

3.3.3 UNB Interference characterization

By considering a multiple access channel, we have derived the interference pattern expression, as follows.

For the general case, at the BS side, the received signal is the sum of active nodes' signals and can be expressed as follows:

$$r(t) = \sqrt{h_c(r_x,t)} * h_e(f_x,t) * s_x(t) + \sum_{y \in \{\mathcal{A}-x\}} \sqrt{h_c(r_y,t)} * h_e(f_y,t) * s_y(t) + w(t) \qquad (3.15)$$

where, for any active node $x, y \in \mathcal{A}$, $s(t)$ is the modulated symbol; $h_e(f,t)$ is the transmission FIR filter centered on the randomly chosen carrier frequency f; $*$ denotes the convolution operator, and $w(t)$ is an additive white Gaussian noise with zero mean and variance σ^2, and

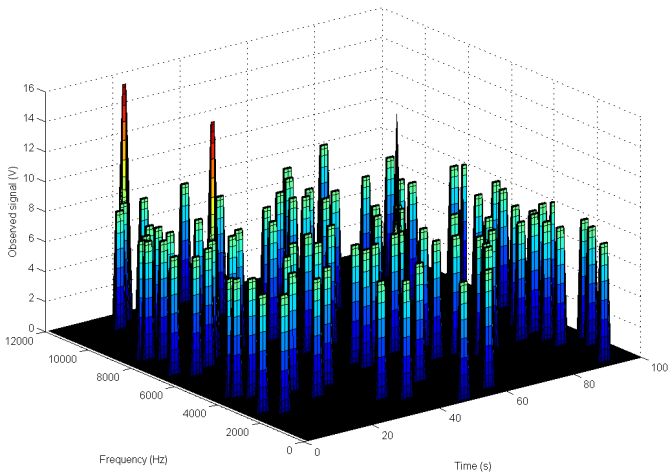

FIGURE 3.22: Example of temporal & spectral repartitions of nodes.

the pathloss described by $h_c(r,t) = g(t) \cdot h_0 \cdot r^{-\alpha},\ r \in [r_m, r_M]$, where $\alpha \geq 2$ is the path loss exponent; g is the Rayleigh channel coefficient, which is a random variable following an exponential distribution of unitary mean $g \sim exp(1)$ considered as constant during the observation instant; and h_0 is the reference gain determined at the reference distance $r_0 = 1$ m.

To recover desired signal, the total signal received at BS is filtered at the carrier frequency of desired node f_x with the matching filter ($h_r(f_x,t) = h_e(f_x,t)$). We deduce :

- the received power corresponding to the signal of the desired node x arriving at the BS: $P_s = h_c(r_x,t) \cdot P_0 = g_x \cdot r_x^{-\alpha} \cdot P_0'$, with $P_0 = < |h_e(f,t) * h_e(f,t) * s(t)|^2 >$ which is identical to all signals, and P_0' which stands for $h_0 \cdot P_0$.
- the interference power I_y caused by a single interferer on the desired signal follows: $I_y = h_c(r_y,t) \cdot \beta(|f_x - f_y|) \cdot P_0 \quad = g_y \cdot r_y^{-\alpha} \cdot \beta(|f_x - f_y|) \cdot P_0'$, with

$$\beta(|f_x - f_y|) = \frac{< |h_e(f_y,t) * h_e(f_x,t)|^2 >}{< |h_e(f_x,t) * h_e(f_x,t)|^2 >} \tag{3.16}$$

  the *rejection coefficient* to characterize the case where the reception filter is centered on a different frequency than the transmission filter. This rejection coefficient quantifies the portion of interfering signal which is kept after filtering. It depends on the frequency spacing between the two carrier frequencies $\delta f = |f_x - f_y|$ as presented in Fig.3.23 (black curve) for a realistic filter as used in SigFox's network. One may note that, β is a rejection coefficient, thus without unit in linear domain, and expressed in dB in logarithm scale. However, in the following, thanks to normalization with respect to the desired user power, the interference power and the rejection coefficient are the same. I will thus use the term "interference".

We can approximate this interference with two kind of models. First, we can note that the actual interference level can be divided into two main areas. Transition occurs between $200 - 400$Hz, depending on the considered criterion. For high δ_f, the interference level is low, below -50dB. So a unique interferer in this area will have almost no impact on the performance of the desired node. On the contrary, a unique node will cause a perceptible interference only if δ_f is very small, as the filter is very selective. As the available bandwidth is very large (we consider at least 12kHz in this paper) compared to the interference width, the interference level can be approximated by a constant in this area. Thus, we model the contribution of a single-interferer by a rectangular function:

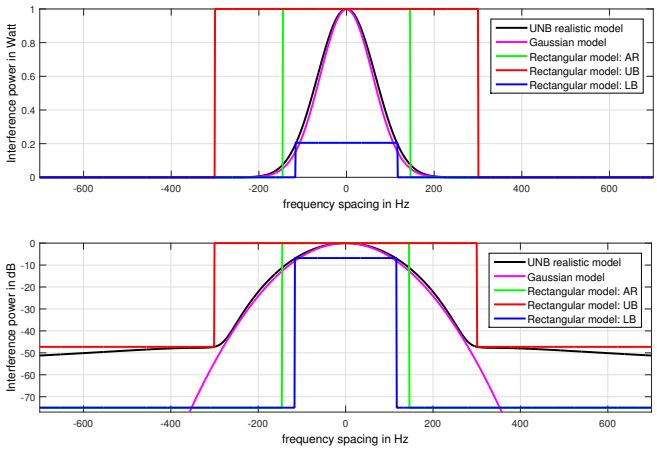

FIGURE 3.23: Behavior of the interference coefficient vs the frequency difference δ_f between the desired node and the interferer

$$\beta(\delta f) = \begin{cases} I_{max} & for \quad \delta f \leq \triangle/2, \\ I_{min} & for \quad \delta f > \triangle/2. \end{cases} \tag{3.17}$$

where $\triangle$ corresponds to the width of δ_f that creates high interference level.

We have determined the empirical parameters for several cases (upper bound, lower bound and optimal model)(in red, blue and green respectively). The values reported in Table.3.1 were obtained by searching for the parameter set that minimizes the simulated BER (resp OP) difference with the theoretical BER (resp. OP) (eq.3.22 and eq.3.23 that will be presented in few pages).

TABLE 3.1: List of simplified models using rectangular function

Models	I_{max} for $\lvert\delta_f\rvert \leq \frac{\triangle}{2}$	I_{min} for $\lvert\delta\rvert > \frac{\triangle}{2}$
Upper bound	$I_{max\_up} = 0$ dB & $\triangle_{up} = 440$ Hz	$I_{min\_up}(\triangle_{up})$ dB
Lower bound for BER	$I_{max\_low}(\triangle_{low})$ dB & $\triangle_{low} = 100$ Hz	$I_{min\_low} = -90$ dB
Lower bound for OP	$I_{max\_low}(\triangle_{low})$ dB & $\triangle_{low} = 220$ Hz	$I_{min\_low} = -90$ dB
Optimal model	$I_{max} = -1.77$ dB & $\triangle = 232$ Hz	$I_{min} = -90$ dB

We have also approximated the interference power by a zero-mean Gaussian function, depending on the frequency difference δf (pink curve on Fig.3.23):

$$\beta\left(\delta f\right) = \frac{150}{\sigma\sqrt{2\pi}} \exp^{\frac{-\delta f^2}{2\sigma^2}} \tag{3.18}$$

with $\sigma = 60$.

When considering several interferers, the AIP (Aggregated Interference Power) is the sum of all interferers' contribution. AIP is plotted on Fig.3.24. We can observe that for a number of active nodes smaller than 20, AIP remains small. On the other case, AIP gradually converges to the left, near 0 dB (which corresponds to $\delta_f = 0$ for a single interferer case) and more. In fact, when the number of active nodes increases, the probability that at least one node chooses a carrier frequency close to the one of desired node is also increased. This contribution will dominate the other and leads to a high level of interference. Thus, in practice, failure is due to a unique interferer. In this case, we say that there is a collision between two packets. We have thus considered this hypothesis throughout all this work.

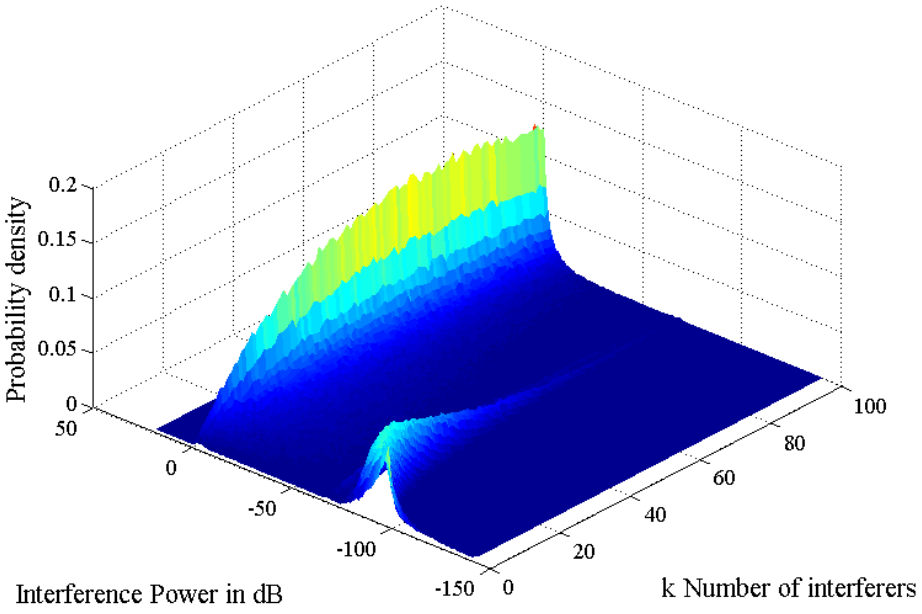

FIGURE 3.24: PDF of the aggregate interference power [dB], for $k = 100$ interferers, for BW = 12 kHz.

3.3.4 UNB associated MAC

In SigFox's network, when devices have a data to transmit, they choose a carrier frequency within the 192kHz available band. In theory, such selection can be done either:

- in a discrete way: the carrier is elected among a finite set of frequencies. We call this DR-FDMA (Discrete Random Frequency Division Multiple Access). DR-FDMA scheme is characterized by $\triangle_f$ the spacing between the possible values of carrier's frequency (CFS: Carrier Frequency Spacing).
- in continuous way: the carrier is chosen at random in the continuous available frequency band. We call this CR-FDMA (Continuous Random Frequency Division Multiple Access). We can note that the CR - FDMA scheme allows the use of transmitters whose time and frequency are unconstrained (except for being in the transmission total band). In practice, the randomness in frequency domain is easily done, thanks to the frequency jitter. It is reasonable, however, to assume that this frequency remains constant during the transmission of a whole packet. Finally, we can note that CR-FDMA corresponds to DR-FDMA scheme with an infinitely small CFS.

We have computed the OP (Outage Probability) for these 2 cases. We consider that a packet is lost if the intended packet undergoes an interference level higher than a given threshold.

If the $k+1$ transmitting nodes are all perceived at the BS with the same power, and no jitter is considered, than the OP is given by:

- in the DR-FDMA scheme:

$$\mathrm{OP}(k) = 1 - \left(1 - \frac{1 + 2 \times \lfloor \frac{\delta_0}{\triangle_f} \rfloor}{\lfloor \frac{BW}{\triangle_f} \rfloor}\right)^k \tag{3.19}$$

- in the CR-FDMA scheme:

$$\mathrm{OP}\,(k) = 1 - \left(1 - \frac{(2 \times \delta_0)}{(BW)}\right)^k \tag{3.20}$$

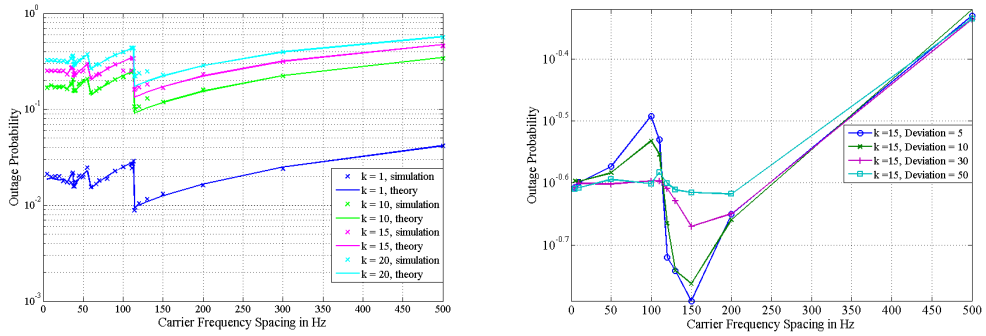

(a) Validation (no jitter)

(b) With jitter, $K = 10$

FIGURE 3.25: R-FDMA OP vs $\triangle_f$ for k interferers, $BW = 12$ kHz

We can verify on Fig.3.25(a) that the theoretical model fits with the simulation results. However, one should note that the theoretical model is less pertinent when the number of nodes increases, especially for $\triangle_f$ slightly higher than 113 Hz, due to the fact that the aggregated interference was neglected. Besides, we can also observe that the OP curves follow a saw-tooth pattern, whose local maximums and minimums do not depend on the number of active interferers, but only on $\triangle_f$, as predicted by the theoretical analysis. Finally, DR-FDMA is optimal for $\triangle_f = 113$ Hz and is more performing than CR-FDMA scheme (as CR-FDMA corresponds to $CFS \rightarrow 0$).

We have confronted such results to jitter impact. To this aim, we modeled the frequency jitter by an additive random frequency variable, which follows a Gaussian distribution with zero mean and known standard deviation σ. We can observe on Figure 3.25(b), that the DR-FDMA performances are degraded when taking into account jitter. Indeed, the sawtooth pattern is more and more smoothed as the jitter standard deviation increases. Indeed, the statistical distribution of the interferer's carrier around the targeted frequencies tends to reduce the gap between the performances of close $\triangle_f$ values, and especially where there was a discontinuity. Without jitter, all the nodes that choose $\delta_f = 112$ Hz (resp. $\delta_f = 113$ Hz) lead (resp. do not lead) to OP. On the contrary, with jitter, in both cases, we get about half carriers under 113 Hz, creating OP while the second half does not create OP. Thus, there is no discontinuity anymore. As a consequence, the benefit brought by DR-FDMA disappears when jitter is present. In this case, CR-FDMA becomes as efficient as DR-FDMA. Thus, CR-FDMA will be used. Besides, one may note that it allows the use of the cheapest oscillators component without loss of performance network, as for $\sigma > 50$ the same performances will be obtained.

Finally, there are three main inherent features to UNB systems, that will restraint the available choices for Multiple Access Protocols definition, as illustrated in Fig.3.26:

- Asynchronicity: the data transmission of active node is made in a asynchronous manner, both in time without any scheduling strategies. This feature permits to suppress the traffic overload needed for global synchronization. However, it leads to the packet collision during the transmission of a given packet due to the fact that packets do not simultaneously start and stop.

- Lack of contention-based protocols is considered as a third impact on the data transmission of an active node in the frequency domain. As the contention-based protocol is mitigated for all active nodes, each node is transmitting its packet regardless of carrier frequencies being used by other active nodes in a given bandwidth. As a result, the spectral overlap between their individual transmission bands (i.e., interference) is induced when at least two nodes are transmitting at the same moment. For example, in Figure 3.26, the green node starts transmitting even if the red one is already using the band in common. There is a spectral and temporal overlap between them.

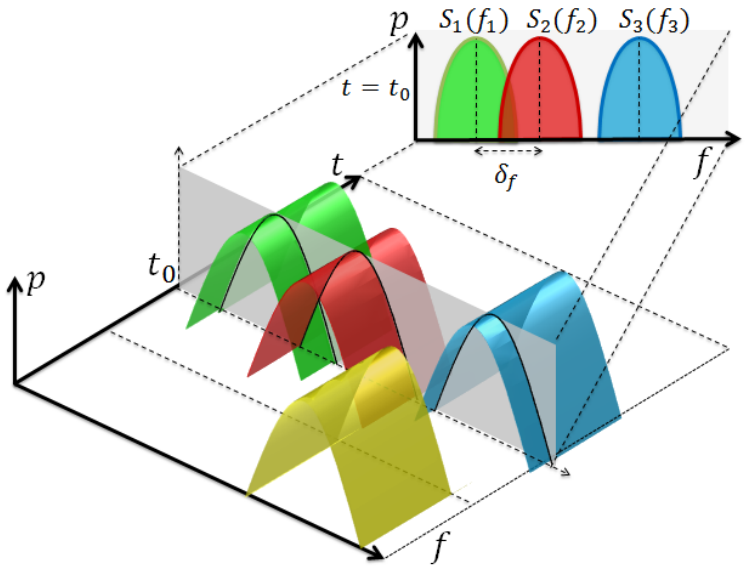

FIGURE 3.26: Example of temporal and spectral repartition of nodes

- Randomness in frequency domain as treated previously which concerns the position of carrier frequency of active nodes in the total bandwidth. Active nodes can choose randomly and continuously their carrier frequencies to transmit their data.

As the CR-FTDMA is an extension of Aloha protocol, we have derived the network throughput as a function of the load. Assuming that each node transmits a message of duration τ seconds, at a randomly chosen time, every D_p seconds on average, we have shown that the ALOHA success probability with slotted or unslotted time, and slotted or unslotted frequency, and uniform distribution in time and frequency domain, is given by:

$$P_{2D} = e^{-\alpha_t \alpha_f G_{tf}} \tag{3.21}$$

with $G_{tf} = N p_t p_f = \dfrac{N\ \tau\ b}{D_p\ BW}$, and $\alpha_f = 2$ (resp.1) for frequency-unslotted (FU) (resp. frequency slotted (FS)) ALOHA.

We plot on Fig.3.27 the throughput as a function of the load G_{tf}. As time and frequency can be independently slotted or unslotted, there are 4 possible scenarios : frequency-slotted (resp. unslotted) time-slotted : FSTS (resp. FUTS), and frequency-slotted (resp. unslotted) time-unslotted : FSTU (resp. FUTU). We can first note that the FSTS case is the best one as the time-frequency space is divided into orthogonal channels, thus minimizing the probability of collision. On the opposite, FUTU is the worst one as partial overlapping is possible both in time and frequency domain. Finally, FSTU and FUTS coincide due to the time-frequency duality. Thus, there are in fact only 3 distinct curves, according to the possible values of the product $\alpha_t \cdot \alpha_f$.

One may note that the time-frequency duality brings flexibility. Indeed, if both precise frequency and timing are difficult to handle simultaneously, FSTS can not be achieved. The duality between FSTU and FUTS allows to decide which constraint to relax, independently of the impact on the performances, but based for example, on the network deployment cost.

3.3.5 UNB performances for same received power at the BS

Now that the specific interference model, and access method is known, we can focus on the performance analysis. In order to have an insight on the specific interference pattern, we have first considered the case where nodes are perceived at the BS with the same emission power. This corresponds to the case where all nodes are at the same distance from the BS, and are affected by the same channel conditions, or to the case where power control is performed.

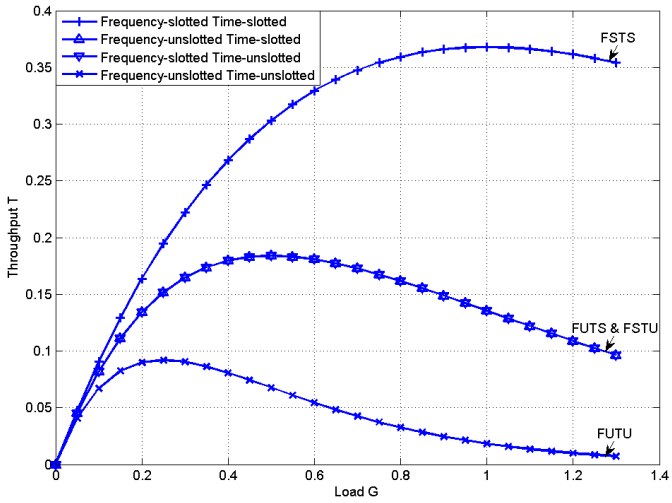

FIGURE 3.27: Network throughput as a function of the load for all (α_t, α_f).

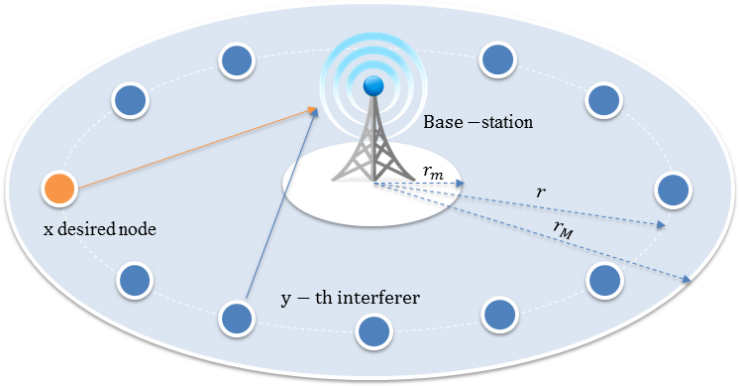

FIGURE 3.28: Network Topology for a unique cell with equal received power

The BS is considered to be always in reception mode, and to scan the whole bandwidth for potential transmissions (as done in SigFox network). For each detected transmission (even simultaneous ones), the BS processes the incoming message(s). If the SINR is higher than a threshold (usually set to 7dB in our work), and the packet is considered correctly received. In all the following work, instantaneous metrics will be considered: we make the assumption that the transmission conditions remain the same over the packet duration. We thus analyze the SINR at a given moment.

One transmission We have shown that, for $k+1$ total simultaneously active users (i.e. k interferers), the BER and OP can be theoretically obtained with:

$$\text{BER}(k) = \sum_{n_L=0}^{n_L=k} \mathbb{P}(N_L = n_L) \cdot erfc\left(\sqrt{\frac{P_s}{P_I(k, n_L)}}\right) \tag{3.22}$$

$$\text{OP}\,(k) = \sum_{n_L / P_I(k,n_L) > \gamma} \mathbb{P}\,(N_L = n_L) \tag{3.23}$$

with

$$\mathbb{P}(N_L = n_L) = C_k^{n_L} \cdot p^{n_L} \cdot (1-p)^{(k-n_L)} \tag{3.24}$$

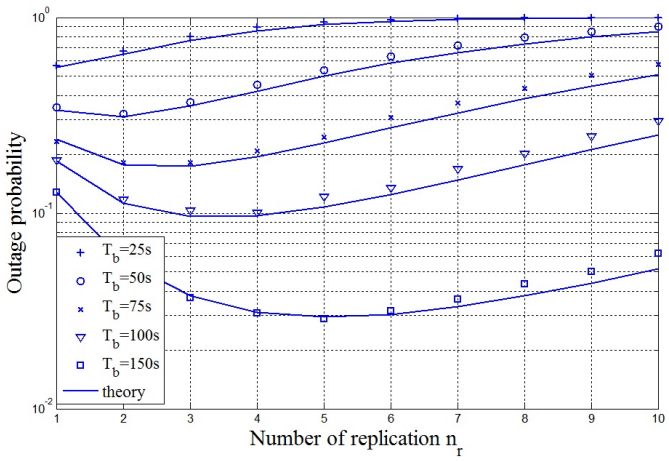

FIGURE 3.29: OP vs number of replications n_r with different message period T_b, $BW = 12$ kHz, $N = 1000$.

From this, we have derived the network capacity, expressed as the maximum number of simultaneously active users while guaranteeing satisfactory OP (Table.3.2). We can verify the accuracy of the rectangular model, as well as the parameter set and the theoretical expressions, as the optimal model provides a good estimation of the simulation, while the bounds actually provide lower and higher estimations.

TABLE 3.2: Maximum Nodes Numbers For $OP = 10^{-1}$, Non Path-loss

BW	N up	N simu	N opt	N low (BER)	N low (OP)
12 kHz	3	6	6	13	6
24 kHz	6	11	11	26	12
48 kHz	12	23	23	51	23
64 kHz	16	30	30	68	31
96 kHz	23	44	45	102	46
1 MHz	124	450	455	1054	479

Multiple transmissions To improve the system capacity, we have considered the use of replications during the transmission. As replications are identical, the message is successfully received if at least one of this replication is correctly received at the base station. We make the assumption that the replications experience independent transmission conditions, and that the success probability of any replication is independent of the collision on the previous ones. We derive the theoretical expression for the outage probability, as a function of the main system parameters: the whole transmission band BW; the frequency occupancy with respect to the carrier $[-b; b]$ Hz; the wake-up duty cycle of nodes T_b; the time duration of a message d, and the replication number n_r. Accordingly, the outage probability of one useful message, transmitted with n_r replication, is:

$$\mathrm{OP} = \left(1 - \left(1 - \frac{2b \times d}{BW \times T_b} \times n_r\right)^{N-1}\right)^{n_r} \tag{3.25}$$

We can observe, on Fig.3.29, that there is an optimum number of replications. This is due to the fact that, at first, when n_r increases, the replications bring redundancy and a better reliability. However, when n_r is too high, it overloads the network, and the performances drop due to excessive number of collisions.

As can be seen in eq.3.25, OP depends on many parameters. However, by derivating eq.3.25, and numerically evaluating the optimal n_r, we have shown that the optimal

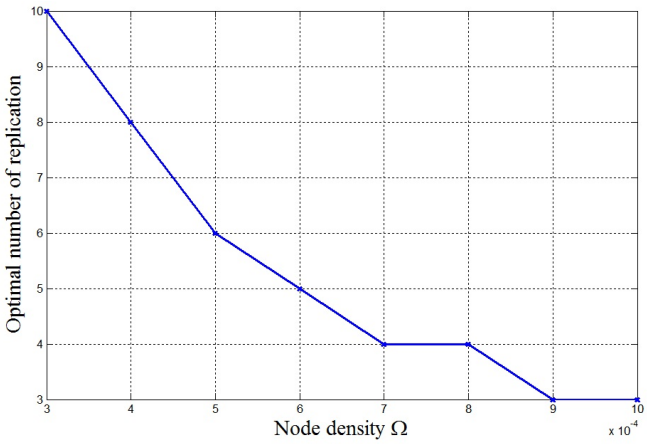

FIGURE 3.30: Node density Ω vs optimal number of replications $n_{r_{opt}}$.

number of replications depends on a single parameter: the resources occupation parameter $\Omega = \frac{N}{BW \times T_b}$. We can thus plot the optimal number of replications as a function of this parameter (Fig.3.30). We can observe that, $n_{r_{opt}}$ decreases when the node density gets high (this is due to the fact that the increase of the network load reduces the available time/frequency resources for the replication process). This result is very interesting and promising because its urges the potential ability of configuring the network by relying on a single global parameter: node density over the temporal and frequency resources Ω.

3.3.6 UNB performances for diverse received power at the BS

Finally, to derive more realistic performances of the network, we have considered the case where the different nodes encounter diverse propagation conditions. We have taken 2 complementary approaches to derive the OP. We first derive an analytic expression of a UNB-based system performance, when considering both the attenuation effect and the actual specific behavior of the interference in the spectral domain. Secondly, we use the stochastic geometry model to also take into account the Rayleigh fading effect, but with a simplified interference model.

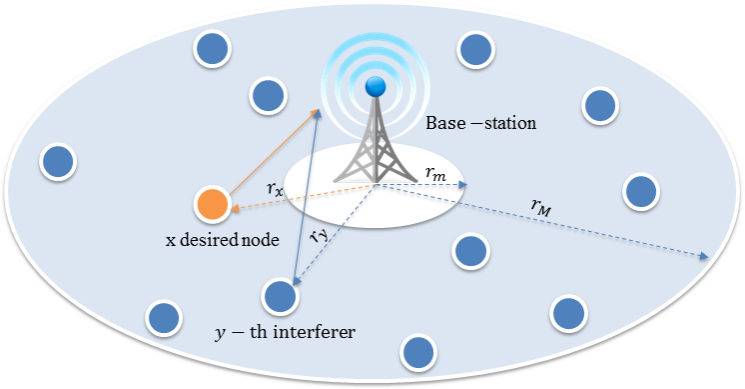

FIGURE 3.31: Topology network of adopting the spatial node distribution.

We suppose that nodes are uniformly distributed in a disk form area, whose range is $[r_m, r_M]$, as shown in Fig. 3.31. Nodes are positioned inside the cell, except for the inner disk of the cell (to ensure mathematical tractability by avoiding singularity at the base-station location [BBM09]). Nodes are distributed according to a spatial homogeneous Poisson point process (HPPP) of density λ that lies in the Euclidean plan $\mathbb{R}^2$. We assume that nodes emit with the same emission power.

Stochastic geometry approach Stochastic geometry is a powerful tool that permits to handle spatial randomness, and its implications on metrics observation. In addition to the geometric pathloss, stochastic geometry permits to take into account Rayleigh fading and noise in the interference expression. It is thus perfectly adapted to our need. However, all previous works using this tool were considering channelized transmission, We have thus introduce the partial collision in frequency domain ($\beta(\delta f)$) in the stochastic geometry model by considering a marked spatial Poisson Point Process (PPP), where the mark models the residual proportion of interference which is perceived on the desired transmission. However, due to the shape of the rejection coefficient function, according to our very first calculations, such approach leads to intractable expressions. We obtained tractable expressions, by considering the rectangular model as presented in (3.17).

We have shown that the OP can be computed as:

$$\mathrm{OP} = 1 - \exp(-W \cdot s) \cdot \mathcal{L}_{P_I}(s) \tag{3.26}$$

with $\mathcal{L}_{P_I}$ the Laplace transform of the AIP Probability Density Function (PDF), expressed in a general way for any desired node at a distance r_x from the BS, as:

$$\mathcal{L}_{P_I}(s) = \mathbb{E}_{P_I}[\exp(-P_I \cdot s)]. \tag{3.27}$$

$$= \exp\left(-2\pi\lambda\left(\underbrace{\int_{r_m}^{r_M} r_y dr_y}_{A} - \underbrace{\int_{r_m}^{r_M} \frac{p}{1+s\cdot b\cdot r_y^{-\alpha}} r_y dr_y}_{B(s)} - \underbrace{\int_{r_m}^{r_M} \frac{1-p}{1+s\cdot c\cdot r_y^{-\alpha}} r_y dr_y}_{C(s)}\right)\right) \tag{3.28}$$

For free space $\alpha = 2$, we have:

$$\mathcal{L}_{P_I}(s) = \left(\frac{r_m^2 + sb}{r_M^2 + sb}\right)^{\pi\lambda psb} \cdot \left(\frac{r_m^2 + sc}{r_M^2 + sc}\right)^{\pi\lambda(1-p)sc} \tag{3.29}$$

For flat earth model $\alpha = 4$, we have:

$$\mathcal{L}_{P_I}(s) = \exp\left(\pi\lambda p \cdot\sqrt{sb}\cdot \arctan\left(\frac{r_m^2\sqrt{sb} - r_M^2\sqrt{sb}}{sb + r_M^2 r_m^2}\right) + \pi\lambda(1-p)\cdot\sqrt{sc}\cdot\arctan\left(\frac{r_m^2\sqrt{sc} - r_M^2\sqrt{sc}}{sc + r_M^2 r_m^2}\right)\right) \tag{3.30}$$

Exact interference shape To take into account the exact interference shape $\beta(\delta f)$, we have computed the OP in a more simple case: without fading and noise, and considering free space propagation ($\alpha = 2$). Contrarily to stochastic geometry where aggregated interference was considered, we consider here that interference comes from a single interferer. With a free space propagation model, the SIR of the desired node is:

$$SIR_1 = \frac{P_0\left(\frac{r_0}{r_x}\right)^2}{P_0\left(\frac{r_0}{r_y}\right)^2 \beta(\delta f)} = \left(\frac{r_y}{r_x}\right)^2 \frac{1}{\beta(\delta f)} \tag{3.31}$$

Consequently, OP can also be expressed as:

$$OP = P\left(r_y \leq r_x\sqrt{S\beta\left(\delta f\right)}\right) \tag{3.32}$$

$$= 0 + \int_{b_1}^{b_2}\left(\frac{{r_x}^2\gamma^*\beta\left(\delta f\right) - {r_m}^2}{k^2}\right)\mathbb{P}\left(\delta f\right)\,\mathrm{d}\delta f + \int_{b_0}^{b_1} 1\cdot\mathbb{P}\left(\delta f\right)\,\mathrm{d}\delta f$$

$$= \left[75a\gamma^*\,\mathrm{erf}\left(\frac{\delta f}{\sqrt{2\sigma^2}}\right) + \frac{150a\gamma^*\sigma}{B\sqrt{2\pi}}\exp\left(\frac{-\delta f^2}{2\sigma^2}\right) + e\frac{\delta f^2}{2} - eB\delta f\right]_{b_1}^{b_2}$$

$$+ \frac{B}{2}\left[\delta f - \frac{\delta f^2}{2B}\right]_{b_0}^{b_1} \tag{3.33}$$

with the following constants:

$$d = \frac{2{r_x}^2}{Bk^2}, \qquad e = \frac{2{r_m}^2}{B^2k^2}, \qquad b_0 = 0$$

$$b_1 = min\left(\beta^{-1}\left(\left(\frac{r_M}{r_x}\right)^2\frac{1}{\gamma^*}\right), B\right), \qquad b_2 = min\left(\beta^{-1}\left(\left(\frac{r_m}{r_x}\right)^2\frac{1}{\gamma^*}\right), B\right)$$

(3.32) represents the OP when there are 2 active nodes. For N active nodes, any of the $N-1$ nodes (i.e. all nodes except the desired node) can be an interfering node. Accordingly, transmission success means that the desired node is not interrupted by any of $N-1$ nodes. Consequently, the outage probability is given by:

$$OP_{(N)} = 1 - (1 - OP)^{N-1} \tag{3.34}$$

Validation We have validated these expressions (eq.3.26 and eq.3.34 in the realistic SigFox's case ($R_b = 100$ bps, $b = 100$ Hz, $B = 192$ kHz, $\gamma^* = 6.8$ dB). For the rectangular model, we derived new sets of parameters for the optimal model (AR), upper and lower bound. Indeed, we have identified that higher distance leads to a wider rectangle. Thus, $r_x = r_{max}$ provides the most pessimistic rectangular model over the cell.

TABLE 3.3: Simplified models using rectangular function used in this part

Models	$\triangle$	I_{max}	I_{min}
Optimal model (AR)	145 Hz	0 dB	-75 dB
Upper bound (UP)	300 Hz	0 dB	-47.28 dB
Lower bound for OP (LB)	116 Hz	-6.8 dB	-75 dB

We present on Fig.3.32 the comparison between simulation and theory results. Specific simulations have been run for the fading and no-fading case to validate the theoretical expressions in the corresponding case. Theories validation aside, we can note that OP (no-Rayleigh) is lower than OP (Rayleigh) when r_x is small. But when r_x exceeds a certain distance, these two cases have identical outage probabilities (and close to the real shape simulation results). Rayleigh fading can amplify or attenuate the received signal power. If the received power of the desired node gets attenuated, the area where interfering nodes may lead to error becomes larger. Hence we have more potential nodes in this case. Meanwhile, if the desired node's received power gets amplified, this area becomes smaller, which leads to less interfering nodes. When r_x is small, the expected area's increase is much bigger than the expected area's decrease. Thus, such a node is sensitive to fading. On the contrary, for high r_x, the area increase is bounded by the cell limit, and thus is less important. In addition, for high r_x, the inner interferers are not impacted by fading in average. Hence, such node is barely affected by the fading.

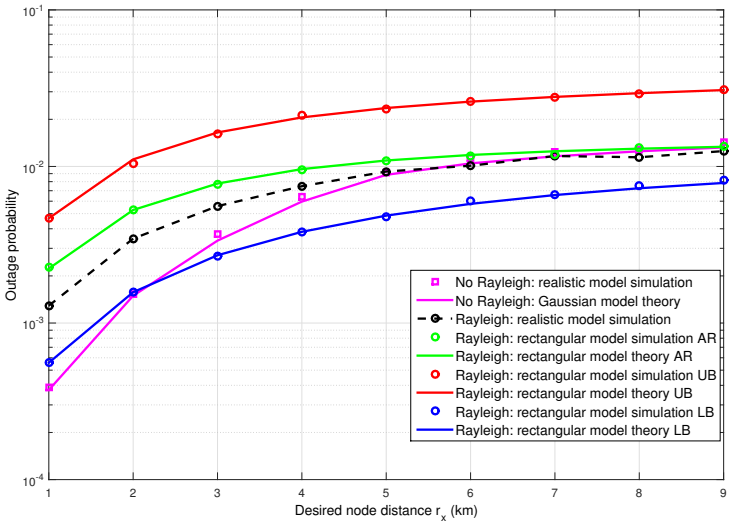

FIGURE 3.32: OP as a function of the desired node's distance r_x, for $B = 96$ kHz, $N = 6$, $r_M = 10$ km, $r_m = 1$ m, $\gamma^* = 6.8$ dB and path loss $\alpha = 2$.

Network spectral efficiency We finally determine the network network spectral efficiency defined as the ratio of the maximum node number and the bandwidth $\frac{N_{max}}{B}$. We compare the spectral efficiency in two cases : without and with a guard band, for different values of α, as shown in Fig.3.33. The *without guard band* corresponds to the ideal case, where targeted frequencies can be obtained, thus allowing the frequency random selection on the whole B. However, in practice, we could obtain such ideal case only if the used bands are placed right next to each other. But, in an UNB network, the oscillator jitter causes imprecise carrier position, which can lead to an overlap between adjacent bands. Therefore, the bands should be separated by a guard interval, which must be taken into account in the spectral efficiency. We consider here a 1736 Hz guard band, which corresponds to the operating frequency transmission 868 MHz and standard deviation of frequency jitter of 2 ppm. This permits to ensure that no actual carrier frequency would fall outside the intended band.

We choose the rectangular model (with AR set of parameter) to study this criteria while varying the path loss exponents. By observing Fig.3.33, we can note that for small bandwidth such as $B = 12$ kHz, the spectral efficiency is highly degraded by the guard band. This is due to the fact that a big portion of the band is wasted for the guard band to counteract the frequency jitter. Meanwhile, the impact of guard band diminishes as B increases. Hence for the large bandwidth length, the spectral efficiency seems the same for both cases. More interestingly, for each B, there exists a highest spectral efficiency obtained with an optimal α. This is because when α increases, the signal power of both the desired node and interfering nodes diminishes. In the first part of the curves, as the desired node is near to the BS, this decrease of power is more important for interfering nodes, which can be anywhere in the cell. Meanwhile, in the second part, when α exceeds a certain value, the power reduction is so severe that the desired node has no more advantage. Thus N_{max} first increases then decreases. One may note that this behavior is smoothened when r_x is closer to r_M.

Following the previous conclusion, we have plotted in Fig. 3.34 the optimal bandwidth B (for the guard band case) to achieve the highest ratio $\frac{N_{max}}{B}$, as a function of the path loss exponent α. This figure provides the optimal choice for B, according to the propagation characteristics. We observe that for urban areas such as $\alpha = 4$, we need a thiner bandwidth than for rural areas to reach the highest spectral efficiency. Hence it also permits us to make effective use of the available bandwidth.

3.3.7 Interference Cancellation

Finally, to improve the network performances (and thus its capacity), we have considered the use of SIC receiver (Successive Interference Cancellation). We have followed the same methodology than for (3.32), by considering the rectangular interference model. However,

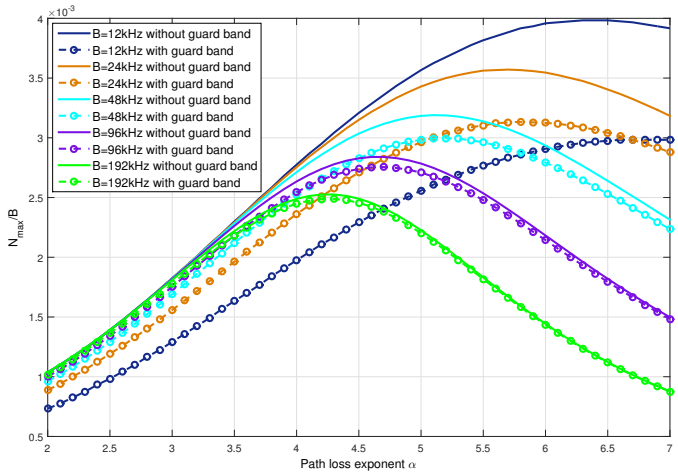

FIGURE 3.33: Maximum node number to bandwidth ratio $\frac{N_{max}}{B}$ (nodes/Hz) vs exponent path-loss α, for $r_M = 10$ km, $r_x = 2$ km, $r_m = 1$ m, $\gamma^* = 6.8$ dB, with and without guard band

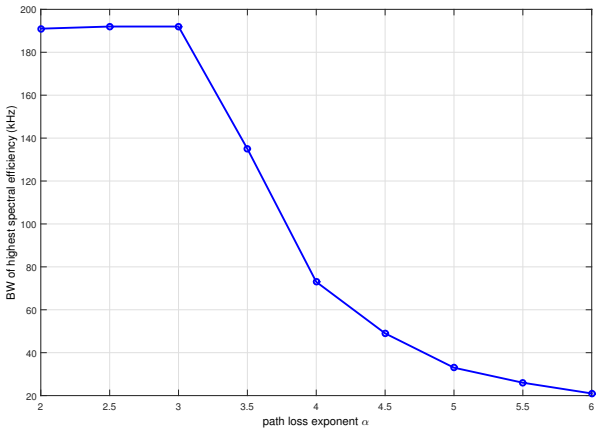

FIGURE 3.34: Bandwidth for highest spectral efficiency ($\frac{N_{max}}{B}$) vs exponent path-loss α, for $r_M = 10$ km, $r_x = 2$ km, $r_m = 1$ m, $\gamma^* = 6.8$ dB, with guard band

in this case, we derive the performances obtained on average in the cell, and not for a fixed r_x. We suppose that the SIC is able to iteratively decode and perfectly remove the highest SINR packets, as long as its SIR is above the required threshold. Thus a packet is successfully received if its SINR is higher than the threshold, or if the colliding packet is itself decodable. Thus, we get:

$$\begin{aligned} OP_{SIC} &= P\left(SIR_x \leq S\right) - P\left(SIR_x \leq S \cap SIR_y > S\right) \\ &= \int_{b_3}^{b_2} \left(\frac{(d-d_1)}{SIR_{th}\beta\left(\delta f\right)} + (e-e_1)SIR_{th}\beta\left(\delta f\right) + (f-f_1) \right) P\left(\delta f\right) \, \mathrm{d}\delta f \\ &\quad + \int_{b_4}^{b_3} P\left(\delta f\right) \, \mathrm{d}\delta f \end{aligned} \tag{3.35}$$

with the following integral edges: $b_1 = min\left(\beta^{-1}\left(\left(\frac{r_m}{r_M}\right)^2 \frac{1}{S}\right), B\right)$, $b_2 = min\left(\beta^{-1}\left(\frac{1}{S}\right), B\right)$ $b_3 = min\left(\beta^{-1}\left(\left(\frac{r_M}{r_m}\right)^2 \frac{1}{S}\right), B\right)$, and $b_4 = 0$;

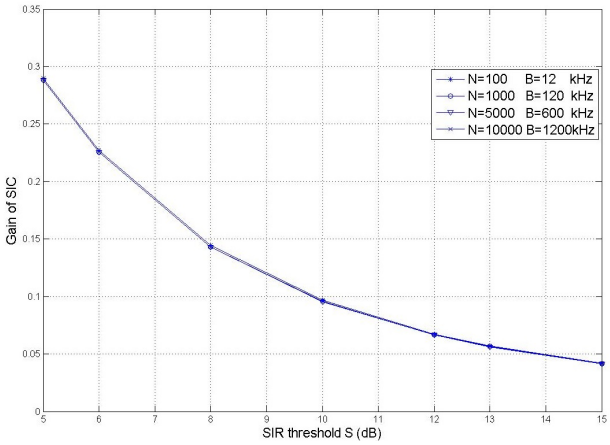

FIGURE 3.35: Gain of SIC, for different SIR threshold S (dB), and constant node density $\frac{100N}{B}$, $r_m = 30$ m, $r_M = 1000$ m.

and the following constants:

$$d = \frac{r_M^4}{2k^4} - \frac{r_m^2 r_M^2}{k^4} - \frac{r_M^2}{k^2} \qquad d_1 = \frac{{r_M}^4}{2k^4},$$
$$e = -\frac{r_m^4}{2k^4} \qquad e_1 = \frac{{r_m}^4}{2k^4},$$
$$f = \frac{r_m^4}{k^4} + \frac{r_M^2}{k^2} \qquad f_1 = -\frac{{r_M}^2 {r_m}^2}{k^4}$$

where $k^2 = r_M^2 - r_m^2$;

After theoretical expression validation, we have determined the SIC benefits, by computing the error reduction percentage $\frac{PER_{noSIC} - PER_{SIC}}{PER_{noSIC}}$. As seen in Fig.3.35, we have shown that, no matter how the scale of node number $\frac{100N}{B}$ becomes, as long as the node density is constant, the SIC improvement is identical.

3.4 Conclusion

In the presented work we have considered long range networks, by considering two distinct ways of realizing it: multi-hop network and long range transmission technologies. In the first case, we have proposed ways of taking advantages of diversity while limiting the number of additional packets. To do so, we have proposed the use of fountain coding, and network coding, both in the multi-hop, relay channel, and realistic network. We have highlighted the compromise between energy consumption (linked to the transmission number) and the end-to-end delay for full information recovery.

In these studies, the MAC layer was considered as perfect, i.e. all transmissions were performed in different slots. We have thus put aside the collision phenomenon. However, this feature also needs to be taken into account.

In the second case, i.e. long range transmissions, we have specifically focused on the collisions statistics for the specific UNB based scenario. In particular, we have evaluated the collision probability when the nodes are equally distant from the BS, and in the more realistic case of random deployment. Thanks to these theoretical analysis, we have been able to estimate the number of nodes that can be supported for a targeted QoS. We have also proposed the use of SIC receiver to suppress the removable interference contribution, and derived the theoretical performances.

In these studies, the performance evaluation was done for a given moment. However, as transmissions are not slotted, the interference pattern might change during the packet. This degree of freedom should also be considered.

Bibliography

[AY05] Kemal Akkaya and Mohamed Younis. "A survey on routing protocols for wireless sensor networks". In: *Ad hoc networks* 3.3 (2005), pp. 325–349.

[BBM09] F. Baccelli, Bartlomiej Blaszczyszyn, and P. Muhlethaler. "Stochastic analysis of spatial and opportunistic aloha". In: *Selected Areas in Communications, IEEE Journal on* 27.7 (2009), pp. 1105–1119. ISSN: 0733-8716. DOI: 10.1109/JSAC.2009.090908.

[BDK16] Alexandros-Apostolos A Bouleogeorgos, Panagiotis D Diamantoulakis, and George K Karagiannidis. "Low Power Wide Area Networks (LPWANs) for Internet of Things (IoT) Applications: Research Challenges and Future Trends". In: *arXiv preprint arXiv:1611.07449* (2016).

[BM+17] Sergio Barrachina-Muñoz et al. "Multi-hop Communication in the Uplink for LPWANs". In: *Computer Networks* (2017).

[Cen+16] Marco Centenaro et al. "Long-range communications in unlicensed bands: The rising stars in the IoT and smart city scenarios". In: *IEEE Wireless Communications* 23.5 (2016), pp. 60–67.

[Karst] P Karn. *The VMSK Delusion*. last accessed September 2017. URL: http://www.ka9q.net/vmsk/,.

[Lub+01] Michael G Luby et al. "Efficient erasure correcting codes". In: *IEEE Transactions on Information Theory* 47.2 (2001), pp. 569–584.

[LYC03] S. Y. R. Li, R. W. Yeung, and Ning Cai. "Linear network coding". In: *Information Theory, IEEE Transactions on* 49.2 (2003), pp. 371–381.

[Mac05] David JC MacKay. "Fountain codes". In: *IEE Proceedings-Communications* 152.6 (2005), pp. 1062–1068.

[Per+13] M.H. Perrott et al. "A Temperature-to-Digital Converter for a MEMS-Based Programmable Oscillator With $< \pm 0.5 - ppm$ Frequency Stability and $< 1 - ps$ Integrated Jitter". In: *Solid-State Circuits, IEEE Journal of* 48.1 (Jan. 2013), pp. 276–291. ISSN: 0018-9200. DOI: 10.1109/JSSC.2012.2218711.

[PFS05] Payam Pakzad, Christina Fragouli, and Amin Shokrollahi. "Coding schemes for line networks". In: *Information Theory, 2005. ISIT 2005. Proceedings. International Symposium on*. IEEE. 2005, pp. 1853–1857.

[RKS17] Usman Raza, Parag Kulkarni, and Mahesh Sooriyabandara. "Low power wide area networks: An overview". In: *IEEE Communications Surveys & Tutorials* 19.2 (2017), pp. 855–873.

[Sha48] Claude E Shannon. "A mathematical theory of communication, Part I, Part II". In: *Bell Syst. Tech. J.* 27 (1948), pp. 623–656.

[Sho06] Amin Shokrollahi. "Raptor codes". In: *IEEE transactions on information theory* 52.6 (2006), pp. 2551–2567.

[TB06] Alberto Tarable and Sergio Benedetto. "Efficiency of precode-only raptor codes and Turbo-fountain codes". In: *Information Theory Workshop, 2006. ITW'06 Chengdu. IEEE*. IEEE. 2006, pp. 61–65.

[Wal] H. R. Walker. In: *http://www.vmsk.org* ().

[Xia03] Chen Xiaoyi Yao Qingdong Liu Xiaocheng. "The VMSK modulation delusion [J]". In: *Journal of Electronics and Information Technology* 11 (2003), p. 018.

[Zha13] Shikai Zhang. "Spectrum aanlyses of UNB modulation formats". In: *Consumer Electronics, Communications and Networks (CECNet), 2013 3rd International Conference on*. IEEE. 2013, pp. 594–597.

Chapter 4

Perspectives

4.1 Introduction

Since I joined the CITI laboratory, my research directions have been driven by the expected forthcoming applications relying on wireless communications. This has been fostered by the CITI scientific scope and aim. Indeed, this laboratory was created so as to cover all aspects of WSN, from wireless communications to applications, along with security, implementation and network challenges. Since then, the laboratory theme has evolved to "humans connected to the digital society", with a broadened scope extended to RF devices architectures and robotics. Nonetheless, the laboratory consistency was kept surrounding the applications rather than the individual scientific skills. In this context, I brought my expertise in transmission systems to reinforce the existing wireless team composed by Jean-Marie GORCE and Guillaume VILLEMAUD.

As developed in the previous chapters, during the last 10 years, I have focused on two main application domains: WBAN and LPWA IoT. One may note that, according to the technology adoption lifecycle, I started working on these subjects as an early adopter (and even innovator for SigFox context). Indeed, as shown on Fig.4.1, the first contracts on both subjects were obtained at the very beginning of these topics. I am willing to pursue this thematic accuracy, by trying to identify the forthcoming applications and scientific and technical obstacles. I will thus present three short term perspectives, as well as two long term ones (but highly less reliable) that I would like to launch during the next 10 years, sooner or later.

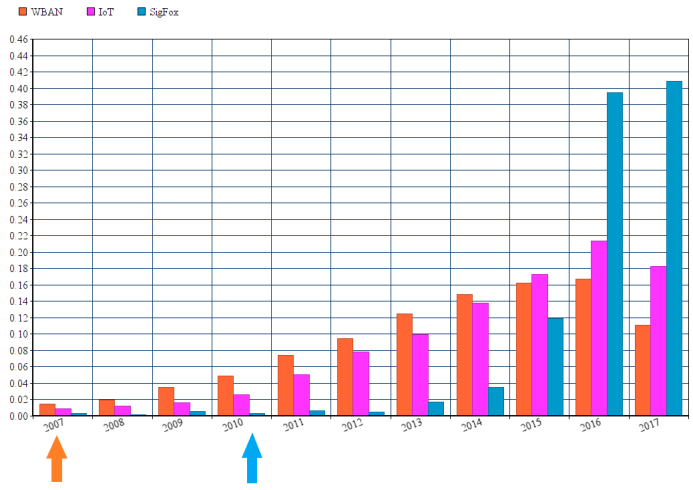

FIGURE 4.1: Percentage (with respect to the total amount of results in each category) of results returned by Google Scholar for different keywords, obtained on September 2017

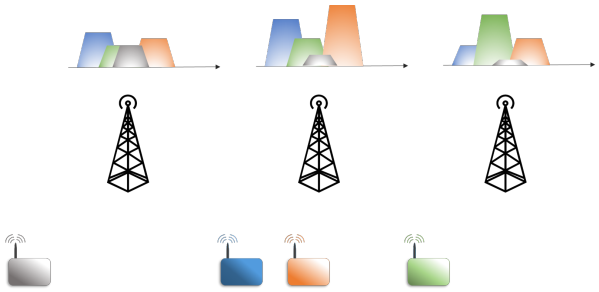

FIGURE 4.2: Spatial diversity example

4.2 Multiple Base Station, or Massive MIMO for uplink

This perspective is the most direct one as it constitutes the objectives fixed for Yuqi MO's PhD last year. Previously, we studied SigFox network performances from the a single receiver (single cell) point of view, as presented in 3.3. This supposes that a BS send and/or receive transmissions to and/or from nodes in its vicinity that it is serving. However, it is commonly known that, due to the need of full coverage (no white space), some nodes can be in connection with multiple BSs. Thanks to the very long range of UNB communications, it appears that all nodes are sensed by multiple stations. This brings spatial diversity that we want to take advantage of.

In most cellular systems, one BS is supposed to serve devices in a specific service area. While devices send data to their intended BS, they also create interference to adjacent BSs. Thus, a BS actually receives the sum of the useful information, contribution of devices intended to neighboring BSs' and noises. If the BSs independently decode the signal, the neighbor devices are seen as interferers. Nonetheless, BSs can cooperate to cover a given area. In this case, all BSs and sensor nodes share the same available time/frequency resource. However, each BS gets a different point of view of the transmitted signal, as shown in Fig.4.2, as they are not located at the same distance from the transmitting devices, and as the transmitted signals experience diverse channel conditions to reach the BS. Therefore, ways to take advantage of multiple BSs' diversity, in terms of time, space and spectrum domain, has been brought up and studied in many research works.

The earliest works on multiple BSs consider them independent and non-collaborative. As BSs do not cooperate with each other, one message can be received by several BSs. The spatial diversity of multiple BSs can still be beneficial in this case. Since the relative distances and the propagation environment between the node and BSs are different, each BS may receive signals of different qualities (in terms of Signal to Interference plus Noise Ration (SINR) or Received Signal Strength Indication (RSSI)). The profit is that when one message fails to be decoded by one BS, it is still possible to be seized by other BSs. Therefore, how to take advantage of BSs' spatial diversity becomes studied. It can help, for example, on the deployment of BSs. In random access networks, multiple non-cooperated BSs are proved to be more efficient than increasing retransmissions trials for heavy input traffic [Sak92], in terms of overall throughput and the average transmission delay. The impacts of multiple BSs' placements and mobility are also evaluated, most of which are for the purpose of prolonging the Wireless Sensor Network's (WSN) lifetime by reducing the energy consumption of nodes [AYY07].

As time goes on, people start to pay attention to the interaction and cooperation among BSs. Solid works from information-theoretic point of view have been conducted. The well-known Wyner's cellular model considers each BS as an antenna of a global receiver, and it treats the cellular network as a Gaussian multiple access channel. This global receiver collects all the information and decodes all the signals jointly. Research works have been made established on this principle, such as finding out the optimal number for cooperating BS [HKD09]; evaluating the benefits of cooperation among neighboring BSs and distant ones; making a comparison between centralized and distributed data processing. One may note that I do not plan to consider in my work the specific equipments that have to be deployed at the BSs to sample and transfer the received signal to a centralized sink before being jointly treated.

When focusing specifically on the uplink, the main issues are to improve the uplink throughput, to estimate channel capacity limits, as well as to reduce nodes' transmission power [AEH06]. To achieve these goals, multiple BSs' joint detection, nodes' cooperative transmission (relaying), and joint power control [Lu+10] are proposed and analyzed. Joint detection, in a general sense, is to combine the signals each BS receives, even if none of them can decode it. For example, if one message from a specific node can not be decoded by any of the BSs that perceive it, we can combine all the signals that where received by the BSs. In this case, the desired user contribution is constructively added, while interference and noise are averaged, leading to a significant increase in the SINR. Thus, this signal may be decoded. There are actually digital combination and signal processing as ways to combine these signals. When the channel can be previously estimated, and when multiple antennas are available on the BSs, MIMO can be performed as presented for example in [PNR17]. Contrarily, we can use the set of BSs to build a virtual MIMO system. This is called Network MIMO (NMIMO) [Wei+16]. The antennas are geographically distributed, and collect the incoming signals before transferring them to a server that will process the streams to recover the data. This approach is more consistent with what we plan to do. However, MIMO needs prior channel estimation, which is not appropriate in SigFox's network.

The objective is thus to take advantage of the available spatial diversity in an opportunistic way, such as presented in [MCL15]; [Li+17]; [Jak+15]. The first one [MCL15], presents the general concept of multiple receivers along with interference cancellation techniques, and provides simulations with different channel models. Similarly, in [Jak+15]; [Mas+], the authors give an insight in spatial-temporal cooperation, along with SIC. With spatial cooperation, neighboring BSs inform each other whenever they collect a user within their coverage overlap, and interference subtraction is done across neighboring BSs in a given slot. Data is transmitted on several slots, so temporal cooperation corresponds to (temporal) successive interference cancellation performed locally at each BS, across different slots in the frame; spatial-temporal cooperation combines both two approaches over the decoding process. All these methods are proved to be beneficial in enhancing the throughput, while each having a different compromise with the synchronization and cost aspects. More recently, [Li+17] focuses on satellites communication. Channel impact is limited to the propagation delay, that generates diversity on the temporal signatures of the different receivers.

I want to complete these studies by taking into account the specific interference pattern of UNB signals. I aim at deriving a theoretical expression that consider the spatial correlation between the BSs, based on a similar approach than [DRG16]; [HYA16] where stochastic geometry is used. Then, I also plan to evaluate the performances of other diversity combining schemes such as MRC (Maximal Ratio Combining) and EGC (Equal Gain Combining), and estimate the trade-off between the receiver complexity and efficiency.

4.3 Sparsity exploitation

This perspective comes within the scope of multiple access techniques in IoT networks [SNL16]. The goal is still to address the reliability of sporadic and very short data transmissions made by a very large number of nodes, without overloading the network with reservation mechanism. In SigFox's network, as deployed nodes are intended to be as simple as possible, and network deployment to be "plug and play" transmissions characteristics are similar among the transmitting nodes (same basic modulation, same statistics on the carrier frequency, ...). Thus identification of the transmitter is done by successfully retrieving the packet and extracting the header informations. Besides, when two packets with similar received power are colliding, they can not be separated.

If we accept to design smarter devices, and perform nodes parameterization before deployment, additional features can be obtained. In particular, orthogonal multiple access techniques (OMA), such as TDMA, FDMA, SC-FDMA, or OFDMA can be used [SNL16]. In this case, the perfect orthogonal feature permits a perfect separation on the transmitting streams. The resource allocation can be done prior to transmission, depending on the transmission conditions, but at the cost of reservation mechanism. On the contrary, dedicating a resource to nodes prior to deployment saves this reservation need. Nonetheless, as a bigger

codebook size is obtained by increasing the channel use, this methodology can note scale with the IoT needs.

An alternative is to consider pseudo-orthogonal channels, with Non Orthogonal Multiple Access (NOMA). Each node is assigned with a code (or a set of codes). The objective of the receiver is thus to detect which nodes are transmitting, and, if intended, recover the sent information. The basic idea is to take advantage of the natural sparsity (only a very small portion of nodes actually transmit at a given time), by using Compressed Sensing (CS) framework [Dav+11]. In On-Off random access schemes [FRG09], the receiver objective is to detect the transmitting nodes, by identifying in the received signal their signature, with multiuser detection techniques. This strategy is beneficial to networks where nodes have to transmit the detection of an event, or ask for more communication resources reservation. Similarly, in [Xie+16], the active node detection is done at the receiver, along with symbol demodulation to be able to transmit more than one bit during the communication process. In this case, the sparsity is used to suppress the identifier header.

One of the remaining challenges is the optimization of the code and the receiver algorithm to reduce the mis-detection, and the false-alarm statistics, without overloading the network. To this aim, we are analyzing the detection statistics, and evaluating the benefits of such scheme compared to the ones where the node identifier is sent within the data packet.

Finally, I intend to evaluate how the correlation between the node's position, or the knowledge of prior transmission can be used to improve the receiver performances.

This work is intended to be realized during the thesis of Diane DUCHEMIN.

4.4 VLC

This perspective also concerns IoT, but focuses on domotics applications. Domotics refers to systems that permits to adapt the home equipment behavior to the exact need of the person(s) living in the place. The classical applications case are temperature and/or light controlling, people and/or animals tracking within the home, remote surveillance, home automation. In these systems, data are transmitted to a central collecting point which process the incoming data and triggers the needed actions. This requires transmission capabilities for the deployed equipment, and thus additional features on the device.

Nonetheless, there are, in our places, many other devices that would benefit from communication features, if the additional cost is almost null. This is the case for all objects equipped with LED indicator, such as coffee machine, kettle, cooktop, household appliances. They usually have basic processing capabilities to manage user instructions, but no digital interface to display a message to the user when needed. The idea is thus to take advantage of the LED indicator to send the data packet so that a camera of commonly available devices (smartphone, tablet, wearables like smart-glasses etc.) can receive it. This is called OCC (Optical Camera Communications), and is a new branch of VLC (Visible Light Communications) [Dan+12]; [Hu+15]; [Sch+12]. Apart from domotics, applications can be extended to any LED equipped object, as for example, on racks in a retail store, to provide additional informations on the desired products. Besides, such technique is also appealing to be deployed on child toys, to provide communication capabilities without exposing the child to electromagnetic waves.

With OCC technique, the data is modulated with OOK modulation (On Off Keying), at a very low rate ($1-10$ kHz), making the LED flashing. This LED modulation is not perceptible by human eyes, thanks to retinal persistence, but is captured by the camera. Indeed, a frame is not acquired at once, but rather row by row. Thus, if the LED status changes between the row acquisitions, the final image contains presents vertical pattern. This is called rolling shutter mechanism [Dan+12].

This techniques is studied in the CITI laboratory by Alexis DUQUE, and his supervisor Razvan STANICA. They have built a proof of concept system [Duq+16], and improved the system reliability by using fountain codes [Duq+17], when considering a single LED. We are just starting a collaboration to make an efficient use of RGB (Red Green Blue) LEDs. With such LEDS, one can exploit the two additional channels to increase the data rate [CC14]; [Luo+15]. We are rather intending to add smart redundancy so as to obtain a more reliable transmission.

4.5 Communications for Robotics applications

WSNs have paved the way for not only IoT networks, but also for MRN (Mobile Robot Networks). Robots are defined as sensors which have additional capacities, such has autonomous and intended mobility, as well as capability of making complex decision and taking appropriate action regarding their behavior. Robots can be used complementary to classical sensors to build a more efficient network [Li+12]; [Cha+16]; [Lic+16].

However, robots can also be exploited on their own, for, e.g. patrolling applications [PR11]. In this case, the robots have to perform the same task in a collaborative way. To do so, robots exchange data through wireless transmissions [Kon+17].

In the two aforementioned cases, robots mobility is an important feature. Indeed, on one hand, mobility induces ever changing topology and introduces non-stationarity as the multi-path pattern is strongly impacted [Hol+16]. On the other hand, robots mobility can be exploited to position the robot at an appropriate place [Kon+17]; [Lic+16]; [Ali+16]. However, in this case, the robot might change its initial path to fulfill transmission needs. In a complementary direction, I would like to opportunistically take advantage of this spatial diversity, without modifying the robot's initial movement. In particular, I would like to focus on humanoid robots, and extend the work done on WBAN to this context. Such work would be facilitated by collaborating with Olivier SIMONIN, and the robotic team that he is leading in the laboratory.

4.6 Quantum transmission ?

This last perspective is more a daydream. But who knows ?

Since I heard about quantum physics, the related phenomena has fascinated me. The fact that the measurement action on an intricate photon immediately modifies the state of its twin regardless of the distance that separate them looks like magic to me. But it also arouses my telecommunication curiosity: is it possible to use this property to transfer data in a perfectly reliable way ? If so, it would revolutionize the telecommunication field. Until now, no solution has been found to transfer data by using entanglement, and experts seem pessimistic. Nonetheless, I would enjoy spending spare time (if any) on this subject, just to try !

Bibliography

[AEH06] Emre Aktas, Jamie Evans, and Stephen Hanly. "Distributed base station processing in the uplink of cellular networks". In: *Communications, 2006. ICC'06. IEEE International Conference on*. Vol. 4. IEEE. 2006, pp. 1641–1646.

[Ali+16] Usman Ali et al. "Motion and Communication Co-optimization with Path Planning and Online Channel Estimation". In: *arXiv preprint arXiv:1603.01672* (2016).

[AYY07] Kemal Akkaya, Mohamed Younis, and Waleed Youssef. "Positioning of base stations in wireless sensor networks". In: *IEEE Communications Magazine* 45.4 (2007).

[CC14] Shih-Hao Chen and Chi-Wai Chow. "Color-shift keying and code-division multiple-access transmission for RGB-LED visible light communications using mobile phone camera". In: *IEEE Photonics Journal* 6.6 (2014), pp. 1–6.

[Cha+16] Chao-Tsun Chang et al. "Data Collection for Robot Movement Mechanisms in Wireless Sensor and Robot Networks". In: *Computer Symposium (ICS), 2016 International*. IEEE. 2016, pp. 435–440.

[Dan+12] Christos Danakis et al. "Using a CMOS camera sensor for visible light communication". In: *Globecom Workshops (GC Wkshps), 2012 IEEE*. IEEE. 2012, pp. 1244–1248.

[Dav+11] Mark A Davenport et al. "Introduction to compressed sensing". In: *preprint* 93.1 (2011), p. 2.

[DRG16] Marco Di Renzo and Peng Guan. "Stochastic geometry modeling and system-level analysis of uplink heterogeneous cellular networks with multi-antenna base stations". In: *IEEE Transactions on Communications* 64.6 (2016), pp. 2453–2476.

[Duq+16] Alexis Duque et al. "Unleashing the power of LED-to-camera communications for IoT devices". In: *Proceedings of the 3rd Workshop on Visible Light Communication Systems*. ACM. 2016, pp. 55–60.

[Duq+17] Alexis Duque et al. "SeedLight: Hardening LED-to-Camera Communication with Random Linear Coding". In: *VLCS'17: 4th ACM Workshop on Visible Light Communication Systems*. 2017, p. 6.

[FRG09] Alyson K Fletcher, Sundeep Rangan, and Vivek K Goyal. "On-off random access channels: A compressed sensing framework". In: *arXiv preprint arXiv:0903.1022* (2009).

[HKD09] Jakob Hoydis, Mari Kobayashi, and Mérouane Debbah. "On the optimal number of cooperative base stations in network MIMO". In: *The IEEE Transactions on Signal Processing* (2009).

[Hol+16] Bernd Holfeld et al. "Radio channel characterization at 5.85 GHz for wireless M2M communication of industrial robots". In: *Wireless Communications and Networking Conference (WCNC), 2016 IEEE*. IEEE. 2016, pp. 1–7.

[Hu+15] Pengfei Hu et al. "Colorbars: Increasing data rate of led-to-camera communication using color shift keying". In: *Proceedings of the 11th ACM Conference on Emerging Networking Experiments and Technologies*. ACM. 2015, p. 12.

[HYA16] Kianoush Hosseini, Wei Yu, and Raviraj S Adve. "A Stochastic Analysis of Network MIMO Systems." In: *IEEE Trans. Signal Processing* 64.16 (2016), pp. 4113–4126.

[Jak+15] Dušan Jakovetić et al. "Cooperative slotted aloha for multi-base station systems". In: *IEEE Transactions on Communications* 63.4 (2015), pp. 1443–1456.

[Kon+17] Linghe Kong et al. "AdaSharing: Adaptive Data Sharing in Collaborative Robots". In: *IEEE Transactions on Industrial Electronics* (2017).

[Li+12] Xu Li et al. "Servicing wireless sensor networks by mobile robots". In: *IEEE Communications Magazine* 50.7 (2012).

[Li+17] Pengxu Li et al. "Asynchronous Cooperative Aloha for Multi-Receiver Satellite Communication Networks". In: *IEEE Communications Letters* (2017).

[Lic+16] Daniel Bonilla Licea et al. "Mobility diversity-assisted wireless communication for mobile robots". In: *IEEE Transactions on Robotics* 32.1 (2016), pp. 214–229.

[Lu+10] Xiaojia Lu et al. "Joint power control, receiver beamforming and adaptive multi base station coordination for uplink wireless communications". In: *Personal, Indoor and Mobile Radio Communications Workshops (PIMRC Workshops), 2010 IEEE 21st International Symposium on*. IEEE. 2010, pp. 446–450.

[Luo+15] Pengfei Luo et al. "Experimental demonstration of RGB LED-based optical camera communications". In: *IEEE Photonics Journal* 7.5 (2015), pp. 1–12.

[Mas+] Aleksandar Mastilovic et al. "Cooperative Slotted ALOHA for Multi-Base Station Systems with Multipacket Reception". In: ().

[MCL15] Andrea Munari, Federico Clazzer, and Gianluigi Liva. "Multi-receiver aloha systems-a survey and new results". In: *Communication Workshop (ICCW), 2015 IEEE International Conference on*. IEEE. 2015, pp. 2108–2114.

[PNR17] Anastasios K Papazafeiropoulos, Hien Quoc Ngo, and Tharmalingam Ratnarajah. "Performance of massive MIMO uplink with zero-forcing receivers under delayed channels". In: *IEEE Transactions on Vehicular Technology* 66.4 (2017), pp. 3158–3169.

[PR11] David Portugal and Rui Rocha. "A survey on multi-robot patrolling algorithms". In: *Technological innovation for sustainability* (2011), pp. 139–146.

[Sak92] Katsumi Sakakibara. "Performance approximation of a multi-base station slotted ALOHA for wireless LAN's". In: *IEEE transactions on vehicular technology* 41.4 (1992), pp. 448–454.

[Sch+12] Stefan Schmid et al. "An LED-to-LED Visible Light Communication system with software-based synchronization". In: *Globecom Workshops (GC Wkshps), 2012 IEEE*. IEEE. 2012, pp. 1264–1268.

[SNL16] Qipeng Song, Loutfi Nuaymi, and Xavier Lagrange. "Evaluation of multiple access strategies with power control error and variable packet length in M2M". In: *Wireless Communications and Networking Conference Workshops (WCNCW), 2016 IEEE*. IEEE. 2016, pp. 379–384.

[Wei+16] Mary Ann Weitnauer et al. "Reliability and longer range for low power transmitters with on demand network MIMO". In: *RFID (RFID), 2016 IEEE International Conference on*. IEEE. 2016, pp. 1–10.

[Xie+16] Ronggui Xie et al. "Many access for small packets based on precoding and sparsity-aware recovery". In: *IEEE Transactions on Communications* 64.11 (2016), pp. 4680–4694.